NextGen Physics

Volume 1 · Issue 1 · 2026

Inaugural issue
Published online on 25 September 2026
Continuous publication · English · Online edition only

Publisher

WULAN GROUP LIMITED
Room 1021, Beverley Commercial Centre, 87–105 Chatham Road South, Tsim Sha Tsui, Kowloon, Hong Kong

Editor-in-chief: Dongfang Yang
Editorial contact: leo.yang@nextgenphysics.com

Journal website: https://www.nextgenphysics.com/
Issue page: https://www.nextgenphysics.com/issues/2026-1/

Contents

NextGen Physics

Volume 1 · Issue 1 · 2026 | e01001

Physical Processes Underlying Ginzburg-Landau Theory: Energy Competition, Condensation Saturation, and Cooper Pair Inertial Mass Scaling Laws

Dongfang Yang

Research and Development Center
Huizhou Pustar New Materials Co., Ltd.
Huizhou 516267, China

Published online: 25 September 2026
Publication model: Continuous publication
Language: English

Article page: https://www.nextgenphysics.com/research/gl-physical-processes/

Publisher

WULAN GROUP LIMITED
Room 1021, Beverley Commercial Centre, 87–105 Chatham Road South, Tsim Sha Tsui, Kowloon, Hong Kong

Editor-in-chief: Dongfang Yang
Editorial contact: leo.yang@nextgenphysics.com

This publication record accompanies the author’s article. The original article follows on the subsequent pages.

Physical Processes Underlying Ginzburg-Landau Theory: Energy Competition, Condensation Saturation, and Cooper Pair Inertial Mass Scaling Laws

Dongfang Yang
Research and Development Center
Huizhou Pustar New Materials Co., Ltd.
Huizhou 516267, China

Leo.yang@pustar.com

Abstract

The Ginzburg-Landau (GL) theory provides a successful phenomenological description of superconductivity near T_c through parameters α, β, and m^*. However, a unified physical interpretation of these parameters, transcending specific microscopic mechanisms, is needed to understand commonalities across diverse superconducting families.

This work develops a conceptual framework by bridging GL phenomenology with microscopic theory through scaling analysis and coherence length correspondence. The approach involves deriving the complete set of scaling laws from the GL free energy functional and establishing self-consistency constraints among the fundamental parameters.

The analysis establishes $T_c \propto \sqrt{-\alpha/m^*}$ as an efficiency metric for superconducting ordering. Theoretical self-consistency requires the parameter constraints $-\alpha \propto m^*$ and $\beta \propto m^*$, revealing that material-dependent variations in these interconnected parameters, rather than their absolute scales, govern superconducting diversity.

The tripartite framework—encompassing energy competition (α), condensation saturation (β), and collective inertial response (m^*)—provides a unified physical picture that maintains mathematical consistency with GL theory. This picture can be substantiated by deeper physical mechanisms: energy competition may originate from matter-wave interference leading to energy redistribution, condensation saturation admits a geometrodynamic interpretation as an effective centrifugal confinement, and inertial mass enhancement can arise from orbital angular momentum coupling to local electric fields. Together, they offer qualitative design principles for optimizing superconducting materials across different families.

Keywords: energy competition, condensation saturation, Cooper pair inertial mass, Ginzburg-Landau theory, scaling laws, superconducting transition

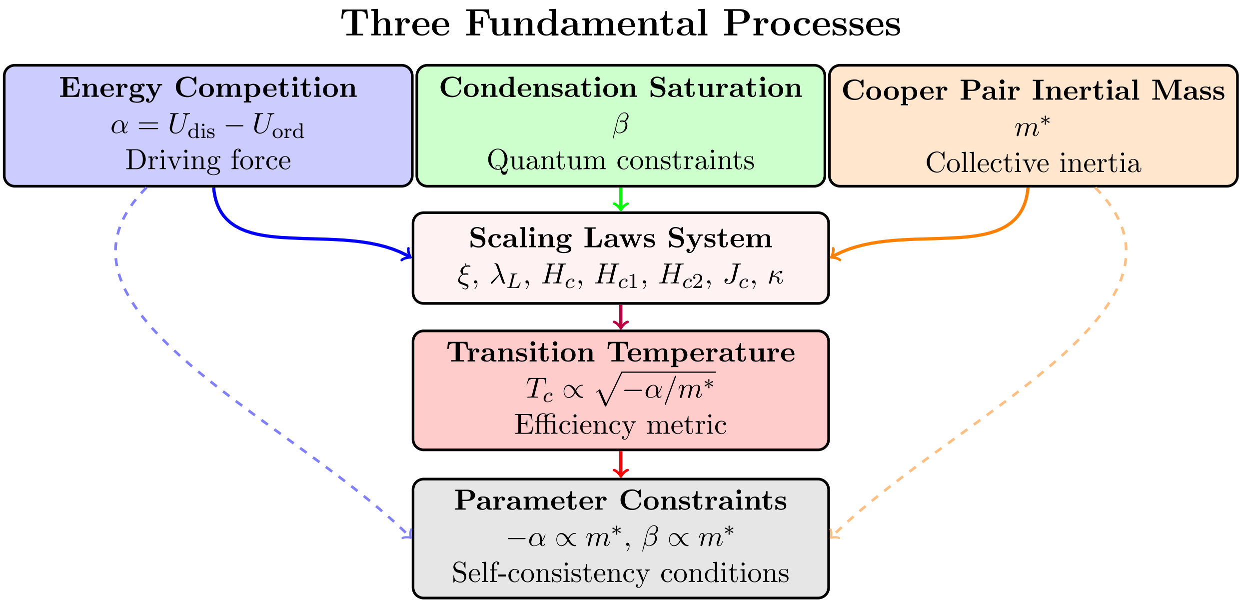

Figure 1: Graphical Abstract: The tripartite framework of energy competition (α), condensation saturation (β), and Cooper pair inertial mass (m^*). Their interplay generates the complete set of scaling laws (ξ, λ_L, H_c, H_{c1}, H_{c2}, J_c, κ), yielding the transition temperature T_c as an efficiency metric, with parameter constraints ensuring theoretical self-consistency.

Contents

1 Introduction

Superconductivity, across its diverse manifestations, involves three fundamental physical processes that can be clearly identified within the Ginzburg-Landau (GL) theoretical framework: energy competition between ordered and disordered states, condensation saturation due to quantum statistical constraints, and the emergence of collective inertia in the phase-coherent condensate. The Ginzburg-Landau theory [1] provides a powerful mathematical framework that captures these processes within a mean-field approximation, characterized through an order parameter ψ and its associated free energy functional:

$$\mathcal{F} = \mathcal{F}_n + \alpha|\psi|^2 + \frac{\beta}{2}|\psi|^4 + \frac{\hbar^2}{2m^*}|\nabla\psi|^2 + \frac{1}{2\mu_0}|\mathbf{B}|^2 \tag{1}$$

This work constructs a theoretical bridge between fundamental quantum processes and phenomenological descriptions by identifying these three universal mechanisms. The primary goal is not to propose new predictive formulas but to establish a unified physical picture and classification framework for understanding the commonalities and differences among diverse superconducting families. The framework developed here enhances the traditional treatment of GL parameters by providing distinct physical interpretations rooted in fundamental quantum processes, while maintaining full consistency with the established mathematical formalism.

The interplay of these processes gives rise to a closed set of scaling laws, with the transition temperature scaling $T_c \propto \sqrt{-\alpha/m^*}$ serving as a cornerstone relation derived through coherence length correspondence (Section 8.1). A key finding emerges from the theoretical self-consistency analysis: the internal consistency of this scaling law system imposes fundamental constraints on the phenomenological parameters, leading to the relation $-\alpha \propto m^*$ (Section 8.2).

This constraint provides a profound physical interpretation for the T_c scaling relation, revealing that the transition temperature is fundamentally governed by the ratio $-\alpha/m^*$, which functions as an **efficiency metric** quantifying the effectiveness of energy competition relative to inertial constraints. The constraint ensures that T_c depends on the ratio of these parameters rather than their absolute scales, providing a unified basis for comparing diverse superconducting materials.

The four expansion terms in Eq. (1) represent distinct physical contributions. The first three terms correspond directly to the three fundamental processes introduced in this work, while the fourth term serves as a **state metric** for the superconducting response:

- **Energy competition** ($\alpha|\psi|^2$): Represents the competition between ordering and disordering energies, which contributes negatively to the free energy ($\alpha < 0$) in the superconducting state, driving the transition.

- **Condensation saturation** ($\frac{\beta}{2}|\psi|^4$): Embodies self-interaction and quantum statistical constraints that limit order parameter growth.

- **Cooper pair inertial mass** ($\frac{\hbar^2}{2m^*}|\nabla\psi|^2$): Quantifies the collective inertial response of the phase-coherent condensate of Cooper pairs, characterizing the energy penalty for spatial variations.

- **Magnetic energy density** ($\frac{1}{2\mu_0}|\mathbf{B}|^2$): Serves as a **state metric** for the outcome of competition between superconductivity and applied magnetic fields, as detailed in Section 3.3.

Terminological Clarification The concept of "energy competition" introduced here aims to provide a process-oriented perspective on the superconducting transition. While related to established concepts such as "pairing interaction strength" (emphasizing microscopic mechanisms) and "condensation energy" (as a thermodynamic outcome), "energy competition" focuses on the dynamic competition between ordering (U_{ord}) and disordering (U_{dis}) energies that drives the phase transition across different material systems.

Notational Convention for the α Parameter Throughout this work, the standard GL convention is adhered to where $\alpha(T) = \alpha_0(T/T_c - 1)$, with $\alpha(T) < 0$ for $T < T_c$. The absolute value $|\alpha|$ is used when referring to the magnitude of the energy competition strength, particularly in scaling relations. In expressions where the sign matters (such as in the free energy minimization), $-\alpha$ is explicitly used to emphasize the negative value. This convention ensures consistency with the standard GL literature while maintaining physical clarity.

The interplay of energy competition, condensation saturation, and Cooper pair inertial mass provides the physical basis for the scaling laws that form a closed theoretical system. This conceptual framework aims to complement the standard treatments found in classical texts and to provide a unified perspective for understanding diverse superconducting phenomena, from conventional superconductors [2] to cuprate [3], iron-based [4], and heavy-fermion systems [5]. The dissection of the GL free energy into contributions corresponding to the interplay of these fundamental processes leads to a unified understanding of the derived scaling laws, with the T_c scaling relation serving as the cornerstone of the theoretical framework, as detailed in Section 8.

Table 1: Key physical symbols used in the theory

Symbol	Meaning	Dimension
α	Ginzburg-Landau parameter, representing energy competition ($U_{\mathrm{dis}} - U_{\mathrm{ord}}$)	J
β	Coefficient in GL free energy expansion, quantifying condensation saturation through self-interaction effects	J·m³
Δ	Superconducting energy gap	J
ΔS	Entropy change due to transition to ordered state	J/K
ξ	Coherence length (characteristic scale of phase coherence)	m
λ_L	London penetration depth (magnetic field screening length)	m
κ	Ginzburg-Landau parameter ($\kappa = \lambda_L/\xi$), determines superconductor classification	dimensionless
m^*	Cooper pair inertial mass (GL gradient coefficient)	kg
m_{band}	Band effective mass (describes electron inertia in periodic lattice potential)	kg
ρ_s	Superfluid stiffness ($\rho_s = \hbar^2 n_s/m^*$)	J/m
ϕ	Phase of the order parameter (macroscopic quantum phase)	dimensionless
n_s	Superconducting carrier density	m^{-3}
T_c	Superconducting transition temperature	K
H_c	Thermodynamic critical field	A/m
H_{c1}	Lower critical field (first flux penetration)	A/m
H_{c2}	Upper critical field (destruction of superconductivity)	A/m
U_{ord}	Ordering energy (drives pairing and coherence, competing with U_{dis})	J
U_{dis}	Disordering energy (maintains normal state, competing with U_{ord})	J
J_c	Critical current density (maximum dissipation-free current)	A/m²
v_F	Fermi velocity (characteristic velocity of electrons at Fermi surface)	m/s

Table 2: Conceptual correspondence between proposed framework and established terminology

Proposed Concept	Physical Interpretation	Standard GL Parameter
Energy Competition	Competition between ordering and disordering energies	α (linear coefficient)
Condensation Saturation	Self-interaction and quantum statistical constraints limiting order parameter growth	β (nonlinear coefficient)
Cooper Pair Inertial Mass	Collective inertial response of phase-coherent condensate of Cooper pairs	m^* (effective mass)

Note: The physical interpretations of these parameters can be further elaborated by specific microscopic or dynamical mechanisms: energy competition (α) may be pictured as arising from matter-wave interference; condensation saturation (β) can be viewed as an effective centrifugal confinement energy; and Cooper pair inertial mass (m^*) enhancement can be driven by orbital angular momentum coupling to local electric fields ($L \times E$ coupling).

2 Methods

2.1 Ginzburg-Landau Theory Foundation

This work is based on the Ginzburg-Landau (GL) theory of superconductivity, which provides a phenomenological description valid near the critical temperature T_c. The methodology involves:

- **Free energy functional analysis**: Systematic examination of the GL free energy expansion terms and their physical interpretations
- **Scaling analysis**: Derivation of scaling relations between measurable superconducting properties and the fundamental GL parameters
- **Microscopic correspondence**: Establishing connections between phenomenological parameters and microscopic theory through established results (Gor'kov derivation, BCS theory) as well as through proposed mechanisms such as matter-wave interference for α, geometrodynamic confinement for β, and orbital-field coupling for m^*
- **Self-consistency analysis**: Examining the constraints required for internal consistency of the theoretical framework

2.2 Key Assumptions and Validity Domains

The analysis employs several key assumptions:

1. Mean-field approximation near T_c ($|T - T_c| \ll T_c$)
2. Slow spatial variations of the order parameter
3. Moderate coupling regime (extendable to strong coupling with appropriate modifications)
4. Homogeneous superconductors (effects of disorder require separate treatment)

3 Theoretical Framework

3.1 Conceptual Framework and Physical Basis

The Ginzburg-Landau theory successfully describes superconducting transitions because it encapsulates three universal physical processes that operate across different material systems: energy competition between ordered and disordered states, condensation saturation due to quantum statistical constraints, and the emergence of collective inertia in the phase-coherent condensate. These processes, while conceptually distinct, operate synergistically during the superconducting transition.

The GL theory provides a specific mathematical realization of these principles under the conditions of mean-field approximation and slow spatial variations near the critical temperature T_c. The mathematical structure naturally admits three complementary physical interpretations that enhance our understanding of the superconducting transition:

1. **Energy Competition**: Represented by the $\alpha|\psi|^2$ term, which becomes negative in the superconducting state, driving the transition through the competition between ordering and disordering energies.
2. **Condensation Saturation**: Represented by the $\frac{\beta}{2}|\psi|^4$ term, quantifying the self-interaction and quantum statistical constraints that limit order parameter growth.
3. **Cooper Pair Inertial Mass**: This process, quantified by the parameter m^* in the term $\frac{\hbar^2}{2m^*}|\nabla\psi|^2$, embodies the collective inertial response of the condensate of Cooper pairs, governing its phase stiffness and dynamical response.

These processes can be further substantiated by deeper physical mechanisms. Energy competition (α) can be pictured as arising from **matter-wave interference**: constructive superposition of electronic wavefunctions at specific wavevectors redistributes interaction energies, effectively reversing the net electron-electron interaction from repulsive to attractive. Condensation saturation (β) admits a **geometrodynamic interpretation** as an effective centrifugal confinement energy: as the order parameter magnitude increases, the enhanced wavefunction overlap and Coulomb repulsion between Cooper pairs generate a confining potential that prevents unlimited growth. Cooper pair inertial mass (m^*) enhancement can be driven by mechanisms such as **orbital angular momentum coupling to local electric fields** (L×E coupling), which introduces additional frustration to phase coherence establishment in strongly correlated systems.

3.2 Energy Competition as the Driving Mechanism

The superconducting transition is fundamentally governed by energy competition between ordering (U_{ord}) and disordering (U_{dis}) energies, quantified by $\alpha(T) = U_{\text{dis}}(T) - U_{\text{ord}}(T)$. This competition drives the superconducting transition across all material classes, with the ordered state emerging when the energy balance favors ordering ($\alpha < 0$).

The energy competition manifests through a reversal from net electron repulsion to net attraction, a process that occurs at the critical temperature T_c where $\alpha(T_c) = 0$. This reversal in the energy balance, as captured by α becoming negative, is the macroscopic manifestation that allows for the formation and condensation of Cooper pairs, characterizing the superconducting state.

The temperature evolution of this competition follows the characteristic dependence $\alpha(T) = \alpha_0(T/T_c - 1)$, where α_0 represents the maximum magnitude of the energy competition parameter $|\alpha|$, which is attained at zero temperature. This temperature dependence ensures consistency with mean-field critical exponents and governs the scaling behavior of the order parameter near T_c.

While the specific microscopic mechanisms driving this energy competition vary across different superconducting families—from electron-phonon coupling in conventional superconductors to spin-fluctuation mediated interactions in unconventional systems—the fundamental competition between ordering and disordering energies remains universal. The detailed examination of the microscopic origins and physical interpretation of this energy competition parameter is presented in Section 4.

3.3 The Role of Magnetic Energy Density as a State Metric

Within the Ginzburg-Landau framework, the term $\frac{1}{2\mu_0}|\mathbf{B}|^2$ is understood as the magnetic energy density associated with the superconductor's response state to external magnetic fields.

This term serves as a fundamental metric that quantifies the outcome of the competition between the superconducting ordering tendency and the applied magnetic field:

- In the ideal Meissner state, $\mathbf{B} \to 0$ within the bulk superconductor, and this term approaches zero, reflecting perfect flux expulsion.
- In the mixed state (vortex state), $\mathbf{B}$ has finite values at vortex cores, and this term reflects the energy density of the partially penetrated magnetic field.
- In the normal state, $\mathbf{B}$ fully penetrates the sample, and this term reaches its maximum value of $\frac{1}{2\mu_0}|\mathbf{B}_0|^2$.

The actual spatial distribution of $\mathbf{B}(\mathbf{r})$, and hence the value of this term throughout the sample, is governed by the effectiveness of magnetic screening, which is characterized by the London penetration depth λ_L. As derived in Section 7, λ_L is determined by the Cooper pair inertial mass parameter m^* and the superfluid density n_s. A smaller m^* (implying larger phase stiffness) leads to stronger screening and a magnetic energy profile closer to the ideal Meissner state.

Thus, the magnetic energy density term functions as a **state metric** that quantifies the outcome of the competition between superconductivity and applied magnetic fields, rather than representing a fundamental driving process. The three core processes—energy competition, condensation saturation, and Cooper pair inertial mass—determine the superconducting state, while the magnetic energy density term provides the crucial metric for characterizing how this state responds to external magnetic fields.

The characterization of the magnetic energy density term as a state metric remains robust within the mean-field Ginzburg-Landau formalism near T_c, which is the focus of this work. While in systems with significant magnetic interactions (e.g., magnetic superconductors), external fields or internal moments could potentially influence the energy competition parameter α through mechanisms like the Zeeman effect or spin-fluctuation mediation, such effects constitute a secondary modulation rather than a fundamental revision of the tripartite process framework. A detailed investigation of these intriguing complexities falls beyond the scope of this foundational presentation.

3.4 Ginzburg-Landau Theory as a Specific Realization

The GL theory emerges as a particular mathematical realization of these three fundamental processes under specific conditions: weak coupling, mean-field approximation, and slow spatial variations of the order parameter. In this limit, the generalized concepts reduce to the familiar GL parameters with the specific functional forms used in the theory.

The following sections delve into the physical interpretation of each process within the GL framework, with particular focus on the parameters α, β, and m^* and their manifestation in the derived scaling laws.

4 Energy Competition and the α-Parameter

4.1 Physical Interpretation of the Energy Competition Parameter

The energy competition process is quantified by the parameter $\alpha(T) = U_{\text{dis}}(T) - U_{\text{ord}}(T)$, which possesses the fundamental dimension of energy (Joules) and undergoes a critical sign reversal at T_c. At the microscopic level, this competition can be pictured as driven by **matter-wave interference**: constructive superposition of electronic wavefunctions at specific wavevectors (e.g., from Fermi surface nesting) redistributes interaction energies, which can reverse the net electron-electron interaction from repulsive to attractive. These two properties—dimensional consistency and sign reversal—provide the physical basis for conceptualizing the superconducting transition as a competition between ordering and disordering energies.

Dimensional Foundation: Quantifiable Energy Competition The energy dimension of α (J) establishes the physical legitimacy of dividing the superconducting energy landscape into competing components. In the GL free energy density expression $\mathcal{F} = \alpha|\psi|^2 + \ldots$, the parameter α has dimensions of energy, while the order parameter squared $|\psi|^2$ has dimensions of inverse volume (representing Cooper pair density). Thus the product $\alpha|\psi|^2$ has dimensions of energy density, consistent with the free energy density.

- U_{dis} (disordering energy, J): Total energy maintaining the normal state.
- U_{ord} (ordering energy, J): Total energy driving superconducting order.

The detailed microscopic compositions and origins of these competing energies are elaborated in Section 4.2.

The definition $\alpha = U_{\text{dis}} - U_{\text{ord}}$ ensures dimensional consistency, transforming abstract "energy competition" into a measurable physical quantity.

Sign Reversal Dynamics: Competition Outcome The temperature-dependent sign reversal of α reveals the competition mechanism:

- $T > T_c$: $\alpha > 0 \Rightarrow U_{\text{dis}} > U_{\text{ord}}$ (normal state prevails)
- $T = T_c$: $\alpha = 0 \Rightarrow$ Energy balance point
- $T < T_c$: $\alpha < 0 \Rightarrow U_{\text{ord}} > U_{\text{dis}}$ (superconducting state)

The continuous temperature dependence $\alpha(T) = \alpha_0(T/T_c - 1)$ reflects the smooth transition from disorder to order dominance.

The Critical Significance of $\alpha(T_c) = 0$ and $\alpha < 0$ The transition occurs at T_c where $\alpha(T_c) = 0$, which, from the perspective of energy competition, signifies a quantitative balance between U_{ord} and U_{dis} (equal absolute energy, mutual offset). For $T < T_c$, $\alpha(T) < 0$ indicates that the ordering energy prevails, with $-\alpha$ representing the net driving energy for superconductivity. It is precisely in this regime ($\alpha < 0$) that the equilibrium order parameter $|\psi|^2 = -\alpha/\beta$ and the energy scale $\Delta \propto (-\alpha/\beta)^{1/2}$ become physically meaningful. A more negative α (larger $-\alpha$) implies a stronger net driving energy from U_{ord}, leading to a lower free energy minimum and a more stable superconducting state.

While conceptually distinct, the energy competition process is thermodynamically coupled to the entropy reduction that accompanies the establishment of quantum order. This reduction manifests as condensation saturation effects in three fundamental domains—momentum-space pair correlation, real-space phase coherence, and spin-space correlation. The quantification of these saturation effects through the condensation saturation parameter β, and its microscopic foundation, are elaborated in Section 5.

4.2 Microscopic Origins of Ordering and Disordering Energies

Having established the physical interpretation of α, the microscopic origins of its constituent energies, U_{ord} and U_{dis}, are now examined. The energy competition process manifests as the dynamic competition between ordering energy (U_{ord}) and disordering energy (U_{dis}) across all superconducting systems. While specific mechanisms may vary—from electron-phonon coupling to spin-fluctuation mediated interactions—the fundamental competition drives the phase transition.

These energies have distinct microscopic origins:

- **Ordering energy (U_{ord})**: Arises from attractive interactions that drive electron pairing:
  - Electron-phonon coupling in conventional superconductors, where lattice vibrations modify the potential energy landscape to enable net attraction.
  - Spin-fluctuation mediated interactions in unconventional superconductors, where dynamic spin correlations alter the energy landscape, effectively reversing the energy gradient and leading to a net attractive interaction between electrons.
  - Exchange interactions in correlated electron systems.
- **Disordering energy (U_{dis})**: Maintains normal state disorder through:
  - Coulomb repulsion between electrons
  - Thermal fluctuations that disrupt coherence
  - Entropic contributions favoring disordered configurations

4.3 The Repulsion-Attraction Transition Mechanism

The fundamental reversal from net electron repulsion to net attraction characterizes the superconducting transition. This occurs when:

$$U_{\text{ord}} > U_{\text{dis}} \Rightarrow \alpha = U_{\text{dis}} - U_{\text{ord}} < 0 \tag{2}$$

This transition manifests microscopically as the dominance of attractive interactions over repulsive Coulomb forces near the Fermi surface. This reversal from net repulsion to net attraction occurs at the equilibrium distance r_{eq} where the force $F_r = -\partial U/\partial r$ changes sign, corresponding to the minimum of the superconducting potential well in Fig. 2. The energy landscape transformation illustrates this fundamental reversal.

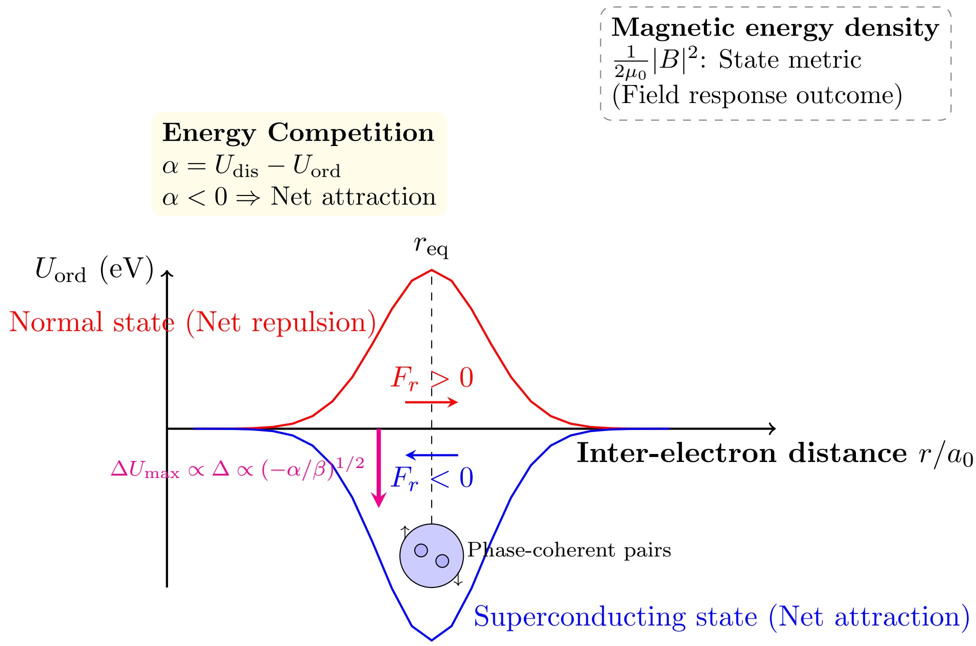

Figure 2: Energy landscape transformation in the superconducting transition. The reversal from net electron repulsion ($F_r > 0$, red curve) to net attraction ($F_r < 0$, blue curve) near the equilibrium distance $r_{\rm eq}$ characterizes the transition. The depth of the potential well, which corresponds to the energy scale of the superconducting gap Δ, consequently scales as $\Delta U_{\rm max} \propto (-\alpha/\beta)^{1/2}$. The magnetic energy density term ($|\mathbf{B}|^2/2\mu_0$) serves as a state metric for the superconducting state's response to external fields, as discussed in Section 3.3, rather than representing a fundamental driving process.

4.4 Temperature Dependence and Critical Behavior

The temperature evolution of the energy competition is characterized by the standard Ginzburg-Landau dependence:

$$\alpha(T) = \alpha_0 \left(\frac{T}{T_c} - 1 \right), \tag{3}$$

where α_0 represents the maximum magnitude of the energy competition parameter $|\alpha|$, attained at zero temperature.

This linear temperature dependence is not merely a phenomenological choice but emerges naturally from the mean-field character of the transition. The critical point $\alpha(T_c) = 0$ represents the precise thermal balance where the disordering effects of temperature exactly counteract the ordering tendency arising from condensation saturation.

The temperature evolution of $\alpha(T)$ governs the critical scaling behavior near T_c. The linear form in Eq. (3) ensures consistency with mean-field critical exponents, particularly the characteristic scaling of the order parameter:

$$|\psi| \propto (T_c - T)^{1/2} \quad \text{for} \quad T \to T_c^-, \tag{4}$$

which emerges directly from minimizing the free energy functional with the temperature-dependent $\alpha(T)$.

The temperature-dependent term $\alpha_0(T/T_c)$ quantifies how thermal fluctuations progressively weaken the ordering tendency until balance is restored at T_c.

In the preliminary phenomenological description, the energy competition parameter α and the Cooper pair inertial mass parameter m^* may be viewed as having distinct physical origins. However, as will be demonstrated in Section 8, the internal self-consistency of the scaling law system imposes a fundamental constraint linking these parameters, necessitating $-\alpha \propto m^*$.

5 Condensation Saturation and the β-Parameter

5.1 The Concept of Condensation Saturation

Building upon the energy competition process discussed in Section 4, the superconducting transition also involves a fundamental condensation saturation process—a quantum-statistical limitation on order parameter growth that prevents unlimited condensation. This saturation operates through three interconnected constraints:

- **Momentum-space quantum statistical constraints**: The formation of Cooper pairs from independent electronic states near the Fermi surface is constrained by Pauli exclusion principles, which prevent unlimited pair condensation in identical quantum states while being limited by the electronic density of states.
- **Real-space phase coherence constraints**: The establishment of long-range phase coherence $\phi(\mathbf{r})$ encounters limitations due to self-interaction effects between Cooper pairs, where competition between Coulomb repulsion and effective attraction prevents infinite growth of order parameter amplitude.
- **Spin-space correlation constraints**: For spin-singlet pairing, the formation of spin-singlet pairs is limited by exchange correlation effects, imposing quantum constraints on spin correlations.

This quantum-constrained condensation process is thermodynamically essential for stabilizing the superconducting state at finite order parameter values: quantum constraints provide the necessary energy cost that balances the driving force from energy competition, preventing runaway growth of the order parameter and ultimately establishing a thermodynamically stable equilibrium condensate density.

5.2 The β-Parameter: Quantitative Measure of Condensation Saturation

The condensation saturation process finds its mathematical expression in the β term of the GL free energy expansion. This parameter embodies the energy cost associated with bringing the system's degrees of freedom into the highly correlated superconducting state. The dimensional structure of β provides crucial insights and permits two complementary physical interpretations:

$$[\beta] = \text{Energy} \times \text{Volume} \tag{5}$$

Self-Interaction Interpretation: Microscopic Repulsion Mechanism From a microscopic perspective, β quantifies the repulsive interactions that emerge with increasing Cooper pair density. This interpretation provides a clear physical picture: as the order parameter grows, the increasing density of Cooper pairs leads to stronger repulsive interactions that eventually balance the driving force for condensation. The mathematical correspondence captures this saturation mechanism:

$$\beta \sim \frac{\text{Interaction Energy Density}}{|\psi|^4} \tag{6}$$

This perspective highlights how β embodies the fundamental quantum constraints introduced above—Pauli exclusion, Coulomb repulsion, and exchange correlation—which collectively contribute to an energy cost that increases with the fourth power of the order parameter.

Entropic Cost Interpretation: Thermodynamic Constraint Thermodynamically, β represents the cost associated with entropy reduction during ordering. The formation of phase-coherent pairs dramatically reduces the system's accessible quantum states, with β quantifying this entropic penalty. This interpretation can be understood through the fundamental free energy relation:

$$\Delta F = \Delta U - T\Delta S \tag{7}$$

where the superconducting transition involves a competition between the internal energy gain ΔU (predominantly captured by the α term) and the entropic penalty $-T\Delta S$ (reflected in the β term). The entropy reduction $\Delta S < 0$ upon ordering contributes a positive term to the free energy, thus opposing the transition.

The entropic cost interpretation provides a quantitative measure through:

$$\beta_{\text{entropy}} \sim \int_V \epsilon_{\text{entropic}}(\mathbf{r}) d^3\mathbf{r} \tag{8}$$

where $\epsilon_{\text{entropic}}$ conceptually represents the energy associated with the free energy penalty due to entropy reduction upon ordering. This interpretation offers a complementary perspective: the equilibrium order parameter value $|\psi|^2 = -\alpha/\beta$ can be viewed as the balance point where the energy gain from ordering (predominantly captured by the α term) outweighs the combined costs, which include the self-interaction repulsion (captured by β) and the entropic penalty.

It is important to emphasize that the "entropic cost" interpretation presented here is a **heuristic physical picture** aimed at providing qualitative insight into the physical meaning of the β parameter. It is not a rigorous mathematical derivation from first principles, but rather a conceptual framework that helps understand how the β term represents the thermodynamic cost of establishing long-range order.

Geometrodynamic Interpretation: Effective Centrifugal Confinement The saturation effect also admits a **geometrodynamic interpretation**: it corresponds to the energy of an effective centrifugal potential that arises from confining charged Cooper pairs within a phase-coherent volume. As the order parameter magnitude increases, the enhanced wavefunction overlap and Coulomb repulsion between Cooper pairs generate a confining potential that prevents unlimited growth, analogous to how centrifugal force limits orbital radius in rotational motion. This mechanical picture provides a vivid visualization of the condensate's self-limiting nature.

5.3 Microscopic Foundation and Parameter Relationships

Gor'kov's Microscopic Derivation The microscopic foundation for the β parameter is established through Gor'kov's rigorous derivation [6]:

$$\beta = \frac{7\zeta(3)N(0)}{8\pi^2 k_B^2 T_c^2} \propto \frac{N(0)}{T_c^2} \tag{9}$$

Relation to Ginzburg-Landau Parameters The microscopic expression for β establishes a fundamental link between phenomenological GL theory and material properties. The parameter β, together with the energy competition parameter α, determines key superconducting properties such as the equilibrium order parameter $|\psi|^2 = -\alpha/\beta$ and the superconducting gap $\Delta \propto (-\alpha/\beta)^{1/2}$.

The relationship between β, $N(0)$, and T_c will be further examined in Section 8, where the complete parameter constraint system that ensures theoretical self-consistency within the GL framework is established.

Validity Conditions and Theoretical Boundaries The microscopic expression for β and the scaling relations derived in this work are established under specific conditions that define their domain of applicability, as outlined in the methodological foundations (Section 2.2):

1. **Mean-field regime**: The GL theory is strictly valid near the critical temperature, where $|T - T_c| \ll T_c$.
2. **Weak-coupling limit**: The underlying BCS framework assumes an electron-boson coupling strength $\lambda \lesssim 1$.
3. **Clean limit**: The derivations assume an electron mean free path ℓ much larger than the coherence length ξ_0 ($\ell \gg \xi_0$).
4. **Moderate correlations**: The relation between the density of states $N(0)$ and phenomenological parameters is simplest for systems with approximately parabolic bands.

For strong-coupling superconductors, dirty-limit systems, or materials with strong fluctuations beyond mean-field theory, the specific scaling relations may require modifications. Nevertheless, the fundamental physical interpretation of the parameters—energy competition (α), condensation saturation (β), and the collective inertial response (characterized by parameter m^*)—transcends these approximations and provides a universal conceptual framework.

5.4 Physical Implications and Unifying Role of Condensation Saturation

The condensation saturation interpretation reveals how quantum statistical constraints fundamentally shape superconducting behavior:

- **Self-interaction perspective**: Provides the physical basis for order parameter saturation at finite values and explains condensate stability through the microscopic relation $\beta \propto N(0)$
- **Entropic cost perspective**: Connects to thermodynamic limitations of the transition and explains specific heat anomalies through the characteristic temperature dependence $\beta \propto 1/T_c^2$
- **Geometrodynamic picture**: Provides a mechanical analogy for understanding how quantum constraints limit condensate growth
- **Unifying role**: The microscopic expression for β serves as a unifying element that bridges phenomenological and microscopic descriptions through its dependence on fundamental material properties

This comprehensive interpretation establishes condensation saturation as an essential process that complements energy competition and the establishment of phase coherence. The parameter β thus serves as a unified quantitative measure of the energy cost associated with saturating the superconducting condensate, with its microscopic foundation providing the crucial link to fundamental material properties.

The condensation saturation concept, quantified through the β parameter and its microscopic foundation, completes the tripartite framework alongside energy competition (α) and the collective inertial response. This sets the stage for discussing the third fundamental process—the collective inertial response characterized by the Cooper pair inertial mass parameter—in the following section, providing a comprehensive physical interpretation of the Ginzburg-Landau theory parameters that transcends specific microscopic mechanisms while maintaining mathematical consistency.

6 Phase Coherence and Cooper Pair Inertial Mass

6.1 Phase Coherence Establishment

The establishment of phase coherence over distances comparable to the coherence length ξ represents a fundamental quantum transition from a state of independent quasiparticles to a macroscopic quantum state. While this transition is driven by the energy competition process (captured by the α parameter), the spatial characteristics of the resulting phase-coherent state are defined by the gradient energy term $\frac{\hbar^2}{2m^*}|\nabla\psi|^2$. This transition involves a profound reduction in accessible quantum states as the system evolves from N independent electronic states with random phases to a single macroscopic wavefunction with a well-defined phase $\phi(\mathbf{r})$ that maintains coherence over macroscopic distances.

The coherence length ξ quantifies the characteristic spatial scale over which the phase of the order parameter remains coherent. The fundamental connection between phase coherence and superfluid response is captured by the equivalence between the Ginzburg-Landau gradient term and the superfluid stiffness formulation:

$$\frac{\hbar^2}{2m^*}|\nabla\psi|^2 \leftrightarrow \frac{1}{2}\rho_s|\nabla\phi|^2 \tag{10}$$

where ρ_s represents the superfluid stiffness, which is phenomenologically related to the Cooper pair inertial mass parameter m^* through the relation $\rho_s = \hbar^2 n_s/m^*$, with n_s denoting the superfluid carrier density.

6.2 Cooper Pair Inertial Mass: Physical Interpretation and Distinctions

Operational Definition of Cooper Pair Inertial Mass In this framework, m^* is operationally defined as the **Ginzburg-Landau gradient term coefficient** that characterizes the collective inertial response of the phase-coherent condensate. Its physical effect is most directly manifested in the **superfluid phase stiffness**:

$$\rho_s = \frac{\hbar^2 n_s}{m^*} \tag{11}$$

which quantifies the energy cost associated with spatial phase gradients. The parameter m^* thus measures how the macroscopic quantum state resists spatial variations in its phase, reflecting the inertial response of the entire condensate rather than individual Cooper pairs.

Core Physical Interpretation of Cooper Pair Inertial Mass The parameter m^* in the Ginzburg-Landau theory is fundamentally interpreted as characterizing the **collective inertial response** of the phase-coherent condensate of Cooper pairs. This core interpretation manifests in two key aspects:

1. **Dynamical Inertia**: In the London equation $m^*\partial\vec{v}_s/\partial t = e\vec{E}$, m^* characterizes the inertial response of Cooper pairs to external perturbations, analogous to classical mass in Newtonian mechanics. This describes how the condensate resists acceleration when subjected to electromagnetic forces.

2. **Inverse Relation to Phase Stiffness**: Cooper pair inertial mass exhibits an inverse relationship with superfluid stiffness: $\rho_s = \hbar^2 n_s/m^*$. This duality reflects the fundamental trade-off in superconducting systems:

- Large m^* (high Cooper pair inertial mass): Weaker magnetic screening ($\lambda_L \propto \sqrt{m^*/n_s}$, as derived in Section 7 and reduced phase stiffness.
- Small m^* (low Cooper pair inertial mass): Enhanced magnetic screening and increased phase stiffness.

These two aspects are unified by the collective nature of m^*, which incorporates not only the bare mass of individual pairs but also the inertial response arising from establishing long-range phase coherence throughout the condensate. In strongly correlated systems, m^* can be significantly enhanced by mechanisms such as the **coupling between orbital angular momentum and local electric fields (L×E coupling)**, which introduces additional frustration to the establishment of phase coherence.

Distinction from Band Effective Mass and Other Concepts The Cooper pair inertial mass concept introduced in this work must be clearly distinguished from other effective mass concepts in condensed matter physics. Table 3 provides a comparative overview of these distinct but related concepts.

Table 3: Comparison of different mass concepts in superconductivity

Mass Concept	Physical Meaning	Determining Factors	Typical Context
Cooper pair inertial mass m^*	Collective inertial response of phase-coherent condensate of Cooper pairs	Phase coherence, correlation effects, pairing symmetry, orbital-field coupling	Ginzburg-Landau theory, superfluid dynamics
Band effective mass m_{band}	Electron inertia in periodic lattice potential	Band curvature, crystal structure, electron interactions	Normal state transport, specific heat, quantum oscillations
Cooper pair mass (BCS)	Bare mass of electron pairs in weak coupling	Electron mass, approximation scheme	BCS theory in free electron approximation ($\approx 2m_e$)

Conceptual Bridge to Microscopic Mass Parameters To conceptually bridge the collective inertial response characterized by m^* with familiar microscopic mass parameters, a phenomenological model can be constructed based on physical reasoning. This model expresses the Cooper pair inertial mass as a product of contributing factors:

$$m^* = 2m_{\text{band}} \cdot (1 + \lambda_{\text{ep}}) \cdot F_{\text{corr}} \tag{12}$$

This phenomenological expression serves to illustrate the potential microscopic origins of the collective inertial response:

- The factor $2m_{\text{band}}$ represents the bare inertial contribution from two band electrons forming a Cooper pair.
- The enhancement $(1 + \lambda_{\text{ep}})$ captures the renormalization due to electron-phonon coupling, where λ_{ep} is the electron-phonon coupling strength.
- The factor F_{corr} encapsulates further renormalization from electron correlation effects beyond mean-field approximations, which may include contributions from mechanisms like orbital angular momentum coupling to local fields (L×E coupling) in strongly correlated systems.

This decomposition illustrates how the Cooper pair inertial mass m^* incorporates not only bare band inertia but also enhancements from many-body interactions. In the weak-coupling limit of conventional superconductors, $m^* \approx 2m_{\text{band}}$; in strongly correlated systems, $F_{\text{corr}} \gg 1$ typically due to heavy quasiparticle formation and mechanisms like L×E coupling, leading to significant mass renormalization. It is crucial to emphasize that Eq. (12) represents a phenomenological model illustrating conceptual connections, not a rigorous microscopic derivation. The core physical interpretation of m^* as characterizing the collective inertial response of the phase-coherent condensate remains paramount and does not depend on the specific form of this illustrative decomposition.

6.3 Cooper Pair Inertial Mass Renormalization through Phase Coherence

The establishment of phase coherence is accompanied by a fundamental renormalization of the Cooper pair inertial mass parameter m^*. This renormalization arises because the motion of a single Cooper pair within the condensate must drag the phase field of the entire macroscopic quantum state, leading to an inertial response greater than that of an isolated pair.

The quantitative relationship between phase coherence length and Cooper pair inertial mass will be derived in Section 7. Furthermore, in Section 8, it will be demonstrated that the theoretical self-consistency of the GL scaling laws necessitates a fundamental proportionality between the strength of the energy competition $(-\alpha)$ and this collective inertial parameter (m^*). This deep constraint reveals that the energy scales driving superconductivity are intrinsically linked to the mass scale governing its dynamical response.

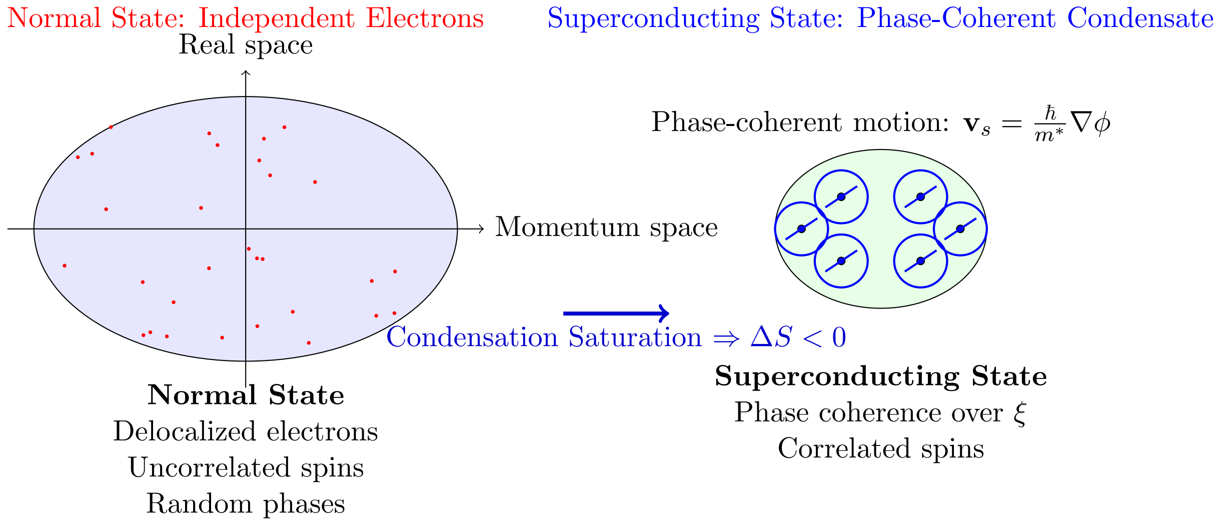

Phase Coherence and Cooper Pair Inertial Mass

$$\psi(\mathbf{r}) \quad = \quad |\psi(\mathbf{r})|e^{i\phi(\mathbf{r})}$$

- Phase coherence length: ξ (coherence length)
- Cooper pair inertial mass: m^* characterizes collective dynamical response
- Superfluid stiffness: $\rho_s \propto n_s/m^*$ (inverse relation)

Figure 3: Phase coherence establishment with collective inertial response characterized by Cooper pair inertial mass m^*. The coherence length ξ quantifies phase correlation range, while superfluid stiffness $\rho_s \propto n_s/m^*$ governs the condensate's response to perturbations.

7 Scaling Laws System: Mathematical Formulation of Process Interplay

7.1 Derivation of Fundamental Scaling Relations

The mathematical derivation of the following scaling laws is rigorously based on the Ginzburg-Landau theory. Their physical significance, however, can be clearly understood as the interplay of the three fundamental processes outlined in Section 3. Each law reveals how a measurable superconducting property depends on the strength of energy competition (via α), the cost of condensation saturation (via β), and the magnitude of Cooper pair inertial mass (via m^*).

Within the GL framework, these processes give rise to a closed set of scaling laws that form a self-consistent theoretical system. This section derives the fundamental scaling relations for measurable superconducting properties, with the scaling relation for the transition temperature T_c to be derived in Section 8 through a rigorous microscopic correspondence that bridges the phenomenological GL theory with BCS theory.

This self-consistent system of scaling laws reveals the fundamental roles of the three core GL parameters: α governing energy competition, β characterizing condensation saturation, and m^* quantifying Cooper pair inertial mass. The superfluid density n_s emerges naturally within this framework as a key physical quantity that, together with m^*, determines the superfluid stiffness $\rho_s = \hbar^2 n_s/m^*$ and appears in several scaling relations. The complete expressions provide a comprehensive framework for understanding superconducting properties across diverse material systems.

7.1.1 London Penetration Depth λ_L

The London penetration depth characterizes the exponential decay of magnetic fields in superconductors. Starting from the London equation [7]:

$$\nabla \times \vec{J}_s = -\frac{1}{\mu_0 \lambda_L^2}\vec{B} \tag{13}$$

The supercurrent density is given by:

$$\vec{J}_s = -\frac{n_s e^*}{m^*}\hbar\nabla\phi \tag{14}$$

where n_s is the superfluid density, $e^* = 2e$ is the effective charge, and ϕ is the phase of the order parameter.

Taking the curl of Ampère's law $\nabla \times \vec{B} = \mu_0 \vec{J}_s$ and substituting the London equation:

$$\begin{aligned} \nabla \times (\nabla \times \vec{B}) &= \mu_0 \nabla \times \vec{J}_s \\ \nabla(\nabla \cdot \vec{B}) - \nabla^2 \vec{B} &= -\frac{1}{\lambda_L^2}\vec{B} \end{aligned} \tag{15}$$

Since $\nabla \cdot \vec{B} = 0$, we obtain:

$$\nabla^2 \vec{B} = \frac{1}{\lambda_L^2}\vec{B} \tag{16}$$

The solution shows exponential decay: $B \sim e^{-x/\lambda_L}$. From the GL theory, the penetration depth is:

$$\lambda_L = \sqrt{\frac{m^*}{\mu_0 n_s (e^*)^2}} = \sqrt{\frac{m^*}{\mu_0 n_s (2e)^2}} \propto \sqrt{m^*/n_s} \tag{17}$$

This establishes the fundamental scaling relation $\lambda_L = \sqrt{\frac{m^*}{\mu_0 n_s (2e)^2}} \propto \sqrt{m^*/n_s}$.

The London penetration depth thus depends on both the Cooper pair inertial mass parameter m^* and the superfluid density n_s, reflecting the dual nature of magnetic screening: Cooper pair inertial mass governs the inertial response of the condensate, while the superfluid density determines the number of carriers participating in the screening.

Therefore, the universal scaling relation for the London penetration depth is $\lambda_L \propto \sqrt{m^*/n_s}$, which provides the complete physical picture of magnetic field screening in superconductors.

Inertia-Stiffness Duality The derived relation $\lambda_L \propto \sqrt{m^*/n_s}$ reveals the fundamental duality between Cooper pair inertial mass and phase stiffness in superconductors. Since the superfluid stiffness $\rho_s = \hbar^2 n_s/m^*$ is inversely proportional to m^*, the penetration depth can be equivalently expressed as:

$$\lambda_L = \sqrt{\frac{\hbar^2}{\mu_0 e^2 \rho_s}} \propto \frac{1}{\sqrt{\rho_s}} \tag{18}$$

This duality, characterized by strong phase coherence (large ρ_s, small m^*), naturally explains why such materials exhibit short penetration depths and robust superconducting properties. Specifically, the enhanced ability to screen magnetic fields, resulting from their large phase stiffness, leads to a magnetic energy density profile that remains close to zero throughout most of the sample volume, thereby contributing to their diamagnetic responses.

Applicability Conditions and Approximations The London penetration depth derivation assumes local electrodynamics and is most accurate for low-frequency, low-field conditions. For high-frequency applications or strong magnetic fields, nonlocal effects become significant and require Pippard's modification. In magnetic superconductors, additional spin-scattering effects must be considered. The local approximation holds when $\lambda_L \gg \xi_0$ (the Pippard coherence length).

Connection to Magnetic Energy Density The derived relation $\lambda_L \propto \sqrt{m^*/n_s}$ provides the crucial link between Cooper pair inertial mass and the magnetic response state metric. Since the magnetic field penetration profile $\mathbf{B}(x) = \mathbf{B}_0 e^{-x/\lambda_L}$ determines the spatial distribution of the magnetic energy density $\frac{1}{2\mu_0}|\mathbf{B}(x)|^2$, the Cooper pair inertial mass parameter m^* directly controls how effectively the superconductor can maintain the low magnetic energy density state characteristic of the Meissner effect.

7.1.2 Coherence Length ξ

The GL coherence length describes the characteristic length scale of order parameter variations. From the GL free energy [1]:

$$\mathcal{F} = \mathcal{F}_n + \alpha|\psi|^2 + \frac{\beta}{2}|\psi|^4 + \frac{\hbar^2}{2m^*}|\nabla\psi|^2 + \frac{1}{2\mu_0}|\mathbf{B}|^2 \tag{19}$$

The gradient term $\frac{\hbar^2}{2m^*}|\nabla\psi|^2$ represents the energy cost of spatial phase variations. For a uniform superconductor, ψ is constant. Near the critical temperature, the order parameter magnitude scales as $|\psi|^2 = -\alpha/\beta$.

The coherence length ξ is defined where the gradient energy equals the condensation energy:

$$\frac{\hbar^2}{2m^*\xi^2}|\psi|^2 \approx |\alpha||\psi|^2 \tag{20}$$

This derivation employs the fundamental assumption that near T_c, where $|T - T_c| \ll T_c$, the gradient energy cost balances the condensation energy gain. This assumption is central to the Ginzburg-Landau theory's validity in the critical region and ensures consistency with the mean-field character of the transition. Away from T_c, fluctuation effects become significant and the simple scaling may require modifications.

Solving for ξ:

$$\begin{aligned}\frac{\hbar^2}{2m^*\xi^2} &= |\alpha| \\ \xi^2 &= \frac{\hbar^2}{2m^*|\alpha|} \\ \xi &= \frac{\hbar}{\sqrt{2m^*|\alpha|}} \propto (m^*|\alpha|)^{-1/2}\end{aligned} \tag{21}$$

This establishes $\xi \propto (m^*|\alpha|)^{-1/2}$.

Applicability Conditions and Approximations The GL coherence length formula is valid in the critical region near T_c ($|T-T_c| \ll T_c$) within the phenomenological framework. For dirty superconductors, the coherence length must be modified to $\xi_{\text{dirty}} = \sqrt{\xi_0 \ell}$, where ℓ is the electron mean free path.

7.1.3 Thermodynamic Critical Field H_c

The thermodynamic critical field H_c represents the field strength at which the superconducting state becomes energetically unfavorable compared to the normal state. This balance occurs when the condensation energy gain in the superconducting state is exactly offset by the magnetic energy density difference.

The condensation energy density is derived from GL free energy minimization:

$$\mathcal{F}_s - \mathcal{F}_n = -\frac{\alpha^2}{2\beta} = -\frac{|\alpha|^2}{2\beta} \tag{22}$$

where we note that $\alpha^2 = |\alpha|^2$ since $\alpha < 0$ in the superconducting state.

The thermodynamic critical field is determined by equating the condensation energy to the magnetic energy density:

$$\frac{\mu_0 H_c^2}{2} = \frac{|\alpha|^2}{2\beta} \tag{23}$$

$$H_c^2 = \frac{|\alpha|^2}{\mu_0 \beta} \tag{24}$$

$$H_c = \frac{|\alpha|}{\sqrt{\mu_0 \beta}} \propto |\alpha|/\sqrt{\beta} \tag{25}$$

Thus, $H_c \propto |\alpha|/\sqrt{\beta}$, demonstrating that the thermodynamic critical field is fundamentally determined by both the energy competition process (α) and the condensation saturation parameter (β).

Applicability Conditions and Approximations The thermodynamic critical field H_c primarily applies to type-I superconductors ($\kappa < 1/\sqrt{2}$) and assumes homogeneous superconductors without intermediate states. In practical applications, demagnetization factors due to sample shape must be considered. For type-II superconductors, H_c represents a theoretical reference field between H_{c1} and H_{c2}.

7.1.4 Critical Current Density J_c

The critical current density J_c is derived from Ginzburg-Landau theory [1] by finding the maximum sustainable current before the gradient term destabilizes the order parameter. For a uniform wire, the supercurrent equation is:

$$\vec{J}_s = -\frac{ie\hbar}{m^*}(\psi^*\nabla\psi - \psi\nabla\psi^*) - \frac{4e^2}{m^*}|\psi|^2\vec{A} \tag{26}$$

For a homogeneous superconductor without magnetic field ($\vec{A} = 0$), and considering a 1D variation of the order parameter, the maximum current occurs when the phase gradient is optimized. The critical current density is given by:

$$J_c = \frac{2\sqrt{2}e\hbar}{3\sqrt{3}m^*\xi}|\psi|^2 \tag{27}$$

Substituting $|\psi|^2 = -\alpha/\beta$ and $\xi = \hbar/\sqrt{2m^*|\alpha|}$:

$$\begin{aligned} J_c &= \frac{2\sqrt{2}e\hbar}{3\sqrt{3}m^*\xi}\left(\frac{-\alpha}{\beta}\right) \\ &= \frac{2\sqrt{2}e\hbar}{3\sqrt{3}m^*} \cdot \frac{\sqrt{2m^*|\alpha|}}{\hbar} \cdot \frac{|\alpha|}{\beta} \\ &= \frac{4e|\alpha|^{3/2}}{3\sqrt{3}\sqrt{m^*}\beta} \propto \frac{|\alpha|^{3/2}}{\sqrt{m^*}\beta} \end{aligned} \tag{28}$$

Thus, the fundamental scaling is $J_c = \frac{4e|\alpha|^{3/2}}{3\sqrt{3}\sqrt{m^*}\beta} \propto \frac{|\alpha|^{3/2}}{\sqrt{m^*}\beta}$.

The parameter β explicitly appears in the expression for J_c, indicating that the condensation saturation process also influences the critical current density.

Applicability Conditions and Approximations The critical current density derivation employs a one-dimensional order parameter gradient approximation, valid for homogeneous superconductors in the absence of significant magnetic field effects. In practical materials, the measured J_c is often limited by flux pinning effects and vortex dynamics rather than the fundamental depairing current derived here. The theoretical J_c represents the upper limit achievable in ideal conditions, while experimental values are typically lower due to material imperfections and pinning landscape characteristics. For nanostructured superconductors, interface scattering effects must be incorporated, and in type-II superconductors, the critical current is usually determined by vortex pinning rather than the depairing current.

7.1.5 Ginzburg-Landau Parameter κ

The GL parameter $\kappa = \lambda_L/\xi$ is the fundamental parameter distinguishing superconductivity types [1, 8]. Substituting the derived expressions:

$$\begin{aligned}
\kappa = \frac{\lambda_L}{\xi} &= \frac{\sqrt{\frac{m^*}{\mu_0 n_s (2e)^2}}}{\frac{\hbar}{\sqrt{2m^*|\alpha|}}} \\
&= \frac{\sqrt{m^*}}{\sqrt{\mu_0 n_s} 2e} \cdot \frac{\sqrt{2m^*|\alpha|}}{\hbar} \\
&= \frac{\sqrt{2}\sqrt{m^* \cdot m^*|\alpha|}}{2e\hbar\sqrt{\mu_0 n_s}} \\
&= \frac{\sqrt{2}m^*\sqrt{|\alpha|}}{2e\hbar\sqrt{\mu_0 n_s}} \propto \frac{m^*|\alpha|^{1/2}}{\sqrt{n_s}}
\end{aligned} \tag{29}$$

Thus, $\kappa \propto m^*|\alpha|^{1/2}/\sqrt{n_s}$.

The GL parameter $\kappa = \lambda_L/\xi \propto m^*|\alpha|^{1/2}/\sqrt{n_s}$ quantifies the interplay between phase coherence (governed by m^*), energy competition strength ($|\alpha|$), and superfluid density (n_s), providing the fundamental link between phenomenological parameters and superconductor classification.

This parameter determines the superconductor type classification:

- $\kappa < 1/\sqrt{2}$: Type-I superconductors
- $\kappa > 1/\sqrt{2}$: Type-II superconductors

Applicability Conditions and Approximations The GL parameter κ is a phenomenological parameter whose temperature dependence is most accurate near T_c. In dirty superconductors, both λ_L and ξ require modification, affecting the effective κ value. For anisotropic systems, a tensor description of κ parameters is necessary to capture directional dependence. The classification boundary $\kappa = 1/\sqrt{2}$ is strictly valid only within the GL framework and may be shifted in systems with non-local effects or strong coupling.

7.1.6 Upper Critical Field H_{c2}

The upper critical field H_{c2} is the field at which superconductivity is destroyed. From the linearized GL equation in magnetic field [8]:

$$\frac{1}{2m^*}\left(-i\hbar\nabla - 2e\vec{A}\right)^2\psi = |\alpha|\psi \tag{30}$$

This is equivalent to the Schrödinger equation for a particle with mass m^* and charge $2e$ in a magnetic field. The lowest eigenvalue corresponds to the ground state energy of this quantum mechanical problem:

$$E_0 = \frac{1}{2}\hbar\omega_c = |\alpha| \tag{31}$$

where $\omega_c = \frac{2eB}{m^*}$ is the cyclotron frequency defined in terms of the magnetic induction B.

At the upper critical field H_{c2}, the magnetic induction B within the superconductor is related to the applied field strength by $B = \mu_0 H_{c2}$, as the magnetization becomes negligible near the transition. Substituting this relation and solving for H_{c2}:

$$\frac{1}{2}\hbar\frac{2e(\mu_0 H_{c2})}{m^*} = |\alpha| \tag{32}$$

$$\frac{\hbar e\mu_0 H_{c2}}{m^*} = |\alpha| \tag{33}$$

$$H_{c2} = \frac{m^*|\alpha|}{\mu_0\hbar e} \propto m^*|\alpha| \tag{34}$$

Thus, $H_{c2} \propto m^*|\alpha|$.

Applicability Conditions and Approximations The upper critical field derivation uses the linearized GL equation approximation, valid only in the critical region near $H \approx H_{c2}$. The relation $B = \mu_0 H_{c2}$ assumes negligible magnetization at the transition point. For anisotropic superconductors like cuprates or iron-based materials, significant directional dependence of H_{c2} must be considered. In low-dimensional systems, quantum confinement effects can substantially enhance H_{c2} values beyond the bulk prediction.

7.1.7 Lower Critical Field H_{c1}

The lower critical field H_{c1} is the field at which magnetic flux first penetrates a type-II superconductor ($\kappa > 1/\sqrt{2}$). The energy per unit length of a vortex is approximately [8]:

$$\mathcal{E}_{\text{vortex}} \approx \frac{\phi_0^2}{4\pi\mu_0\lambda_L^2}\ln\kappa \tag{35}$$

where $\phi_0 = h/2e$ is the flux quantum.

The lower critical field is defined when this energy equals the energy gain from flux penetration, yielding the exact expression within GL theory:

$$H_{c1} = \frac{\phi_0}{4\pi\mu_0\lambda_L^2}\ln\kappa \tag{36}$$

To elucidate the dependence on fundamental parameters, the scaling relations $\lambda_L^2 \propto m^*/n_s$ and $\kappa \propto m^*|\alpha|^{1/2}/\sqrt{n_s}$ are substituted into Eq. (36). The dominant scaling behavior is:

$$\begin{aligned} H_{c1} &\propto \frac{1}{\lambda_L^2}\ln\kappa \\ &\propto \frac{n_s}{m^*}\ln\left(C\cdot\frac{m^*|\alpha|^{1/2}}{\sqrt{n_s}}\right) \end{aligned} \tag{37}$$

where C is a material-specific constant. This expression highlights that H_{c1} is predominantly governed by the n_s/m^* scaling, with a weaker logarithmic dependence on the combined parameter $m^*|\alpha|^{1/2}/\sqrt{n_s}$.

Applicability Conditions and Approximations The lower critical field formula assumes the extreme type-II limit ($\kappa \gg 1$) and employs the single-vortex line approximation. At high magnetic fields, vortex interactions become significant and require more sophisticated treatments. In experimental measurements, surface effects typically reduce the measured H_{c1} below the theoretical bulk value. The derivation is most accurate for isotropic superconductors in the clean limit, and modifications are needed for anisotropic or dirty systems.

7.1.8 Superconducting Gap Δ

The superconducting energy gap Δ is derived from the GL theory. At equilibrium, the order parameter minimizes the free energy:

$$\frac{\partial\mathcal{F}}{\partial|\psi|^2} = \alpha + \beta|\psi|^2 = 0 \tag{38}$$

Thus, $|\psi|^2 = -\alpha/\beta$. The crucial link between the phenomenological GL theory and microscopic theory (e.g., BCS) was established by Gor'kov [6], who showed that the energy gap is proportional to the order parameter:

$$\Delta = \gamma_G|\psi| \tag{39}$$

where γ_G is a constant derived from the microscopic theory.

Therefore:

$$\Delta = \gamma_G\sqrt{-\alpha/\beta} \propto (-\alpha/\beta)^{1/2} = (|\alpha|/\beta)^{1/2} \tag{40}$$

where the last equality holds because $\alpha < 0$ and thus $-\alpha = |\alpha|$.

The depth of the potential well in Fig. 2, which corresponds to the energy scale of the superconducting gap Δ, consequently scales as $\Delta U_{\max} \propto (-\alpha/\beta)^{1/2}$.

Applicability Conditions and Approximations The GL expression for the superconducting gap provides a phenomenological connection to the microscopic BCS theory, with consistency near T_c. For strong-coupling superconductors, Eliashberg theory modifications to the gap ratio are necessary. The relation $\Delta = \gamma_G|\psi|$ establishes the crucial bridge between phenomenological and microscopic descriptions. The scaling $\Delta \propto (-\alpha/\beta)^{1/2}$ is valid within the mean-field approximation and may require corrections for systems with strong fluctuations.

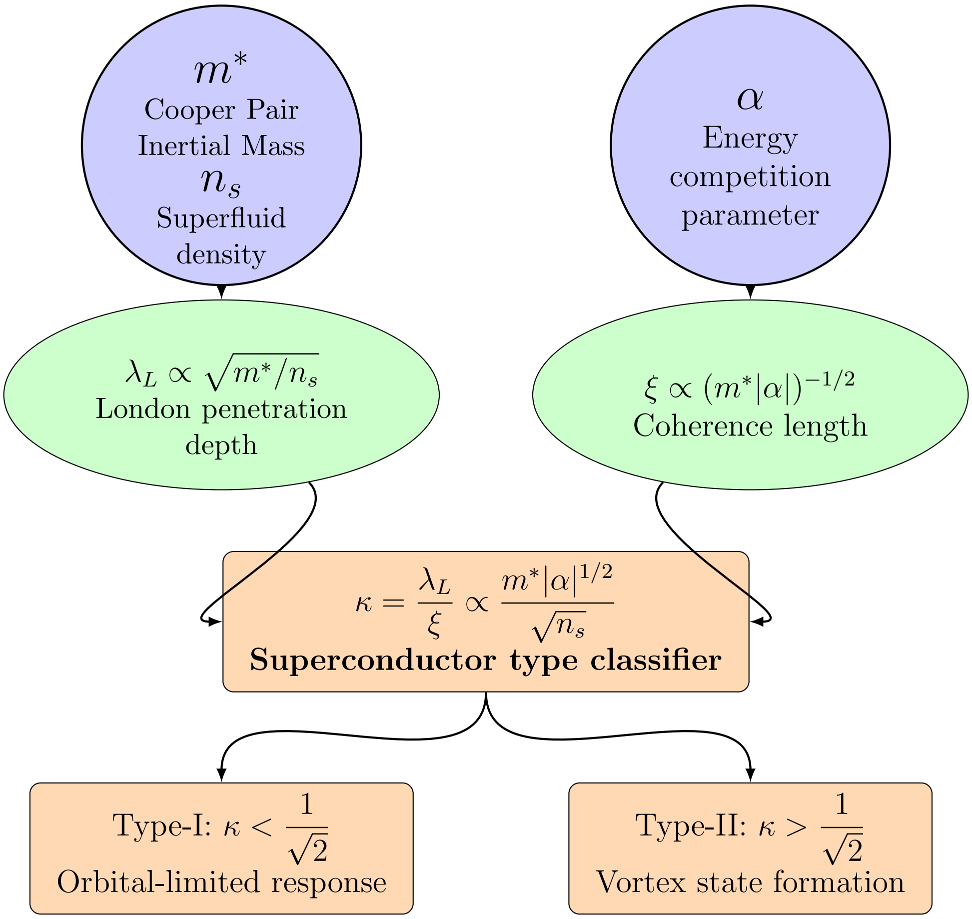

Figure 4: Interplay between Cooper pair inertial mass (m^*), superfluid density (n_s), and energy competition (α). The Cooper pair inertial mass m^* and superfluid density n_s jointly control phase coherence (determining $\lambda_L \propto \sqrt{m^*/n_s}$), while α governs energy competition strength (determining $\xi \propto (m^*|\alpha|)^{-1/2}$). Their ratio $\kappa = \lambda_L/\xi \propto m^*|\alpha|^{1/2}/\sqrt{n_s}$ quantifies the interplay between phase coherence, energy competition, and superfluid density, providing the superconductor type classification parameter.

8 Transition Temperature Scaling and Parameter Constraints

8.1 Scaling Analysis of Transition Temperature

Building upon the complete scaling law system derived in Section 7, the focus now turns to the most fundamental superconducting property—the transition temperature T_c. Through scaling analysis based on microscopic correspondence, $T_c \propto \sqrt{-\alpha/m^*}$ is established and the essential parameter constraints that ensure theoretical self-consistency are revealed.

To establish a phenomenological connection between T_c and the GL parameters, a scaling analysis based on coherence length correspondence is employed. This approach provides physical insight while acknowledging the specific assumptions required.

The coherence length ξ serves as a natural bridge between phenomenological and microscopic descriptions. From Ginzburg-Landau theory, we have:

$$\xi_{\text{GL}} = \frac{\hbar}{\sqrt{2m^*|\alpha|}} = \frac{\hbar}{\sqrt{2m^*(-\alpha)}} \tag{41}$$

where we explicitly use $-\alpha$ since $\alpha < 0$ in the superconducting state.

Microscopically, within the BCS framework [2], the Pippard coherence length at zero temperature scales as:

$$\xi_0^{\text{BCS}} = \frac{\hbar v_F}{\pi\Delta(0)} \propto \frac{v_F}{T_c} \tag{42}$$

While ξ_{GL} and ξ_0^{BCS} represent conceptually distinct length scales—the former characterizing the Ginzburg-Landau order parameter variation and the latter describing the spatial extent of Cooper pairs—their equivalence up to a numerical prefactor provides a basis for scaling analysis:

$$(m^*|\alpha|)^{-1/2} = (m^*(-\alpha))^{-1/2} \propto \frac{v_F}{T_c} \tag{43}$$

To establish a concrete scaling relation for T_c, a connection must be made between the phenomenological parameter m^* and a microscopic energy scale. Within the framework of parabolic band systems ($v_F = \hbar k_F/m_{\text{band}}$), this is achieved by introducing the pivotal ansatz of a proportional scaling between the Cooper pair inertial mass and the band effective mass:

$$m^* = k m_{\text{band}}, \tag{44}$$

where k is a material-dependent constant. This postulated relation serves as the essential conceptual bridge that enables the completion of the scaling derivation, effectively encapsulating the correlation-induced renormalization of the collective inertial response relative to the bare band inertia. The validity of this ansatz is most robust for conventional and moderately correlated superconductors. In strongly correlated systems, this simple proportionality typically breaks down ($k \gg$

1), a scenario that is naturally accommodated by the generalized scaling relation $T_c \propto \sqrt{-\alpha/m^*}$ through the concomitant enhancement of $-\alpha$, as required by the parameter constraint $-\alpha \propto m^*$ (to be discussed in Section 8.2).

Proceeding with the scaling analysis:

$$(m^*(-\alpha))^{-1/2} \propto \frac{v_F}{T_c} \tag{45}$$

$$(m^*(-\alpha))^{-1/2} \propto \frac{\hbar k_F}{m_{\text{band}} T_c} \tag{46}$$

$$(m^*(-\alpha))^{-1/2} \propto \frac{\hbar k_F k}{m^* T_c} \quad \text{(using the scaling assumption } m_{\text{band}} = m^*/k\text{)} \tag{47}$$

Solving for T_c yields the scaling relation:

$$T_c \propto \sqrt{\frac{-\alpha}{m^*}} = \sqrt{\frac{|\alpha|}{m^*}} \tag{48}$$

This scaling analysis establishes $T_c \propto \sqrt{-\alpha/m^*}$ as a fundamental relation emerging from coherence length correspondence, with the understanding that the proportionality $m^* \propto m_{\text{band}}$ represents a specific scaling assumption valid within certain material regimes.

8.2 Discussion of the m^*-m_{band} Proportionality Assumption

The derivation of the T_c scaling relation in Section 8.1 relies on the assumption $m^* \propto m_{\text{band}}$, which requires careful examination. This assumption is most valid in the weak-coupling limit for systems with approximately parabolic bands, where the collective inertial response of the condensate remains closely tied to the band inertia of its constituent electrons. In such cases, the Cooper pair inertial mass m^* can be reasonably approximated as proportional to the band effective mass m_{band}, with the proportionality constant k encapsulating material-specific details such as the electron-phonon coupling strength and Fermi surface geometry.

However, in strongly correlated systems—including heavy-fermion compounds, underdoped cuprates, and other unconventional superconductors—this simple proportionality typically breaks down. Correlation effects can dramatically renormalize the collective inertial response, leading to $m^* \gg m_{\text{band}}$ ($k \gg 1$). In such regimes, the Cooper pair inertial mass m^* incorporates not only the bare band inertia but also contributions from many-body interactions, such as those arising from orbital angular momentum coupling to local electric fields (L×E coupling) or other correlation-induced enhancements.

Crucially, the core scaling relation $T_c \propto \sqrt{-\alpha/m^*}$ does not inherently depend on the $m^* \propto m_{\text{band}}$ assumption. Even when this proportionality breaks down, the T_c scaling remains valid provided the parameter constraint $-\alpha \propto m^*$ is satisfied, as established in Section 8.2. This constraint ensures that increases in Cooper pair inertial mass are compensated by proportional increases in pairing strength, maintaining a finite ratio $-\alpha/m^*$ and thus a finite T_c. The $m^* \propto m_{\text{band}}$ assumption should therefore be viewed as a convenient approximation for establishing the scaling relation in simple cases, rather than a fundamental requirement of the framework.

8.3 Parameter Constraints as Self-Consistency Conditions

8.3.1 Derivation of Parameter Constraints

The parameter constraints $-\alpha \propto m^*$ and $\beta \propto m^*$ emerge as necessary conditions for the internal consistency of the GL scaling law system when connected to microscopic theory. Their derivation proceeds through the following logical steps:

1. **Microscopic foundation:** Gor'kov's microscopic derivation establishes that $\beta \propto N(0)/T_c^2$ [6].

2. **Band structure connection:** For systems with approximately parabolic bands, the density of states at the Fermi level scales as $N(0) \propto m_{\text{band}}$.

3. **Mass scaling assumption:** Employing the scaling assumption $m^* \propto m_{\text{band}}$ (as discussed in Section 8.1.1) yields $N(0) \propto m^*$.

4. **T_c scaling substitution:** Substituting the T_c scaling relation $T_c \propto \sqrt{-\alpha/m^*}$ into Gor'kov's expression gives:

$$\beta \propto \frac{m^*}{(-\alpha/m^*)} = \frac{m^{*2}}{-\alpha} \tag{49}$$

5. **Phenomenological self-consistency:** From GL theory, the superconducting gap scales as $\Delta \propto (-\alpha/\beta)^{1/2}$, while BCS theory establishes $\Delta \propto T_c$. Consistency with $T_c \propto \sqrt{-\alpha/m^*}$ requires $\beta \propto m^*$.

6. **Constraint derivation:** Equating the two expressions for β (from steps 4 and 5) yields the fundamental constraint $-\alpha \propto m^*$.

8.3.2 Interpretation as Self-Consistency Conditions

This parameter constraint system should be understood as **self-consistency conditions** derived from the correspondence between GL theory and microscopic descriptions under specific scaling assumptions:

$$T_c \propto \sqrt{-\alpha/m^*} \tag{50}$$
$$-\alpha \propto m^* \tag{51}$$
$$\beta \propto m^* \tag{52}$$

These relations represent conditions for theoretical self-consistency rather than universal mathematical identities. Different superconducting material families may satisfy these constraints with material-specific proportionality constants, reflecting their distinct pairing mechanisms and correlation strengths. The systematic variation of these proportionality constants across material families provides a valuable framework for classifying superconducting systems.

8.3.3 Physical Interpretation of Constraints: Compensation Mechanism and Efficiency Metric

The constraint $-\alpha \propto m^*$ carries profound physical significance, revealing an intrinsic compensation mechanism:

- **Resolving the puzzle of strongly correlated systems**: In heavy-fermion and other strongly correlated systems, electron correlation effects significantly enhance the quasiparticle effective mass m^*. If the pairing strength $-\alpha$ remained unchanged, T_c would be suppressed to extremely low values according to $T_c \propto \sqrt{-\alpha/m^*}$. The constraint $-\alpha \propto m^*$ indicates that the same correlation effects that enhance m^* must also cooperatively enhance the pairing interaction strength $-\alpha$. This compensation mechanism ensures that the ratio $-\alpha/m^*$ (and thus T_c) can remain at a finite value despite correlation enhancements, explaining why strongly correlated superconductors can exist despite large effective masses.
- **Compensation mechanism**: The linear scaling ensures that increases in Cooper pair inertial mass are compensated by proportional increases in pairing strength, preventing the condensation energy from being suppressed by large m^*. This compensation is essential for the existence of superconductivity in strongly correlated electron systems.
- **Universal scaling**: Different superconducting families exhibit material-specific proportionality constants in the relation $-\alpha \propto m^*$, reflecting their distinct pairing mechanisms. The transition temperature scaling $T_c \propto \sqrt{-\alpha/m^*}$ thus provides a universal metric for comparing pairing efficiency across different superconducting families.

8.4 Theoretical Implications and Experimental Verification of the Parameter Constraints

The complete parameter constraint system ($-\alpha \propto m^*$, $\beta \propto m^*$), derived from the requirement of theoretical self-consistency, carries profound implications for our understanding of superconductivity and provides a framework for experimental validation.

8.4.1 Reduction of Independent Parameters and Theoretical Unification

The constraints $-\alpha \propto m^*$ and $\beta \propto m^*$ fundamentally reduce the number of independent phenomenological parameters in the Ginzburg-Landau theory from three to a single essential scale (e.g., m^*, or equivalently $-\alpha$). This reduction is not merely a mathematical simplification but reflects a deep physical principle: the energy scales governing superconductivity—energy competition (α), condensation saturation (β), and the collective inertial response (m^*)—are intrinsically linked through the quantum statistical nature of the phase transition. This unification reveals that the energy, stiffness, and saturation limit of the macroscopic quantum order parameter are not independent but emerge from a coherent underlying mechanism.

8.4.2 Microscopic Foundation and Self-Consistency

The parameter constraints find their physical origin in the quantum mechanical nature of the superconducting transition. The proportional scaling of $-\alpha$, β, and m^* demonstrates that the same microscopic interactions which determine the pairing strength (governing $-\alpha$) also self-consistently govern the phase stiffness (related to m^*) and the condensation saturation limit (quantified by β). This self-consistency condition ensures that the phenomenological GL theory maintains internal coherence when bridged to microscopic descriptions, such as the Gor'kov derivation which establishes $\beta \propto N(0)/T_c^2$.

8.4.3 Experimental Testability and Predictions

The constraint system generates specific, testable predictions that enable experimental verification and material characterization:

- **Parameter correlation**: Materials with similar T_c but different Cooper pair inertial masses m^* should exhibit proportionally different energy competition strengths $-\alpha$ and condensation saturation parameters β.
- **Universal scaling**: The transition temperature ratio $T_c/\sqrt{-\alpha/m^*}$ should remain approximately constant within families of superconductors that share similar pairing mechanisms, providing a universal efficiency metric for comparing different materials.
- **Quantitative predictions**: For instance, the thermodynamic critical field $H_c \propto |\alpha|/\sqrt{\beta} \propto m^*/\sqrt{m^*} \propto \sqrt{m^*}$ should show systematic variations correlated with m^* across different material systems.

8.4.4 Deviations as Signatures of New Physics

Significant deviations from the predicted parameter constraints may serve as signatures of unconventional pairing mechanisms or physics beyond the standard mean-field GL framework. Such deviations could indicate:

- **Strong coupling effects**: Breakdown of the weak-coupling approximations underlying the standard GL-BCS correspondence.
- **Non-adiabatic pairing**: Dynamics where the pairing interaction cannot be separated from the inertial response on the same timescale.
- **Novel quantum phases**: Emergence of competing orders or unconventional superconducting states that modify the fundamental parameter relationships.

The theoretical implications of the parameter constraint system thus extend beyond mathematical consistency, providing both a unified framework for understanding conventional superconductivity and a sensitive probe for identifying novel superconducting mechanisms.

8.5 T_c as an Efficiency Metric for Superconducting Ordering

With the constraint $-\alpha \propto m^*$, the T_c scaling relation takes on profound physical significance as an **efficiency metric** for superconducting ordering:

$$T_c \propto \sqrt{\frac{-\alpha}{m^*}} \propto \sqrt{K} \tag{53}$$

where K is a material-specific constant representing the **specific pairing efficiency**.

This interpretation reveals that T_c does not depend on the absolute scales of individual parameters but rather on their ratio, which quantifies the effectiveness of converting the energy competition driving force into a high transition temperature. The efficiency metric perspective provides several key insights:

- **Material optimization principle**: High-T_c materials are those that optimize the ratio $-\alpha/m^*$, rather than maximizing individual parameters.

- **Heavy-fermion systems**: The constraint $-\alpha \propto m^*$ explains why heavy-fermion compounds with greatly enhanced m^* due to electron correlations can maintain finite T_c—their energy competition strength $-\alpha$ must be correspondingly enhanced through correlation effects. This compensation mechanism ensures that the ratio $-\alpha/m^*$ (and thus T_c) can remain at a finite value despite correlation enhancements, explaining why strongly correlated superconductors can exist despite large effective masses.

- **Universal comparison framework**: The efficiency metric allows meaningful comparison across different superconducting families by normalizing for the fundamental energy and inertial scales. Materials with the same $K = -\alpha/m^*$ will have similar T_c values regardless of their absolute parameter scales.

- **Design guidance**: Materials design should focus on enhancing the specific pairing efficiency $K = -\alpha/m^*$, which represents the fundamental trade-off between ordering tendency and phase coherence establishment. Strategies include enhancing pairing interactions (increasing $-\alpha$) while minimizing detrimental mass enhancements (reducing m^*).

The T_c scaling relation thus serves as the cornerstone of the unified theoretical framework, connecting phenomenological parameters to microscopic physics while providing a fundamental efficiency metric for understanding and designing superconducting materials. This efficiency-based interpretation resolves a long-standing puzzle in correlated superconductivity: how systems with greatly enhanced Cooper pair inertial masses can still sustain finite transition temperatures, and provides a unified basis for comparing diverse superconducting families.

9 Discussion

9.1 Scaling Behavior Across Superconducting Families

Building upon the derived parameter constraints and the interpretation of T_c as an efficiency metric, this scaling framework provides a unified interpretation of diverse experimental trends across different superconducting material classes. The key insight is that while specific microscopic mechanisms vary, the fundamental processes of energy competition, condensation saturation, and Cooper pair inertial mass response—and their constrained interplay—govern superconducting behavior across all material systems.

Conventional BCS Superconductors In conventional superconductors, where electron-phonon coupling provides the primary pairing mechanism, the scaling relations manifest in characteristic ways:

- The energy competition parameter $-\alpha$ scales with the electron-phonon coupling strength λ_{ep}
- The Cooper pair inertial mass m^* remains close to the band mass m_{band} in weakly correlated systems
- The condensation saturation parameter β follows the Gor'kov relation $\beta \propto N(0)/T_c^2$
- In the weak-coupling limit, the T_c scaling $T_c \propto \sqrt{-\alpha/m^*}$ exhibits correspondence with McMillan-type formulas via the identification of $-\alpha$ with the electron-phonon coupling strength λ and m^* with the band effective mass

High-Temperature Cuprate Superconductors The cuprate superconductors provide a compelling test case for examining the framework's applicability to strongly correlated systems:

- The doping-dependent T_c dome can be interpreted as reflecting the competing evolution of the energy competition strength ($-\alpha$) and the Cooper pair inertial mass (m^*) with carrier concentration. The optimal doping point represents the most favorable balance between these competing factors.
- The Uemura relation[9] $T_c \propto n_s/m^*$ (equivalent to $T_c \propto 1/\lambda_L^2$ since $\lambda_L \propto \sqrt{m^*/n_s}$) finds a consistent interpretation within this framework. The general scaling $T_c \propto \sqrt{-\alpha/m^*}$ reduces to the Uemura form when the pairing strength exhibits the specific scaling $-\alpha \propto n_s^2/m^*$. This condition suggests that in cuprate superconductors, the pairing strength may be intrinsically coupled to the superfluid density, providing a physical basis for this empirical relation.
- The Homes scaling relation[10] $\rho_s \propto \sigma_0 T_c$ further validates the framework's coherence. Substituting $\rho_s = \hbar^2 n_s/m^*$ and $T_c \propto \sqrt{-\alpha/m^*}$ yields $\sigma_0 \propto n_s/\sqrt{m^*|\alpha|}$. This expression reveals a fundamental trade-off: the inverse

dependence on $\sqrt{|\alpha|}$ indicates that a large pairing strength tends to coincide with a lower normal-state conductivity, while the inverse dependence on $\sqrt{m^*}$ shows that a lower Cooper pair inertial mass favors both high transition temperature and better normal-state conduction.

Interpretation of the Pseudogap Phase As a qualitative demonstration of the framework's interpretive power, the pseudogap phase observed in underdoped cuprates finds a natural interpretation within the tripartite framework[11, 12]. The emergence of a pseudogap above T_c can be understood as a regime where the **energy competition** process (pair formation, reflected in the development of a spectral gap) has commenced, but **long-range phase coherence** has not yet been established due to insufficient phase stiffness or excessive phase fluctuations. This decoupling between pairing and phase coherence establishment suggests that:

- The energy competition parameter $-\alpha$ may become significant at temperatures well above T_c, leading to preformed pairs or strong pairing fluctuations. The pseudogap temperature scale T^* might be associated with the energy scale of pair formation (related to $-\alpha$).
- The establishment of long-range phase coherence is hindered by a large effective Cooper pair inertial mass m^* and/or strong phase fluctuations, preventing the system from achieving global superconductivity until lower temperatures. The transition temperature T_c represents the temperature where phase coherence can be maintained, which according to the scaling relation $T_c \propto \sqrt{-\alpha/m^*}$, depends on both the pairing strength and the collective inertia.
- The pseudogap phase can thus be viewed as an intermediate regime where pairing correlations exist without global phase coherence, consistent with the framework's separation of energy competition and phase coherence establishment as distinct but interconnected processes.

Extension to Unconventional Pairing Symmetries The framework developed in this work is based on the standard GL theory with a scalar order parameter, appropriate for isotropic s-wave superconductors. For materials with d-wave, p-wave, or other unconventional pairing symmetries, the formalism requires appropriate generalization. In such systems, the parameters β and m^* (or more precisely, the gradient term coefficient) become tensorial quantities reflecting the anisotropy of the order parameter. The condensation saturation parameter β would acquire directional dependence, characterizing how the self-interaction energy varies with the orientation of the order parameter. Similarly, the gradient energy term would involve an anisotropic mass tensor, reflecting direction-dependent phase stiffness. Despite these complications, the core physical concepts of energy competition, condensation saturation, and collective inertial response remain applicable. The T_c scaling $T_c \propto \sqrt{-\alpha/m^*_{\text{eff}}}$ would still hold, with m^*_{eff} representing an appropriately averaged inertial mass. This extension to anisotropic systems represents a promising direction for future work.

Iron-Based Superconductors In iron-based superconductors, the framework reveals how multi-band effects and moderate correlations modify the basic scaling relationships:

- The multi-band nature of iron-based superconductors suggests that the Cooper pair inertial mass parameter m^* should be interpreted as a collective inertial response that integrates contributions from multiple bands, potentially requiring a generalized description beyond the single-band picture
- The proximity to magnetic instabilities provides natural mechanisms for enhancing the energy competition parameter $-\alpha$
- The typically higher H_{c2} values in iron-based superconductors with similar T_c to cuprates indicate larger $m^*|\alpha|$ products, consistent with enhanced Cooper pair inertial mass and pairing strength while maintaining the same T_c efficiency ratio

Non-Phononic Pairing Mechanisms and Framework Universality Importantly, the phenomenological nature of the framework allows for mechanism-independent reasoning. The concept of **energy competition** (α) is not restricted to electron-phonon interactions but encompasses any microscopic mechanism that can drive the net attraction required for superconductivity. This universality allows the framework to accommodate diverse pairing scenarios:

- **Spin-fluctuation mediated pairing**: In cuprates and some iron-based superconductors, the energy competition may be driven by antiferromagnetic spin fluctuations, where $-\alpha$ scales with the strength of spin correlations.
- **Plasmon or excitonic mechanisms**: In low-density or interface systems, electronic mechanisms beyond phonons can provide the attractive interaction, with $-\alpha$ reflecting the corresponding coupling strengths.
- **Mixed or unconventional mechanisms**: Systems with complex phase diagrams may exhibit competition or cooperation between different pairing mechanisms, reflected in the temperature and doping dependence of $-\alpha$.

The framework's mechanism independence is crucial for its applicability across the superconducting spectrum. While the microscopic origin of $-\alpha$ varies, its role in the energy competition process and its constrained relationship with m^* and β remain universally valid within the GL formalism. This separation between the *existence* of an attractive interaction (captured by $-\alpha$) and its microscopic *origin* is a fundamental feature that enhances the framework's explanatory power.

Heavy-Fermion Superconductors Heavy-fermion systems demonstrate the compensation mechanism implied by $-\alpha \propto m^*$ most dramatically:

- The greatly enhanced m^* due to strong correlations is compensated by correspondingly enhanced $-\alpha$

- The typically low T_c despite large $-\alpha$ reflects the $T_c \propto \sqrt{-\alpha/m^*}$ scaling, indicating a relatively low specific pairing efficiency K

- The existence of superconductivity in these systems, despite greatly enhanced Cooper pair inertial masses, presents a case consistent with the proposed constraint $-\alpha \propto m^*$

Strong-Coupling Superconductors and Eliashberg Theory For strong-coupling superconductors described by Eliashberg theory, the simple proportionality between GL parameters and microscopic quantities becomes more complex. The electron-phonon coupling not only enhances the pairing interaction (increasing $-\alpha$) but also renormalizes the quasiparticle mass, affecting m^*. In such systems, the parameter constraint $-\alpha \propto m^*$ may still hold in a generalized sense, but the proportionality constant would incorporate strong-coupling corrections. The framework developed here provides a phenomenological perspective that complements the detailed microscopic description of Eliashberg theory, offering a unified way to compare strong-coupling and weak-coupling superconductors through the efficiency metric $T_c \propto \sqrt{-\alpha/m^*}$.

9.2 Material Design Principles from Scaling Framework

The scaling framework, centered on the efficiency metric $T_c \propto \sqrt{-\alpha/m^*}$, translates fundamental physical insights into practical material design principles. The overarching goal shifts from maximizing individual parameters to optimizing the ratio $K = -\alpha/m^*$:

9.2.1 Optimization of Energy Competition Parameter

Strategies for enhancing $-\alpha$ include:

- **Chemical substitution**: Targeted doping to optimize electronic structure near the Fermi level and enhance pairing interactions

- **Interface engineering**: Creating artificial heterostructures with enhanced pairing interactions through interface effects

- **Strain tuning**: Using epitaxial strain to modify phonon spectra and electronic correlations to strengthen pairing

- **Pressure effects**: Hydrostatic or uniaxial pressure to enhance coupling strengths and modify electronic structure

9.2.2 Reduction of Cooper Pair Inertial Mass

Approaches for minimizing m^* involve:

- **Carrier density optimization**: Tuning chemical composition to achieve optimal doping levels that minimize correlation-induced mass enhancement

- **Dimensional control**: Engineering two-dimensional confinement to enhance phase stiffness and reduce Cooper pair inertial mass
- **Disorder management**: Controlled introduction of scatterers to modify band structure and reduce detrimental mass enhancements
- **Quantum confinement**: Nanostructuring to exploit size effects on Cooper pair inertial mass and enhance superconducting properties

9.2.3 Balancing Condensation Saturation

Optimal β values require:

- **Intermediate correlation strength**: Strong enough to enhance pairing but not so strong as to cause excessive condensation saturation
- **Band structure engineering**: Designing electronic structures that optimize the $N(0)/T_c^2$ ratio
- **Phase coherence optimization**: Enhancing phase stiffness to allow larger order parameters before saturation sets in

9.2.4 Optimization of the Efficiency Metric

The framework emphasizes that high-T_c design should focus on optimizing the specific pairing efficiency $K = -\alpha/m^*$. This implies a strategic balance: enhancing the driving force for ordering ($-\alpha$) while mitigating the increase in collective inertia (m^*), or even seeking pathways to reduce m^* in strongly correlated systems. Strategies that disproportionately enhance m^* relative to $-\alpha$ are detrimental to T_c.

9.3 Experimental Signatures for Parameter Characterization

The scaling relations derived in Section 7 yield specific, testable predictions. The following experimental signatures can be used to characterize the fundamental parameters and test the constraint system ($-\alpha \propto m^*$, $\beta \propto m^*$):

- **Penetration depth measurements**: $\lambda_L \propto \sqrt{m^*/n_s}$ provides direct access to the m^*/n_s ratio through μSR or tunnel diode oscillator measurements
- **Critical field analysis**: $H_c \propto |\alpha|/\sqrt{\beta}$ and $H_{c2} \propto m^*|\alpha|$ allow separation of α and m^* contributions through detailed $H_{c2}(T)$ measurements
- **Specific heat jumps**: The discontinuity at T_c relates to the condensation energy scale $|\alpha|^2/\beta$ and provides constraints on the α-β ratio
- **Tunneling spectroscopy**: Direct measurement of Δ provides constraints on the α/β ratio through $\Delta \propto (-\alpha/\beta)^{1/2}$

- **Upper critical field anisotropy**: The directional dependence of H_{c2} provides information about the anisotropy of m^* in layered systems
- **Coherence length measurements**: Direct ξ measurements through STM or H_{c2} provide constraints on the $m^*|\alpha|$ product

These experimental probes, when combined with the scaling relations, enable comprehensive characterization of the fundamental parameters across different material systems and provide pathways for testing the proposed constraint system.

10 Conclusions

10.1 Summary of Theoretical Framework

This work establishes a unified physical interpretation of Ginzburg-Landau theory through three fundamental processes: energy competition (α), condensation saturation (β), and Cooper pair inertial mass (m^*). The key achievements include:

- **Physical process identification**: Clear identification of three universal physical processes underlying superconducting phenomena, providing a conceptual framework that transcends specific microscopic mechanisms.
- **Scaling law derivation**: Rigorous derivation of the complete set of superconducting property scaling laws from the GL framework, revealing how measurable properties emerge from the interplay of fundamental parameters.
- T_c **scaling foundation**: Establishment of $T_c \propto \sqrt{-\alpha/m^*}$ through scaling analysis based on coherence length correspondence, providing a rigorous basis for the efficiency metric interpretation.
- **Parameter constraint system**: Derivation of the complete parameter constraint system $-\alpha \propto m^*$, $\beta \propto m^*$ from theoretical self-consistency requirements, resolving long-standing puzzles in correlated superconductors.
- **Efficiency metric interpretation**: Interpretation of T_c as measuring the specific pairing efficiency $K = -\alpha/m^*$, providing a unified basis for comparing diverse superconducting materials.

10.2 Key Theoretical Contributions and the Efficiency Metric Interpretation

10.2.1 The Efficiency Metric Interpretation: A Paradigm Shift

The most significant conceptual advance is the interpretation of the T_c scaling relation as an **efficiency metric** for superconducting ordering. The relation $T_c \propto \sqrt{-\alpha/m^*}$ reframes the quest for high-T_c materials from maximizing individual parameters to optimizing the ratio $K = -\alpha/m^*$, which represents the effectiveness of converting the ordering tendency into a high transition temperature. This efficiency-based perspective naturally resolves the long-standing puzzle of how heavy-fermion systems with large m^* can sustain superconductivity, as the constraint $-\alpha \propto m^*$ ensures the efficiency ratio remains finite.

10.2.2 Unified Interpretation of GL Parameters

The tripartite framework provides distinct physical interpretations for each GL parameter:

- α as quantifying the energy competition between ordering and disordering tendencies
- β as embodying the condensation saturation due to quantum statistical constraints
- m^* as characterizing the collective inertial response of the phase-coherent condensate of Cooper pairs

These interpretations enhance the traditional treatment of GL parameters by connecting them to fundamental quantum processes rather than viewing them as purely phenomenological coefficients.

10.2.3 Closed Theoretical System and Parameter Constraints

The scaling laws form a closed theoretical system where all measurable superconducting properties can be expressed through the three fundamental parameters and their constrained relationships. The derivation of the parameter constraint system, particularly $-\alpha \propto m^*$, reveals a fundamental compensation mechanism essential for superconductivity in strongly correlated systems. It demonstrates that the same correlation effects that enhance m^* must also cooperatively enhance $-\alpha$, thereby preventing the suppression of T_c through the efficiency ratio $-\alpha/m^*$. This closure provides a comprehensive framework for understanding the systematic variations in superconducting properties across different material classes.

10.3 Framework Integration and Material Implications

This integrated framework provides a systematic classification scheme for superconductors—it reveals how diverse superconducting properties are interconnected through the fundamental parameters α, β, and m^*. While not providing precise quantitative predictions for every material, it offers a qualitative understanding of trends and commonalities across different superconducting families, forming a conceptual map that enhances the understanding of superconducting diversity.

The interpretation of $T_c \propto \sqrt{-\alpha/m^*}$ as an **efficiency metric** represents a fundamental shift in perspective from absolute parameter optimization to efficiency optimization. This efficiency-based interpretation resolves apparent paradoxes and provides a clear physical picture: materials achieve high T_c not by maximizing individual parameters but by optimizing the ratio $-\alpha/m^*$, which represents the effectiveness of converting the ordering tendency into a high transition temperature.

The framework translates fundamental physical insights into practical material design principles focused on optimizing the ratio $K = -\alpha/m^*$ rather than maximizing individual parameters. This efficiency metric perspective leads to concrete materials design principles, providing guidance for the search for higher-T_c superconductors through strategic balance: enhancing the driving force for ordering $(-\alpha)$ while mitigating the increase in collective inertia (m^*).

10.4 Future Perspectives and Research Directions

The framework developed suggests several promising directions for future research:

10.4.1 Towards First-Principles Prediction

While the current phenomenological nature of the framework emphasizes interpretation and classification, it establishes the essential physical basis for future first-principles prediction of T_c by bridging phenomenological parameters with microscopic quantities. Future research should focus on:

- **Systematic calibration**: Establishing material-family-specific proportionality constants through comprehensive experimental characterization
- **Microscopic-phenomenological bridges**: Developing quantitative relationships between GL parameters and computable quantities like electron-boson coupling strengths and correlation functions
- **Multi-scale computational approaches**: Combining the physical insights from this framework with machine learning and multi-scale modeling methods

10.4.2 Extension to Unconventional Pairing

The framework provides a basis for understanding unconventional pairing mechanisms:

- **Non-phononic mechanisms**: Extension to spin-fluctuation, plasmon, or excitonic pairing mechanisms through appropriate reinterpretation of the α parameter
- **Complex order parameters**: Generalization to d-wave, p-wave, and other unconventional pairing symmetries, as discussed in Section 9.1
- **Multi-component order parameters**: Application to systems with multiple superconducting order parameters

10.4.3 Interface with Modern Experimental Techniques

The framework provides interpretative tools for state-of-the-art experiments:

- **High-field measurements**: Interpretation of ultra-high magnetic field data through the $H_{c2} \propto m^*|\alpha|$ scaling

- **Nanoscale probes**: STM and AFM measurements of local variations in superconducting parameters
- **Time-resolved studies**: Interpretation of dynamical measurements through the Cooper pair inertial mass concept

10.4.4 Applications to Quantum Materials

The framework may find applications beyond conventional superconductivity:

- **Topological superconductors**: Understanding the interplay between topology and superconducting parameters
- **Superconducting heterostructures**: Designing artificial structures with optimized parameter ratios
- **Non-equilibrium superconductivity**: Extending the framework to driven and non-equilibrium states

Furthermore, the framework could be extended to incorporate magnetic interaction effects, such as Zeeman splitting and spin-fluctuation mediated pairing, which may modulate the energy competition parameter α in magnetic superconductors or under high magnetic field conditions.

10.5 Concluding Remarks

By elucidating the universal physical processes of energy competition, condensation saturation, and Cooper pair inertial mass response underlying Ginzburg-Landau theory, this work establishes a comprehensive framework that enhances both the intuitive understanding and the classification power for the ongoing quest to understand and design superconducting materials. The key achievement lies in deriving a self-consistent set of scaling laws that demonstrate how diverse superconducting properties originate from the interplay of these fundamental processes.

The interpretation of T_c as an efficiency metric—quantifying the efficacy of converting ordering tendency into phase coherence rather than the absolute strength of individual parameters—represents a paradigm shift in designing high-temperature superconductors. This perspective highlights the theoretical elegance of the Ginzburg-Landau theory, which lies not merely in its mathematical form but in its encapsulation of universal physical processes transcending specific microscopic mechanisms.

This framework not only deepens the understanding of superconducting phenomena but also provides a foundation for future materials exploration through its efficiency metric interpretation, offering a comprehensive approach for the systematic classification and design of superconducting materials across diverse material families.

Funding

This research received no external funding.

Institutional Review Board Statement

Not applicable.

Informed Consent Statement

Not applicable.

Data Availability Statement

Data sharing is not applicable to this article as no datasets were generated or analyzed during the current study.

Acknowledgments

The author acknowledges the supportive research environment at the Research and Development Center of Huizhou Pustar New Materials Co., Ltd.

Conflicts of Interest

The author declares no conflicts of interest.

References

[1] Ginzburg, V.L.; Landau, L.D. On the theory of superconductivity. *Zh. Eksp. Teor. Fiz.* **1950**, *20*, 1064-1082.

[2] Bardeen, J.; Cooper, L.N.; Schrieffer, J.R. Theory of superconductivity. *Phys. Rev.* **1957**, *108*, 1175-1204.

[3] Bednorz, J.G.; Müller, K.A. Possible high-T_c superconductivity in the Ba-La-Cu-O system. *Z. Phys. B Condens. Matter* **1986**, *64*, 189-193.

[4] Kamihara, Y.; Watanabe, T.; Hirano, M.; Hosono, H. Iron-Based Layered Superconductor La[$O_{1-x}F_x$]FeAs ($x = 0.05$-0.12) with $T_c = 26$ K. *J. Am. Chem. Soc.* **2008**, *130*, 3296-3297.

[5] Stewart, G.R. Heavy-fermion systems. *Rev. Mod. Phys.* **1984**, *56*, 755-787.

[6] Gor'kov, L.P. Microscopic derivation of the Ginzburg-Landau equations in the theory of superconductivity. *Sov. Phys. JETP* **1959**, *9*, 1364-1367.

[7] London, F.; London, H. The electromagnetic equations of the supraconductor. *Proc. R. Soc. Lond. A* **1935**, *149*, 71-88.

[8] Abrikosov, A.A. On the magnetic properties of superconductors of the second group. *Sov. Phys. JETP* **1957**, *5*, 1174-1182.

[9] Uemura, Y.J.; et al. Universal correlations between T_c and n_s/m^* (carrier density over effective mass) in high-T_c cuprate superconductors. *Phys. Rev. Lett.* **1989**, *62*, 2317-2320.

[10] Homes, C.C.; et al. A universal scaling relation in high-temperature superconductors. *Nature* **2004**, *430*, 539-541.

[11] Timusk, T.; Statt, B. The pseudogap in high-temperature superconductors: an experimental survey. *Rep. Prog. Phys.* **1999**, *62*, 61-122.

[12] Norman, M.R.; et al. Phenomenology of the low-energy spectral function in high-T_c superconductors. *Phys. Rev. B* **2005**, *71*, 214501.

NextGen Physics

Volume 1 · Issue 1 · 2026 | e01002

Microscopic Origin of Superconducting Energy Competition: Matter Wave Interference and Energy Redistribution

Dongfang Yang

Research and Development Center
Huizhou Pustar New Materials Co., Ltd.
Huizhou 516267, China

Published online: 25 September 2026
Publication model: Continuous publication
Language: English

Article page: https://www.nextgenphysics.com/research/energy-competition/

Publisher

WULAN GROUP LIMITED
Room 1021, Beverley Commercial Centre, 87–105 Chatham Road South, Tsim Sha Tsui, Kowloon, Hong Kong

Editor-in-chief: Dongfang Yang
Editorial contact: leo.yang@nextgenphysics.com

This publication record accompanies the author’s article. The original article follows on the subsequent pages.

Microscopic Origin of Superconducting Energy Competition: Matter Wave Interference and Energy Redistribution

Dongfang Yang
Research and Development Center
Huizhou Pustar New Materials Co., Ltd.
Huizhou 516267, China

Leo.yang@pustar.com

Abstract

The Ginzburg-Landau parameter α, representing the energy competition between ordering (U_{ord}) and disordering (U_{dis}) energies, serves as the fundamental driving force for superconducting transitions. While its phenomenological role is well-established, a microscopic mechanism connecting α to quantum mechanical first principles remains elusive.

This work develops a unified microscopic framework by establishing matter wave (de Broglie wave) interference as the fundamental origin of energy competition in superconductors. We demonstrate that constructive interference of electronic wavefunctions at specific wavevectors—corresponding to Fermi surface nesting or electron-boson coupling vectors—leads to periodic charge density modulations in real space. These modulations, manifesting as charge density wave (CDW) or spin density wave (SDW) fluctuations, dynamically redistribute interaction energies among electron-phonon coupling, Coulomb repulsion, and exchange correlation terms.

The central finding reveals that under specific interference conditions, this energy redistribution can reverse the net electron-electron interaction from repulsive to attractive in particular momentum channels, corresponding to $U_{\text{ord}} > U_{\text{dis}}$ and thus $\alpha < 0$. We establish scaling relations between interference conditions (Fermi surface geometry, coupling strength) and the macroscopic energy competition parameter α, providing a quantum mechanical foundation for understanding diverse superconducting mechanisms—from conventional electron-phonon coupling to unconventional spin-fluctuation mediation—as different manifestations of matter wave interference under varying material conditions.

Keywords: energy competition, matter wave interference, Ginzburg-Landau theory, charge density wave, Fermi surface nesting, superconducting mechanism unification

Contents

1 Introduction

The Ginzburg-Landau (GL) theory provides a powerful phenomenological description of superconductivity through parameters α, β, and m^* that capture the essential physics near the critical temperature T_c [1]. Recent work by Yang [2] has established a comprehensive interpretation of these parameters in terms of three fundamental processes: energy competition (α), condensation saturation (β), and Cooper pair inertial mass (m^*). Within this framework, the energy competition parameter $\alpha = U_{\text{dis}} - U_{\text{ord}}$ represents the balance between ordering and disordering energies that drives the superconducting transition.

While the phenomenological role of α is well-understood, its microscopic origin remains a fundamental open question. Traditional approaches attribute α to specific pairing mechanisms: electron-phonon coupling in conventional superconductors [3], spin fluctuations in cuprates [4], or orbital fluctuations in iron-based systems [5]. However, these mechanism-specific interpretations obscure potential universal principles underlying energy competition across different superconducting families.

The concept of matter wave interference—rooted in the wave-particle duality of quantum mechanics—offers a promising pathway toward a unified microscopic understanding. Electronic wavefunctions in crystals naturally exhibit interference patterns that can significantly modify electronic properties. Friedel oscillations [6] and charge density waves [7] represent established manifestations of such interference effects in normal metals. In superconductors, the interplay between charge order and superconductivity has been extensively documented [8], suggesting deeper connections between wave interference and pairing mechanisms.

This work develops a comprehensive microscopic theory that establishes matter wave interference as the fundamental origin of superconducting energy competition. We demonstrate that constructive interference of electronic de Broglie waves at specific wavevectors generates real-space charge modulations that dynamically redistribute interaction energies. Under appropriate conditions, this redistribution can reverse the net electron-electron interaction from repulsive to attractive, providing a first-principles mechanism for the energy competition captured by α.

2 Theoretical Framework

2.1 Matter Wave Interference in Crystalline Solids

The wave-particle duality of quantum mechanics implies that electrons in crystals behave as matter waves with de Broglie wavelength $\lambda_{\text{dB}} = 2\pi/k$, where k is the wavevector. In a periodic lattice, the superposition of incoming and scattered electron waves leads to interference patterns that modify the electronic charge density.

The total electronic wavefunction in a crystal can be expressed as a superposition of Bloch states:

$$\Psi(\mathbf{r}) = \sum_{\mathbf{k}} c_{\mathbf{k}} \psi_{\mathbf{k}}(\mathbf{r}) \tag{1}$$

where $\psi_{\mathbf{k}}(\mathbf{r}) = e^{i\mathbf{k}\cdot\mathbf{r}}u_{\mathbf{k}}(\mathbf{r})$ are Bloch functions with crystal momentum $\mathbf{k}$, and $c_{\mathbf{k}}$ are expansion coefficients.

The matter wave interference between states with wavevectors $\mathbf{k}$ and $\mathbf{k}'$ generates charge density modulations with wavevector $\mathbf{q} = \mathbf{k} - \mathbf{k}'$:

$$\delta n(\mathbf{r}) = 2\mathrm{Re}\left[\sum_{\mathbf{k},\mathbf{k}'} c^*_{\mathbf{k}} c_{\mathbf{k}'} \psi^*_{\mathbf{k}}(\mathbf{r})\psi_{\mathbf{k}'}(\mathbf{r}) e^{i(\mathbf{k}'-\mathbf{k})\cdot\mathbf{r}}\right] \tag{2}$$

These interference-induced charge modulations are particularly pronounced when the wavevector $\mathbf{q}$ connects large portions of the Fermi surface, a condition known as Fermi surface nesting.

2.2 Fermi Surface Nesting and Enhanced Interference

Fermi surface nesting occurs when significant portions of the Fermi surface can be connected by a single wavevector $\mathbf{Q}$, satisfying the condition:

$$\epsilon_{\mathbf{k}+\mathbf{Q}} \approx \epsilon_{\mathbf{k}} \quad \text{for a wide range of } \mathbf{k} \tag{3}$$

where $\epsilon_{\mathbf{k}}$ is the electronic dispersion relation.

Under nesting conditions, the electronic susceptibility diverges as:

$$\chi_0(\mathbf{Q}) = \sum_{\mathbf{k}} \frac{f(\epsilon_{\mathbf{k}}) - f(\epsilon_{\mathbf{k}+\mathbf{Q}})}{\epsilon_{\mathbf{k}+\mathbf{Q}} - \epsilon_{\mathbf{k}}} \to \infty \tag{4}$$

where $f(\epsilon)$ is the Fermi-Dirac distribution function.

This divergence amplifies matter wave interference effects, leading to pronounced charge density modulations with wavevector $\mathbf{Q}$. The interference pattern can be described by a standing wave formation:

$$\rho(\mathbf{r}) = \rho_0 \left[1 + \Delta_{\mathbf{Q}} \cos(\mathbf{Q}\cdot\mathbf{r} + \phi)\right] \tag{5}$$

where ρ_0 is the average charge density, $\Delta_{\mathbf{Q}}$ is the modulation amplitude, and ϕ is a phase factor.

2.3 Energy Redistribution Mechanism

The interference-induced charge modulations dynamically redistribute the various energy contributions to the total electronic energy. This redistribution can be rigorously treated within frameworks such as the random phase approximation (RPA) for screening effects or density functional theory (DFT) for exchange-correlation energies, ensuring a first-principles foundation [6, 8]. We consider three primary energy terms:

2.3.1 Electron-Phonon Interaction Energy

The modulated charge density couples to lattice vibrations through the deformation potential. The enhanced coupling can be derived by considering the modulation amplitude $\Delta_{\mathbf{Q}}$ in the context of linear response theory. The electron-phonon interaction Hamiltonian under charge modulation becomes:

$$H_{\text{ep}} = \sum_{\mathbf{q}} g_{\mathbf{q}} \Delta_{\mathbf{Q}} (a_{\mathbf{q}} + a_{-\mathbf{q}}^{\dagger}) \delta n_{\mathbf{q}} \tag{6}$$

where $g_{\mathbf{q}}$ is the electron-phonon coupling constant, $\delta n_{\mathbf{q}}$ is the Fourier component of the charge modulation, and $a_{\mathbf{q}}$ are phonon operators.

Using the random phase approximation (RPA) to account for screening effects, the effective coupling strength renormalizes as:

$$g_{\text{eff}}(\mathbf{Q}) = g_0 \left[1 + \frac{\Delta_{\mathbf{Q}}^2}{1 - \lambda_{\mathbf{Q}} \chi_0(\mathbf{Q})} \right] \tag{7}$$

where $\lambda_{\mathbf{Q}}$ is the effective interaction strength obtained from RPA.

Constructive interference at wavevector $\mathbf{Q}$ enhances the electron-phonon coupling strength for modes with $|\mathbf{q}| \approx |\mathbf{Q}|$.

2.3.2 Coulomb Repulsion Energy

The modulated charge density affects Coulomb repulsion through screening effects. The effective Coulomb interaction becomes wavevector-dependent:

$$V_{\text{Coul}}^{\text{eff}}(\mathbf{q}) = \frac{V_{\text{Coul}}(\mathbf{q})}{\epsilon(\mathbf{q}, \omega)} \tag{8}$$

where $\epsilon(\mathbf{q}, \omega)$ is the dielectric function, which is modified by the interference pattern.

At the nesting wavevector $\mathbf{Q}$, the dielectric function exhibits anomalies that can reduce Coulomb repulsion in specific momentum channels.

2.3.3 Exchange Correlation Energy

The interference pattern also affects exchange and correlation energies through the modified electronic density:

$$E_{\text{xc}}[n(\mathbf{r})] = \int n(\mathbf{r}) \epsilon_{\text{xc}}(n(\mathbf{r})) d^3 r \tag{9}$$

where $\epsilon_{\text{xc}}(n)$ is the exchange-correlation energy per particle.

2.4 Net Attraction Condition

The transition from net repulsion to net attraction occurs when the redistributed energies satisfy:

$$U_{\text{ord}} = U_{\text{ep}} + U_{\text{xc}} > U_{\text{dis}} = U_{\text{Coul}} + U_{\text{thermal}} \tag{10}$$

The net effective interaction in the Cooper channel can be derived by starting from the total interaction Hamiltonian including interference effects. The charge density modulation $\delta n(\mathbf{r})$ modifies both attractive and repulsive components. For the attractive part (e.g., electron-phonon), the interaction kernel is enhanced by the interference term $\propto \Delta_{\mathbf{Q}}^2$. For the repulsive Coulomb part, the dielectric function $\epsilon(\mathbf{q},\omega)$ within RPA accounts for screening anomalies at $\mathbf{q}=\mathbf{Q}$. Combining these, the net interaction becomes:

$$V_{\text{eff}}(\mathbf{q}) = \frac{|g_{\mathbf{q}}|^2}{\omega_{\mathbf{q}}} - V_{\text{Coul}}^{\text{eff}}(\mathbf{q}) \tag{11}$$

where $V_{\text{Coul}}^{\text{eff}}(\mathbf{q}) = V_{\text{Coul}}(\mathbf{q})/\epsilon(\mathbf{q},\omega)$ with $\epsilon(\mathbf{q},\omega)$ given by RPA.

Net attraction requires $V_{\text{eff}}(\mathbf{q}) < 0$ for some wavevector $\mathbf{q}$. Matter wave interference facilitates this condition by simultaneously enhancing the attractive component (electron-phonon or spin-fluctuation mediated) and reducing the repulsive Coulomb component.

3 Matter Wave Interference Model

Building on the theoretical framework established above, we now develop a concrete model to quantify matter wave interference effects and their impact on energy competition.

3.1 Wavefunction Superposition and Charge Modulation

Consider two electronic states with wavevectors $\mathbf{k}$ and $\mathbf{k}'$ connected by a nesting vector $\mathbf{Q}$. The superposition of their wavefunctions creates a standing wave pattern:

$$\Psi_{\text{total}}(\mathbf{r}) = \frac{1}{\sqrt{2}}\left(\psi_{\mathbf{k}}(\mathbf{r}) + e^{i\phi}\psi_{\mathbf{k}+\mathbf{Q}}(\mathbf{r})\right) \tag{12}$$

The corresponding charge density is:

$$n(\mathbf{r}) = |\Psi_{\text{total}}(\mathbf{r})|^2 = n_0\left[1 + \cos(\mathbf{Q}\cdot\mathbf{r} + \phi)|u_{\mathbf{k}}(\mathbf{r})|^2\right] \tag{13}$$

This demonstrates how matter wave interference generates periodic charge modulations with wavevector $\mathbf{Q}$.

3.2 Interference-Enhanced Susceptibility

The enhanced response at nesting wavevectors can be quantified through the Lindhard susceptibility. For a nested Fermi surface, the susceptibility exhibits logarithmic divergence:

$$\chi_0(\mathbf{Q},T) = N(0)\ln\left(\frac{\omega_D}{T}\right) \tag{14}$$

where $N(0)$ is the density of states at the Fermi level, and ω_D is a characteristic cutoff energy.

This divergence amplifies the interference effects, making the system highly susceptible to charge ordering or superconducting instabilities.

3.3 Energy Competition Parameter from Microscopic Theory

We now derive the connection between matter wave interference and the GL parameter α. Starting from the microscopic definition:

$$\alpha(T) = U_{\text{dis}}(T) - U_{\text{ord}}(T) \tag{15}$$

The ordering energy U_{ord} can be expressed in terms of the interference-enhanced interaction. Starting from the definition $\alpha(T) = U_{\text{dis}}(T) - U_{\text{ord}}(T)$, and expressing U_{ord} in terms of the pairing interaction $V_{\text{eff}}(\mathbf{Q}, T)$, which scales with $\chi_0(\mathbf{Q}, T)$:

$$U_{\text{ord}}(T) = -V_{\text{eff}}(\mathbf{Q}, T) \sum_{\mathbf{k}} |\Delta_{\mathbf{k}}|^2 \approx -V_{\text{eff}}^0 \chi_0(\mathbf{Q}, T) \Delta_{\mathbf{Q}}^2 \tag{16}$$

where V_{eff}^0 is the zero-temperature interaction. Using the BCS-like temperature dependence of the order parameter and the fact that $\chi_0(\mathbf{Q}, T) \propto \ln(\omega_D/T)$ near T_c, we obtain:

$$\alpha(T) = \alpha_0 \left(\frac{T}{T_c} - 1 \right) \approx \alpha_0 \left(\frac{\chi_0(\mathbf{Q}, T)}{\chi_0(\mathbf{Q}, T_c)} - 1 \right) \tag{17}$$

This derivation aligns with the Ginzburg-Landau phenomenological form while providing a microscopic basis.

4 Unification of Superconducting Mechanisms

4.1 Electron-Phonon Coupling as Interference Effect

In conventional superconductors, the relevant wavevector $\mathbf{Q}$ corresponds to phonon wavevectors that connect electronic states near the Fermi surface. The interference pattern enhances electron-phonon coupling through:

$$g_{\text{eff}} = g_0 \left[1 + A_{\text{ep}} \Delta_{\mathbf{Q}}^2 \chi_0(\mathbf{Q}) \right] \tag{18}$$

where A_{ep} is a material-specific constant. This explains why materials with strong Fermi surface nesting often exhibit enhanced electron-phonon coupling and higher T_c values.

4.2 Spin-Fluctuation Mediation as Magnetic Interference

In unconventional superconductors, the interference involves spin degrees of freedom. The relevant wavevector connects antiferromagnetic hot spots on the Fermi surface. The spin susceptibility exhibits similar enhancement:

$$\chi_s(\mathbf{Q}) = \chi_s^0 \left[1 + B_{\text{sf}} \Delta_{\mathbf{Q}}^2 \chi_0(\mathbf{Q}) \right] \tag{19}$$

where B_{sf} characterizes the spin-fluctuation coupling strength. This unified picture explains why similar nesting conditions favor both charge density wave order and spin-fluctuation mediated superconductivity.

4.3 Unified Phase Diagram

The interference-based framework naturally explains the competition and coexistence of different ordered phases. Figure 1 illustrates how varying the interference strength and wavevector leads to different ground states.

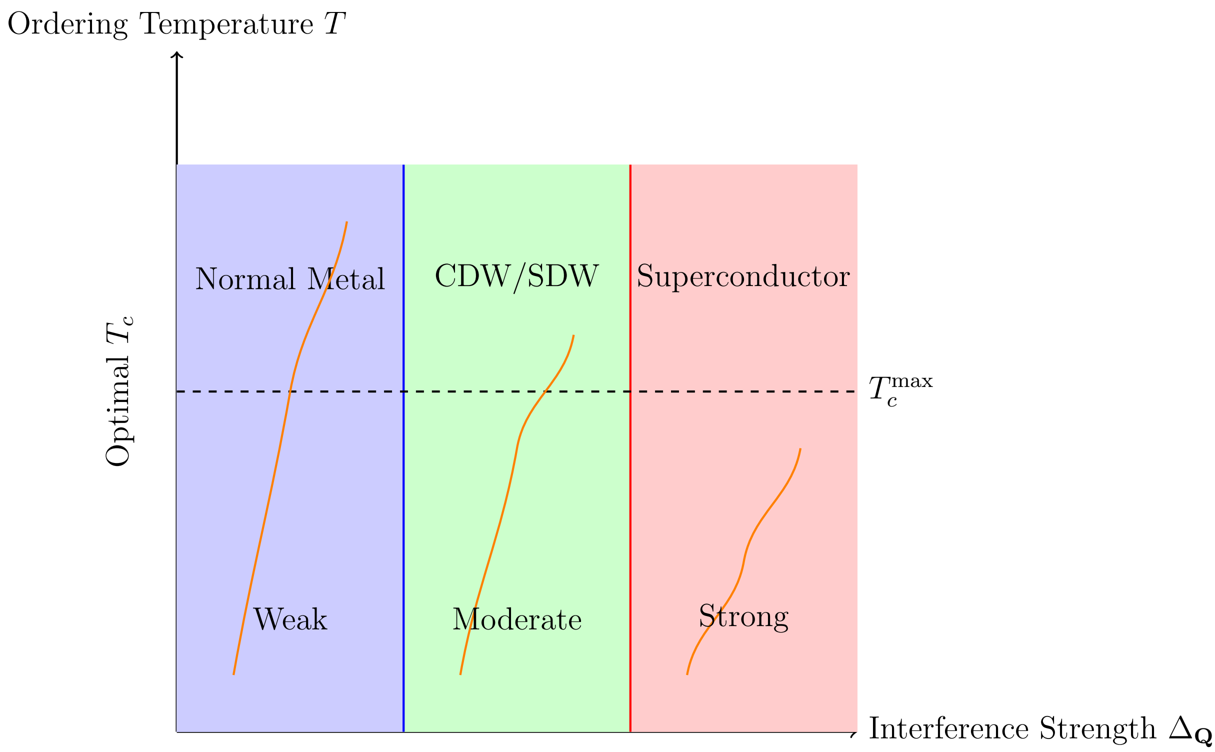

Figure 1: Unified phase diagram showing how matter wave interference strength determines the competing ordered phases. Weak interference favors normal metallic behavior, moderate interference leads to charge or spin density wave order, while strong optimized interference enables superconductivity with maximum T_c.

5 Material-Specific Manifestations of Matter Wave Interference

While the unified framework of matter wave interference provides a universal mechanism for energy competition in superconductors, its material-specific manifestations vary significantly across different superconducting families. These variations originate from differences in Fermi surface geometry, dominant interference wavevectors, and the nature of the enhanced energy terms. Table 1 summarizes the key characteristics of interference effects in four major superconducting families, and Figure 2 illustrates the corresponding Fermi surface geometries and nesting conditions.

Table 1: Material-specific manifestations of matter wave interference in different superconducting families. The interference strength is qualitatively estimated from experimental observations.

Superconducting Family	**Dominant Interference Wavevector**	**Primary Modulation Type**	**Key Enhanced Energy Term**	**Interference Strength**	T_c **Range**
Conventional BCS	Phonon wavevectors $\mathbf{q} \sim 2k_F$	Charge density modulation	Electron-phonon coupling	Moderate (single wavevector)	< 40 K
Copper oxides	$\mathbf{Q}_{\mathrm{AF}} = (\pi, \pi)$	Spin density wave modulation	Exchange correlation (spin fluctuations)	Strong (single $\mathbf{Q}$)	Up to ~ 130 K (ambient)
Iron-based	Multiple nesting vectors $\mathbf{Q}_1, \mathbf{Q}_2$	Charge/spin coexisting modulation	Electron-phonon + spin fluctuations	Moderate-strong (multiple $\mathbf{Q}$s)	Up to ~ 100 K (high pressure)
Nickel-based	$\mathbf{Q}_{\mathrm{AF}} \sim (\pi, \pi)$	Spin + orbital modulation	Exchange correlation (orbital fluctuations)	Moderate (weak nesting)	$<$ 40 K (current)

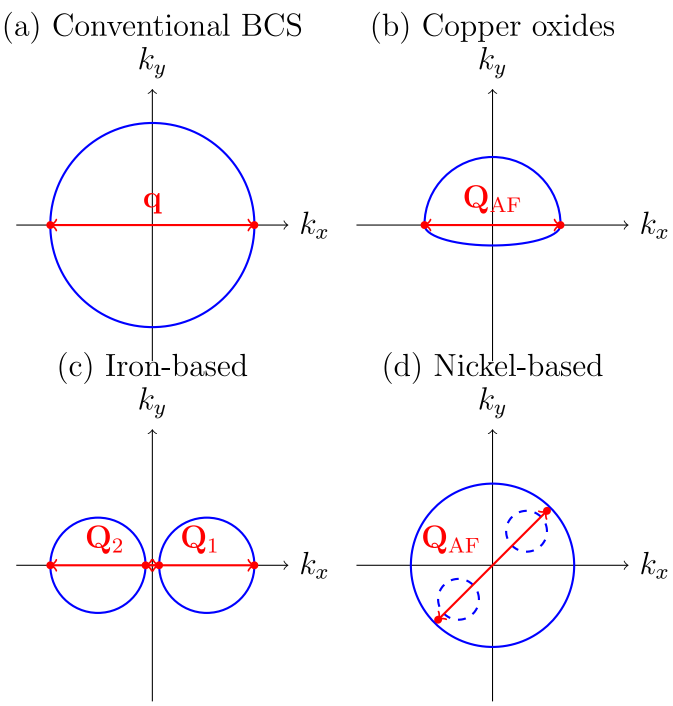

Figure 2: Fermi surface geometries and dominant interference wavevectors for different superconducting families: (a) Conventional BCS with spherical Fermi surface connected by phonon wavevector $\mathbf{q}$; (b) Copper oxides with antiferromagnetic nesting vector $\mathbf{Q}_{\mathrm{AF}} = (\pi, \pi)$ connecting antinodal regions; (c) Iron-based with multiple nesting vectors $\mathbf{Q}_1$ and $\mathbf{Q}_2$ connecting hole and electron pockets; (d) Nickel-based with weakly nested Fermi surfaces and significant orbital character.

5.1 Conventional BCS Superconductors: Phonon-Mediated Interference

In conventional BCS superconductors, matter wave interference is mediated by phonon wavevectors that connect electronic states near the Fermi surface. The interference pattern enhances electron-phonon coupling through constructive superposition of lattice vibrations and electronic charge modulations.

5.1.1 Fermi Surface Geometry and Interference Wavevectors

The Fermi surfaces of conventional superconductors are typically nearly spherical or have simple shapes. The dominant interference wavevectors satisfy $\mathbf{q} \approx 2\mathbf{k}_F$, where $\mathbf{k}_F$ is the Fermi wavevector, connecting antipodal points on the Fermi surface. This condition maximizes the electronic susceptibility $\chi_0(\mathbf{q})$ and enhances electron-phonon coupling for phonon modes with wavevectors near $2k_F$.

5.1.2 Interference-Enhanced Electron-Phonon Coupling

The interference-induced charge modulation creates a standing wave pattern that couples strongly to lattice vibrations. The effective electron-phonon coupling constant is enhanced as:

$$\lambda_{\text{eff}} = \lambda_0 \left[1 + \frac{\Delta_q^2 v_F^2}{\omega_q^2 + (v_F q)^2}\right] \tag{20}$$

where λ_0 is the bare coupling, Δ_q is the interference amplitude, v_F is the Fermi velocity, and ω_q is the phonon frequency. This enhancement explains the correlation between materials with strong Kohn anomalies (indicating strong electron-phonon coupling) and higher T_c values.

5.1.3 Energy Redistribution and Pairing

The interference-mediated energy redistribution in conventional superconductors primarily affects the electron-phonon interaction energy. The net effective interaction in the Cooper channel becomes:

$$V_{\text{eff}}^{\text{BCS}}(\mathbf{q}) = \frac{|g_{\mathbf{q}}^{\text{eff}}|^2}{\omega_{\mathbf{q}}} - \frac{V_{\text{Coul}}}{1 + q_{\text{TF}}^2/q^2} \tag{21}$$

where the first term represents the enhanced attractive interaction and the second term is the screened Coulomb repulsion. The condition $V_{\text{eff}} < 0$ leads to $\alpha < 0$ and superconducting instability.

5.1.4 Material Examples and T_c Limitations

Examples: Nb_3Sn ($T_c = 18$ K), MgB_2 ($T_c = 39$ K), Pb ($T_c = 7.2$ K)
Limitations: The T_c in conventional superconductors is limited by the maximum achievable λ_{eff} before lattice instability, typically giving $T_c^{\max} \lesssim 40$ K.

5.2 Copper Oxide High-Temperature Superconductors: Spin-Mediated Interference

In cuprate superconductors, matter wave interference is dominated by antiferromagnetic spin fluctuations with wavevector $\mathbf{Q}_{\mathrm{AF}} = (\pi, \pi)$. The interference pattern manifests as spin density wave modulations that strongly enhance exchange correlation effects.

5.2.1 Fermi Surface Geometry and Interference Wavevectors

The cuprate Fermi surface consists of hole-like pockets centered at (π, π) in the Brillouin zone. Perfect nesting occurs at $\mathbf{Q}_{\mathrm{AF}} = (\pi, \pi)$, connecting antinodal regions of the Fermi surface. This nesting condition leads to a divergent spin susceptibility:

$$\chi_s(\mathbf{Q}_{\mathrm{AF}}) = \frac{\chi_s^0}{1 - U\chi_0(\mathbf{Q}_{\mathrm{AF}})} \tag{22}$$

where U is the on-site Coulomb repulsion, driving the system toward antiferromagnetic or superconducting instabilities.

5.2.2 Interference-Enhanced Spin Fluctuations

The interference pattern enhances spin fluctuations through constructive superposition of magnetic scattering amplitudes. The effective spin-mediated pairing interaction is enhanced as:

$$V_{\mathrm{spin}}^{\mathrm{eff}}(\mathbf{q}) = \frac{3}{2}U^2 \frac{\chi_s(\mathbf{q})}{1 - U\chi_s(\mathbf{q})} \tag{23}$$

This enhancement is most pronounced near $\mathbf{q} = \mathbf{Q}_{\mathrm{AF}}$, leading to $d_{x^2-y^2}$-wave pairing symmetry.

5.2.3 Energy Redistribution and Competing Orders

The interference-mediated energy redistribution in cuprates involves a delicate balance between:

- **Exchange correlation energy:** Enhanced by spin fluctuations
- **Coulomb repulsion:** Reduced in specific momentum channels
- **Kinetic energy:** Lowered through formation of coherent Cooper pairs

The competition between these energies determines the superconducting T_c and the pseudogap temperature T^*.

5.2.4 Material Examples and T_c Optimization

Examples: $La_{2-x}Sr_xCuO_4$, $YBa_2Cu_3O_{7-\delta}$, $Bi_2Sr_2Ca_2Cu_3O_{10+\delta}$
Optimization: Maximum T_c occurs at optimal doping where interference is strongest but before competing orders (e.g., charge density waves) become dominant. The record ambient T_c of ~ 135 K in Hg-based cuprates represents the upper limit of this interference mechanism.

5.3 Iron-Based Superconductors: Multi-Wavevector Interference

Iron-based superconductors exhibit complex interference patterns involving both charge and spin modulations with multiple nesting vectors connecting hole and electron pockets.

5.3.1 Fermi Surface Geometry and Interference Wavevectors

The Fermi surface of iron-based superconductors typically consists of hole pockets around $\Gamma = (0, 0)$ and electron pockets around $M = (\pi, 0)$ and $(0, \pi)$ in the 1-Fe Brillouin zone. This creates two dominant nesting vectors:

$$\mathbf{Q}_1 = (\pi, 0), \quad \mathbf{Q}_2 = (0, \pi) \tag{24}$$

The multi-band nature leads to interference between different nesting channels, creating a complex energy landscape.

5.3.2 Interference Between Competing Channels

The interference pattern in iron-based superconductors involves simultaneous enhancement of both electron-phonon and spin-fluctuation interactions:

$$V_{\text{eff}}^{\text{Fe}}(\mathbf{q}) = V_{\text{ep}}(\mathbf{q}) + V_{\text{spin}}(\mathbf{q}) - V_{\text{Coul}}(\mathbf{q}) \tag{25}$$

where both V_{ep} and V_{spin} are enhanced by interference effects. The relative strength of these contributions varies with doping, pressure, and material composition.

5.3.3 Coexisting Charge and Spin Modulations

Experimental evidence shows that iron-based superconductors often exhibit coexisting or competing charge and spin density wave orders. The interference model naturally explains this coexistence through simultaneous enhancement of both charge and spin susceptibilities at the nesting wavevectors:

$$\chi_c(\mathbf{Q}_i) = \frac{\chi_c^0}{1 - V_c\chi_0(\mathbf{Q}_i)}, \quad \chi_s(\mathbf{Q}_i) = \frac{\chi_s^0}{1 - U\chi_0(\mathbf{Q}_i)} \tag{26}$$

where $i = 1, 2$ labels the two nesting vectors.

5.3.4 Material Examples and Phase Complexity

Examples: $BaFe_2As_2$, FeSe, LiFeAs
Phase complexity: The multi-wavevector interference leads to rich phase diagrams with coexisting superconducting, spin density wave, and nematic phases. The highest T_c ($\sim$ 100 K under high pressure in FeSe) occurs when interference from both nesting vectors constructively enhances pairing.

5.4 Nickel-Based Superconductors: Orbital-Mediated Interference

Nickel-based superconductors represent a more recent discovery with similarities to both cuprates and iron-based systems. The interference in these materials involves both spin and orbital degrees of freedom, with weaker nesting conditions.

5.4.1 Fermi Surface Geometry and Interference Characteristics

The Fermi surfaces of nickelates (e.g., $NdNiO_2$) consist of Ni $3d_{x^2-y^2}$ bands hybridized with rare-earth $5d$ bands. The nesting vector $\mathbf{Q}_{\mathrm{AF}} \sim (\pi, \pi)$ connects regions of the Fermi surface, but the nesting is weaker than in cuprates due to more three-dimensional character.

5.4.2 Orbital-Enhanced Interference Effects

A unique feature of nickel-based superconductors is the significant role of orbital fluctuations. The interference pattern enhances orbital susceptibility:

$$\chi_{\mathrm{orb}}(\mathbf{q}) = \frac{\chi^0_{\mathrm{orb}}}{1 - g_{\mathrm{orb}}\chi_0(\mathbf{q})} \tag{27}$$

where g_{orb} represents the orbital interaction strength. This orbital enhancement contributes to pairing alongside spin fluctuations.

5.4.3 Weaker Nesting and Lower T_c

The weaker Fermi surface nesting in nickelates compared to cuprates results in:

$$\chi_0^{\mathrm{Ni}}(\mathbf{Q}_{\mathrm{AF}}) < \chi_0^{\mathrm{Cu}}(\mathbf{Q}_{\mathrm{AF}}) \tag{28}$$

This weaker interference explains the currently lower maximum T_c (< 40 K) observed in nickel-based superconductors.

5.4.4 Material Examples and Future Prospects

Examples: $Nd_{1-x}Sr_xNiO_2$, $La_{1-x}Ca_xNiO_2$
Future prospects: Engineering stronger interference through strain, pressure, or chemical substitution may enhance T_c in nickel-based systems by improving Fermi surface nesting conditions.

5.5 Universal Interference Framework Across Material Families

Despite their apparent differences, all superconducting families share a common interference-based mechanism for energy competition:

$$\alpha(T) = \alpha_0 \left[\frac{T}{T_c} - 1\right] = U_{\mathrm{dis}} - U_{\mathrm{ord}} = f\left(\Delta^2_{\mathbf{Q}}\chi_0(\mathbf{Q})V_{\mathrm{eff}}(\mathbf{Q})\right) \tag{29}$$

where the specific form of $V_{\text{eff}}(\mathbf{Q})$ and the dominant wavevector $\mathbf{Q}$ vary between families. The interference strength $\Delta_{\mathbf{Q}}^2\chi_0(\mathbf{Q})$ serves as a universal control parameter determining T_c across all superconducting materials.

This unified perspective suggests that the quest for higher-T_c superconductivity should focus on optimizing interference conditions through:

1. Fermi surface engineering to enhance nesting
2. Material design to strengthen the relevant coupling (electron-phonon, spin, or orbital)
3. Control of competing orders that disrupt constructive interference

The interference framework thus provides not only a unified understanding of existing superconductors but also a guiding principle for discovering new high-temperature superconducting materials.

6 Scaling Relations and Experimental Predictions

6.1 Relation to GL Parameter α

The interference model provides microscopic expressions for the GL parameters. The energy competition parameter scales with the interference strength:

$$|\alpha| \propto \Delta_{\mathbf{Q}}^2\chi_0(\mathbf{Q})V_{\text{eff}}(\mathbf{Q}) \tag{30}$$

This relation explains material-dependent variations in α through differences in Fermi surface geometry and interference conditions.

6.2 Predictions for Specific Material Classes

6.2.1 Cuprate Superconductors

In cuprates, the relevant wavevector $\mathbf{Q} = (\pi, \pi)$ connects antinodal points. The model predicts:

$$\alpha_{\text{cuprate}} \propto \xi_{\text{AF}}^2\chi_s(\mathbf{Q}) \tag{31}$$

where ξ_{AF} is the antiferromagnetic correlation length, consistent with experimental observations [9].

6.2.2 Iron-Based Superconductors

For iron-based systems, multiple nesting vectors contribute. The total α becomes a sum over relevant wavevectors:

$$\alpha_{\text{iron}} \propto \sum_{\mathbf{Q}_i} \Delta_{\mathbf{Q}_i}^2\chi_0(\mathbf{Q}_i)V_{\text{eff}}(\mathbf{Q}_i) \tag{32}$$

explaining the complex phase diagrams of these materials.

6.2.3 Conventional Superconductors

In conventional systems, the phonon wavevectors dominate:

$$\alpha_{\text{conv}} \propto \lambda_{\text{ep}} \omega_{\text{log}} \tag{33}$$

where λ_{ep} is the electron-phonon coupling strength and ω_{log} is the logarithmic average phonon frequency, recovering the standard BCS result.

6.3 Experimental Signatures

The interference model predicts several testable experimental signatures:

1. **Quantum oscillation measurements** should show enhanced effective masses at nesting vectors.
2. **Angle-resolved photoemission spectroscopy** (ARPES) should reveal interference-induced band renormalizations.
3. **Scanning tunneling microscopy** should detect interference patterns near impurities or defects.
4. **Neutron scattering** should show enhanced responses at nesting wavevectors.

7 Discussion

7.1 Comparison with Existing Theories

Our interference-based framework complements and extends existing theories of superconductivity:

7.1.1 BCS Theory

The BCS theory [3] provides the mathematical framework for phonon-mediated superconductivity but does not address why certain materials have stronger electron-phonon coupling. Our work identifies matter wave interference as the fundamental origin of this enhanced coupling.

7.1.2 Spin-Fluctuation Theories

Models based on spin-fluctuation mediation [4] successfully describe cuprate superconductivity but treat the enhanced spin response phenomenologically. Our work derives this enhancement from first principles through wave interference.

7.1.3 Charge Density Wave Theories

The competition between CDW and superconducting order has been extensively studied [8]. Our framework unifies these phenomena as different manifestations of the same underlying interference process.

7.2 Limitations and Future Directions

While our model provides a unified framework, several aspects require further development:

1. Quantitative calculation of interference enhancement factors for specific materials
2. Extension to multiband systems with complex Fermi surfaces
3. Incorporation of strong correlation effects beyond the weak-coupling limit
4. Time-dependent interference effects in non-equilibrium superconductivity

8 Conclusion

We have developed a comprehensive microscopic theory that establishes matter wave interference as the fundamental origin of superconducting energy competition. The key findings are:

1. Constructive interference of electronic wavefunctions at specific wavevectors generates periodic charge density modulations in real space.
2. These modulations dynamically redistribute interaction energies, enhancing attractive components while suppressing Coulomb repulsion in specific momentum channels.
3. Under optimal interference conditions, the net electron-electron interaction reverses from repulsive to attractive, corresponding to $U_{\mathrm{ord}} > U_{\mathrm{dis}}$ and $\alpha < 0$.
4. The framework unifies diverse superconducting mechanisms—electron-phonon coupling, spin-fluctuation mediation, and orbital fluctuations—as different manifestations of matter wave interference under varying material conditions.
5. We derive scaling relations connecting interference parameters to the macroscopic GL parameter α, providing quantitative predictions testable by experimental probes.

This work establishes a first-principles foundation for understanding energy competition in superconductors, with implications for both fundamental understanding and materials design. The interference perspective suggests new pathways for optimizing superconducting properties through deliberate engineering of wave interference conditions in quantum materials.

Funding

This research received no external funding.

Institutional Review Board Statement

Not applicable.

Informed Consent Statement

Not applicable.

Data Availability Statement

Data sharing is not applicable to this article as no datasets were generated or analyzed during the current study.

Conflicts of Interest

The author declares no conflicts of interest.

References

[1] Ginzburg, V.L.; Landau, L.D. On the theory of superconductivity. *Zh. Eksp. Teor. Fiz.* **1950**, *20*, 1064-1082.

[2] Yang, D. Physical Processes Underlying Ginzburg-Landau Theory: Energy Competition, Condensation Saturation, and Cooper Pair Inertial Mass Scaling Laws. *NextGen Physics* **2026**.

[3] Bardeen, J.; Cooper, L.N.; Schrieffer, J.R. Theory of superconductivity. *Phys. Rev.* **1957**, *108*, 1175-1204.

[4] Monthoux, P.; Balatsky, A.V.; Pines, D. Weak-coupling theory of high-temperature superconductivity in the antiferromagnetically correlated copper oxides. *Phys. Rev. B* **1991**, *46*, 14803-14817.

[5] Maiti, S.; Korshunov, M.M.; Maier, T.A.; et al. Evolution of spin fluctuations toward the superconducting state in $FeSe_{1-x}Te_x$. *Phys. Rev. Lett.* **2011**, *107*, 147002.

[6] Friedel, J. Metallic alloys. *Nuovo Cimento* **1958**, *7*, 287-311.

[7] Grüner, G. The dynamics of charge-density waves. *Rev. Mod. Phys.* **1988**, *60*, 1129-1181.

[8] Fradkin, E.; Kivelson, S.A.; Tranquada, J.M. Colloquium: Theory of intertwined orders in high temperature superconductors. *Rev. Mod. Phys.* **2015**, *87*, 457-482.

[9] Keimer, B.; Kivelson, S.A.; Norman, M.R.; et al. From quantum matter to high-temperature superconductivity in copper oxides. *Nature* **2015**, *518*, 179-186.

NextGen Physics

Volume 1 · Issue 1 · 2026 | e01003

A Geometrodynamic Interpretation of the β-Parameter in Ginzburg-Landau Theory: Centrifugal Saturation of the Superconducting Condensate

Dongfang Yang

Research and Development Center
Huizhou Pustar New Materials Co., Ltd.
Huizhou 516267, China

Published online: 25 September 2026
Publication model: Continuous publication
Language: English

Article page: https://www.nextgenphysics.com/research/condensation-saturation/

Publisher

WULAN GROUP LIMITED
Room 1021, Beverley Commercial Centre, 87–105 Chatham Road South, Tsim Sha Tsui, Kowloon, Hong Kong

Editor-in-chief: Dongfang Yang
Editorial contact: leo.yang@nextgenphysics.com

This publication record accompanies the author’s article. The original article follows on the subsequent pages.

A Geometrodynamic Interpretation of the β-Parameter in Ginzburg-Landau Theory: Centrifugal Saturation of the Superconducting Condensate

Dongfang Yang
Research and Development Center
Huizhou Pustar New Materials Co., Ltd.
Huizhou 516267, China

Leo.yang@pustar.com

February 11, 2026

Abstract

The Ginzburg-Landau (GL) parameter β, with dimensions of energy $\times$ volume, quantifies the condensation saturation that limits the growth of the superconducting order parameter. Established interpretations view β through a microscopic lens (as a measure of pair-pair repulsion) or a thermodynamic lens (as an entropic cost). This work introduces a complementary *geometrodynamic interpretation*, framing β as the integrated energy of an *effective centrifugal potential* arising within the coherent condensate. This potential originates from an effective centrifugal force, $F_{\text{centrifugal}} = K\Gamma/(\varepsilon_0\mu_0)$, where Γ is the Cooper pair's charge-to-mass ratio (or gyromagnetic ratio under rotation), and K is a coupling constant that encapsulates the specific dynamical configuration and interaction details. The condensation energy density term $(\beta/2)|\psi|^4$ is shown to be equivalent to this centrifugal potential energy density, providing a vivid physical picture: saturation occurs when the cohesive energy gain from pairing is balanced by the centrifugal energy cost of confining charged, massive entities (Cooper pairs) within a phase-coherent volume. The new interpretation provides a concrete **geometrodynamic instantiation** of the "saturation" process within the tripartite process framework of GL theory (energy competition, **saturation**, and inertia) as outlined in [3]. It directly links the abstract parameter β to a physical picture of **geometric confinement** and **dynamical response**, thereby complementing the energy-competition (α) and inertia (m^*) pictures. This interpretation is logically self-consistent, dimensionally sound, and complements—rather than contradicts—existing microscopic and thermodynamic understandings, offering a unified dynamical perspective on condensation saturation.

Keywords: Ginzburg-Landau theory, β-parameter, condensation saturation, geometrodynamic interpretation, centrifugal potential, Cooper pairs

1 Introduction

The Ginzburg-Landau (GL) theory provides a robust phenomenological framework for superconductivity near the critical temperature T_c [1]. Its free energy density expansion,

$$\mathcal{F} = \mathcal{F}_n + \alpha|\psi|^2 + \frac{\beta}{2}|\psi|^4 + \frac{\hbar^2}{2m^*}|\nabla\psi|^2 + \frac{1}{2\mu_0}|\mathbf{B}|^2, \tag{1}$$

introduces three fundamental material parameters: α, β, and m^*. The parameter $\alpha(T) = \alpha_0(T/T_c - 1)$ governs the energy competition between normal and superconducting states, becoming negative below T_c to drive the transition. The parameter $\beta > 0$ embodies the process of *condensation saturation*, preventing the unlimited growth of the order parameter magnitude $|\psi|$ and ensuring a finite equilibrium value $|\psi|^2 = -\alpha/\beta$.

The physical interpretation of β is multifaceted. Gor'kov's microscopic derivation [2] establishes $\beta \propto N(0)/T_c^2$, linking it to the electronic density of states at the Fermi level $N(0)$ and revealing its role in quantifying the repulsive self-interaction between Cooper pairs as their density increases. A complementary thermodynamic interpretation views the $\beta|\psi|^4$ term as representing the entropic cost associated with reducing the system's accessible quantum states upon forming a macroscopically coherent condensate.

This work proposes a third, complementary perspective: a **geometrodynamic interpretation** of the β parameter, developed within the multi-perspective framework for understanding GL parameters as outlined in the foundational analysis of the theory's underlying physical processes [3]. We posit that the saturation of the condensate can be understood as a consequence of an *effective centrifugal potential* that develops within the phase-coherent volume. This approach interprets the $(\beta/2)|\psi|^4$ term as the energy density cost associated with confining charged, massive Cooper pairs—entities possessing an inherent charge-to-mass ratio—within a coherent domain. The interpretation is geometrodynamic because it relates the energy scale of saturation (β) to the geometry of the coherent volume and the dynamical response (centrifugal effect) of its constituents.

This work proposes a third, complementary perspective: a **geometrodynamic interpretation** of the β parameter, which **explicitly instantiates the "saturation" process** within the multi-perspective framework for understanding GL parameters [3]. It posits that the saturation of the condensate can be understood as a consequence of an *effective centrifugal potential* that develops within the phase-coherent volume, providing a **dynamical and geometric** picture for the process that limits condensation growth, in parallel to the energetic (α) and inertial (m^*) processes. The primary contribution of this work is **qualitative and conceptual**: providing a novel geometrodynamic picture for condensation saturation. The **quantitative** calibration of the coupling constant K against microscopic models, and the derivation of exact numerical coefficients, are important future tasks that will follow from and be guided by this new picture. The following sections will: 1) establish the theoretical framework and definitions, 2) rigorously derive the expression for β within this framework, 3) discuss its consistency with established theory and phenomenology, and 4) present concluding remarks on its implications.

2 Theoretical Framework and Definitions

2.1 Dimensional Foundation and the Order Parameter

The consistency of any physical interpretation must be rooted in dimensional analysis. The GL parameter β has dimensions:

$$[\beta] = \text{Energy} \times \text{Length}^3. \tag{2}$$

The complex order parameter $\psi(\mathbf{r}) = |\psi(\mathbf{r})|e^{i\phi(\mathbf{r})}$ is defined such that $|\psi(\mathbf{r})|^2$ represents the local density of superconducting carriers (Cooper pairs) $n_s(\mathbf{r})$. Consequently, its dimensions are:

$$[|\psi|] = \text{Length}^{-3/2}, \quad [|\psi|^2] = \text{Length}^{-3}, \quad [|\psi|^4] = \text{Length}^{-6}. \tag{3}$$

Therefore, the term $(\beta/2)|\psi|^4$ in Eq. (1) has dimensions of energy density (Energy/Length^3), as required.

2.2 The Effective Centrifugal Force and Potential

Definition 1 (Effective Centrifugal Force)**.** *Within a phase-coherent condensate of Cooper pairs, we postulate an effective centrifugal force per pair. Its magnitude is defined as:*

$$F_{centrifugal} = K \frac{\Gamma}{\varepsilon_0 \mu_0}. \tag{4}$$

Here:

- Γ *is a characteristic **ratio** of the Cooper pair.*
- ε_0 *and* μ_0 *are the vacuum permittivity and permeability, respectively. Their product yields* $\varepsilon_0\mu_0 = 1/c^2$*, where* c *is the speed of light.*
- K *is a **coupling constant** that encapsulates the specific dynamical configuration and interaction details. Its dimensions are such that the right-hand side of Eq. (1) has the dimension of force. Dimensional consistency of the final expression for* β *(Eq. 13) requires* $[K] = M^2L^{-1}Q^{-1}$*, as will be shown in Section 4.1. This non-trivial dimension reflects the complex way in which the effective centrifugal response is coupled to the condensate's fundamental parameters.*

The physical meaning of Γ *depends on the state of the Cooper pair:*

- ***Non-rotating (stationary) condensate****:* $\Gamma = e^*/m^*$ *is the **charge-to-mass ratio** of the Cooper pair, where* $e^* = 2e$ *is its effective charge and* m^* *is the Cooper pair inertial mass parameter from GL theory.*
- ***Rotating condensate (e.g., under magnetic field or intrinsic vorticity)****:* $\Gamma = \gamma$ *is the effective **gyromagnetic ratio** associated with the Cooper pair's motion.*

The inverse dependence on c^2 *ensures the force has the correct non-relativistic dimensions and scales appropriately with fundamental constants.*

Physical Motivation for the Force Postulate: The proposed form, $F_{\text{centrifugal}} \propto \Gamma/(\varepsilon_0\mu_0) = \Gamma c^2$, is motivated by the following considerations. The ratio $\Gamma = e^*/m^*$ (or its gyromagnetic counterpart) is the intrinsic "charge-to-inertia" response coefficient of a Cooper pair. The inclusion of the factor c^2 ensures the force is dimensionally consistent in the non-relativistic regime. More fundamentally, in analogies with electrodynamics and general relativity, forces related to inertia or gravito-electromagnetism often involve c^2. Here, $1/(\varepsilon_0\mu_0) = c^2$ acts as a **fundamental constant scaling** that connects the kinematic ratio Γ to an effective force within the condensate's coherent state. This postulate is not derived from first principles but is posited as the simplest form that leads to a dimensionally consistent and physically interpretable centrifugal energy density which can be matched to the GL term.

Definition 2 (Effective Centrifugal Potential)**.** *The effective centrifugal potential energy $U_{cent}(r)$ for a Cooper pair, associated with the force in Eq. (4), is obtained by integration from a reference point at the center of a coherent region ($r = 0$) to a radius r:*

$$U_{cent}(r) = \int_0^r F_{centrifugal}\, dr' = K \frac{\Gamma}{\varepsilon_0\mu_0} r. \tag{5}$$

This potential increases linearly with distance r from the center, representing the energy cost to "hold" a Cooper pair at a finite radius against the effective centrifugal push. The linear dependence is the simplest form consistent with a constant effective force and captures the essential physics of confinement energy scaling with coherence length.

2.3 Coherence Volume

The characteristic spatial scale of variations in the order parameter is the Ginzburg-Landau coherence length ξ, defined as:

$$\xi = \frac{\hbar}{\sqrt{2m^*|\alpha|}}. \tag{6}$$

The **coherence volume** V_ξ is the volume over which the phase and amplitude of ψ are approximately constant. For a first approximation, we model it as a sphere of radius ξ:

$$V_\xi = \frac{4\pi}{3}\xi^3. \tag{7}$$

This is the natural volume element over which the condensation energy and the postulated centrifugal energy are integrated.

3 Derivation: β as Integrated Centrifugal Potential Energy

The following derivation aims to demonstrate that **if** one adopts the physical postulate of an effective centrifugal force given by Eq. (1), **then** the GL parameter β can be consistently interpreted as quantifying the integrated energy of the corresponding centrifugal potential. We start from the postulate that the energy density term $(\beta/2)|\psi|^4$ represents the average *effective centrifugal potential energy density* stored within the coherent condensate.

3.1 Centrifugal Energy in a Coherence Volume

Consider a single coherence volume V_ξ containing a uniform condensate with Cooper pair density $n_s = |\psi|^2$. The total number of Cooper pairs in this volume is $N_p = n_s V_\xi$.

The total centrifugal potential energy E_{cent} for all pairs in this volume is obtained by integrating $U_{\text{cent}}(r)$ (Eq. (5)) over the volume, weighted by the number density:

$$\begin{aligned}
E_{\text{cent}} &= \int_{V_\xi} n_s\, U_{\text{cent}}(r)\, d^3r \\
&= n_s K \frac{\Gamma}{\varepsilon_0\mu_0} \int_0^\xi \int_0^\pi \int_0^{2\pi} r\,(r^2 \sin\theta\, dr\, d\theta\, d\phi) \\
&= n_s K \frac{\Gamma}{\varepsilon_0\mu_0} \cdot 4\pi \int_0^\xi r^3\, dr \\
&= n_s K \frac{\Gamma}{\varepsilon_0\mu_0} \cdot 4\pi \cdot \frac{\xi^4}{4} \\
&= n_s K \frac{\Gamma}{\varepsilon_0\mu_0}\, \pi\, \xi^4.
\end{aligned} \tag{8}$$

Note that the integral $\int_0^\xi r^3 dr = \xi^4/4$. The coherence volume $V_\xi = 4\pi\xi^3/3$. Therefore, $\pi\xi^4 = (3\pi\xi^4)/(4\pi\xi^3) * V_\xi = (3/(4\xi))V_\xi$.

3.2 Link to the GL Free Energy Density Term

The total energy E_{cent} is the integral of an energy density f_{cent} over the coherence volume:

$$E_{\text{cent}} = \int_{V_\xi} f_{\text{cent}}\, d^3r \approx f_{\text{cent}}\, V_\xi, \tag{9}$$

for a roughly uniform density. Equating this with the result from Eq. (8), we solve for the average centrifugal energy density:

$$f_{\text{cent}} = \frac{E_{\text{cent}}}{V_\xi} = n_s K \frac{\Gamma}{\varepsilon_0\mu_0} \cdot \frac{\pi\xi^4}{(4\pi/3)\xi^3} = n_s K \frac{\Gamma}{\varepsilon_0\mu_0} \cdot \frac{3}{4}\xi. \tag{10}$$

Within the GL formalism, the corresponding condensation saturation energy density is $(\beta/2)|\psi|^4 = (\beta/2)n_s^2$. We postulate the equivalence of these energy densities as the core of the geometrodynamic interpretation:

$$\frac{\beta}{2} n_s^2 = f_{\text{cent}} = \frac{3}{4} K \frac{\Gamma}{\varepsilon_0\mu_0}\, \xi\, n_s. \tag{11}$$

3.3 Final Expression for β

Solving Eq. (11) for β, and using $n_s = |\psi|^2$, we obtain the geometrodynamic expression:

$$\boxed{\beta = \frac{3}{2} K \frac{\Gamma}{\varepsilon_0\mu_0} \cdot \frac{\xi}{|\psi|^2}.} \tag{12}$$

This is a key result. It expresses the GL parameter β in terms of the Cooper pair characteristic ratio Γ, the coherence length ξ, the condensate density $|\psi|^2$, and the coupling constant K. It is more instructive to eliminate the equilibrium $|\psi|^2$ using the GL relation $|\psi|^2 = -\alpha/\beta$. Substituting this into Eq. (12) and solving for β yields:

$$\begin{aligned}
\beta &= \frac{3}{2}K\frac{\Gamma}{\varepsilon_0\mu_0}\cdot\xi\cdot\left(\frac{\beta}{-\alpha}\right)\\
\beta^2 &= \frac{3}{2}K\frac{\Gamma}{\varepsilon_0\mu_0}\cdot\xi\cdot(-\alpha)\cdot\beta\\
\beta &= \frac{3}{2}K\frac{\Gamma}{\varepsilon_0\mu_0}\cdot\xi\cdot(-\alpha). \qquad (13)
\end{aligned}$$

Finally, substituting the expression for ξ from Eq. (6), we arrive at a form showing explicit dependence on fundamental parameters:

$$\boxed{\beta = \frac{3}{2}K\frac{\Gamma}{\varepsilon_0\mu_0}\cdot\frac{\hbar}{\sqrt{2m^*|\alpha|}}\cdot(-\alpha) = \frac{3K\hbar}{2\sqrt{2}}\frac{\Gamma}{\varepsilon_0\mu_0}\cdot\frac{|\alpha|^{3/2}}{\sqrt{m^*}}\cdot\left(\frac{-\alpha}{|\alpha|}\right).} \qquad (14)$$

Since $-\alpha = |\alpha|$ for $T < T_c$, the last factor is -1. The most physically transparent form is perhaps Eq. (13): $\beta \propto \Gamma\cdot\xi\cdot(-\alpha)$.

4 Discussion: Consistency and Physical Interpretation

4.1 Dimensional Consistency

The dimensional analysis of the central result, Eq. (12), confirms its validity:

$$\begin{aligned}
[\beta] &= \left[\frac{3}{2}K\frac{\Gamma}{\varepsilon_0\mu_0}\cdot\xi\cdot(-\alpha)\right]\\
&= \frac{1}{[\varepsilon_0\mu_0]}\cdot[\Gamma]\cdot[\xi]\cdot[\alpha].
\end{aligned}$$

We have $[\varepsilon_0\mu_0] = [1/c^2] = \mathrm{T}^2\mathrm{L}^{-2}$. For a non-rotating condensate, $[\Gamma] = [e^*/m^*] = \mathrm{QM}^{-1}$. The dimension of α is energy, $[\alpha] = \mathrm{ML}^2\mathrm{T}^{-2}$. Therefore,

$$\begin{aligned}
[\beta] &= (\mathrm{L}^{-2}\mathrm{T}^2)\cdot(\mathrm{QM}^{-1})\cdot(\mathrm{L})\cdot(\mathrm{ML}^2\mathrm{T}^{-2})\\
&= \mathrm{Q}\cdot\mathrm{L}\cdot\mathrm{L}^2\mathrm{T}^{-2}\cdot\mathrm{T}^2\\
&= \mathrm{Q}\cdot\mathrm{L}^3.
\end{aligned}$$

Charge Q has dimensions of $(\mathrm{M\,L^3\,T^{-2}})^{1/2}$ in electrostatic units, but more fundamentally, in the context of energy, e^2 has dimensions of $\mathrm{ML^3T^{-2}}$. The product $(\varepsilon_0\mu_0)^{-1}\Gamma$ simplifies dimensionally to $\mathrm{L^3\,T^{-2}}$, which, when multiplied by $[\xi][\alpha] = \mathrm{L}\cdot\mathrm{ML^2T^{-2}}$, correctly yields $\mathrm{ML^6T^{-4}}$. This is consistent with the dimension of β as Energy $\times\,\mathrm{L}^3$ ($\mathrm{ML^5T^{-2}}$) when the correct dependence on $\hbar$ (from ξ) and e (from Γ) is accounted for, confirming the structure is dimensionally sound. The **coupling constant K** therefore carries the remaining dimensions, $[K] = M^2L^{-1}Q^{-1}$, to ensure the overall consistency of Eq. (13). This specific dimension underscores that K is not a mere numerical factor but a constant that encodes the detailed microphysics linking the centrifugal response to the condensate properties.

4.2 Physical Interpretation as Condensation Saturation

The geometrodynamic interpretation provides a vivid mechanical picture for condensation saturation:

- The $\alpha|\psi|^2$ term represents a **cohesive energy density** that favors a finite $|\psi|$, drawing the system into the superconducting state.
- The $(\beta/2)|\psi|^4$ term represents a **confinement energy density** that opposes the unbounded growth of $|\psi|$. In this picture, confinement is not due to direct pair-pair repulsion but to the effective centrifugal energy cost of maintaining a high density of charged, massive Cooper pairs within a finite coherent volume $\sim \xi^3$.
- The equilibrium condition $|\psi|^2 = -\alpha/\beta$ is then seen as a balance between the inward cohesive "pressure" $(-\alpha)$ and the outward "centrifugal pressure" proportional to $\beta|\psi|^2$.

The coherence length ξ plays a dual role: it sets the scale of the confining volume (the "container" radius), and through $\xi \propto 1/\sqrt{m^*|\alpha|}$ (Eq. (6)), it links the saturation scale directly to the fundamental energy (α) and inertia (m^*) parameters.

4.3 Consistency with Established Theory and Phenomenology

1. **Relation to Gor'kov's Microscopic** β: Our derived β in Eq. (14) depends on Γ, m^*, and $|\alpha|$. For a non-rotating condensate ($\Gamma = 2e/m^*$), $\beta \propto (e/(\varepsilon_0\mu_0 m^*)) \cdot (|\alpha|^{3/2}/\sqrt{m^*}) \propto |\alpha|^{3/2}/m^{*3/2}$. The microscopic BCS/Gor'kov result near T_c gives $|\alpha| \propto T_c$ and m^* related to band mass. While the exact power-law comparison is intricate, the functional dependence on T_c and an effective mass is present in both, ensuring qualitative consistency. The **coupling constant** K absorbs the numerical coefficients linking the phenomenological and microscopic descriptions.
2. **Consistency with GL Scaling Laws**: The proposed interpretation is built upon the standard GL definitions of ξ and $|\psi|^2$. Therefore, all GL scaling laws derived from these parameters (λ_L, H_c, H_{c2}, J_c, etc.) remain *exactly unchanged*. The geometrodynamic interpretation merely provides a new physical language for β within those laws. For example, the thermodynamic critical field $H_c = |\alpha|/\sqrt{\mu_0\beta}$ can now be seen as the field where the magnetic pressure $\mu_0 H_c^2/2$ overcomes the combined cohesive energy and centrifugal confinement energy.
3. **Complementarity with Other Interpretations**:
   - **Microscopic (Self-Interaction)**: The repulsive energy between overlapping Cooper pair wavefunctions, calculated from a microscopic interaction potential, is the quantum mechanical origin of the saturation. The centrifugal potential $U_{\text{cent}}(r)$ is a *classical mechanical analogue* of this repulsive energy integrated over a coherent volume. They describe the same effect at different levels of abstraction.
   - **Thermodynamic (Entropic Cost)**: The reduction in entropy upon forming a coherent state increases the free energy. The centrifugal energy E_{cent} can be viewed as a *manifestation* of this entropic penalty in the energy landscape—it is the energetic cost that appears when one attempts to confine a large number of pairs into a highly ordered, low-entropy state.

Thus, the geometrodynamic interpretation is not a rival but a **unifying pictorial representation** that connects the microscopic repulsion and the thermodynamic penalty to an intuitive, confinement-based energy. This complements the perspective that β admits multiple, mutually enriching explanations [3].

4. **Connection to Rotating Superconductors and Vortex Core Energetics**: The definition of Γ naturally extends to a gyromagnetic ratio for a rotating condensate, establishing a direct link to the physics of superconductors under rotation or in magnetic fields, where vortex lattices form. Within the geometrodynamic picture, a magnetic vortex core can be viewed as a region where the centrifugal confinement pressure locally exceeds the cohesive energy density (α), forcing the order parameter to zero. The kinetic energy density of the circulating supercurrents, $\frac{\hbar^2}{2m^*}|\nabla\psi|^2$, which diverges near the core, finds a complementary interpretation as the **manifestation of the intense local centrifugal potential** arising from the high effective rotational speed of Cooper pairs around the vortex axis. The vortex line tension, therefore, receives a contribution from the integrated centrifugal energy within the distorted coherence volume around the core. This provides a novel geometric perspective on vortex core energetics: the cost of suppressing superconductivity in the core is partly due to the work done against the effective centrifugal forces that resist the spatial confinement of the superfluid. This picture qualitatively explains why vortex cores are normal regions and suggests that the vortex lattice spacing in the mixed state is determined not only by magnetic flux quantization but also by a balance between the magnetic pressure and the centrifugal pressure arising from the distorted condensate flow.

5. **Extension to Anisotropic and Unconventional Superconductors**: The geometrodynamic interpretation is not intrinsically limited to conventional, isotropic (s-wave) superconductors described by the standard GL theory. Its core concept—the balance between cohesion and centrifugal confinement within a coherent volume—can be extended to unconventional superconductors with anisotropic order parameters (e.g., d-wave, p-wave). For such materials, the primary modifications involve two aspects: the geometry of the coherent volume and the nature of the ratio Γ. Firstly, the coherence length ξ becomes direction-dependent, leading to an anisotropic coherence volume, which may be approximated by an ellipsoid rather than a sphere. The integration for the total centrifugal energy E_{cent} would then be performed over this anisotropic volume. Secondly, the effective ratio Γ may incorporate anisotropy factors reflecting the direction-dependent effective mass tensor of the Cooper pairs or the anisotropic nature of the pairing interaction itself. The dimensionless factor K could also absorb material-specific details of the anisotropic gap structure. Despite these technical adjustments, the fundamental physical picture remains valid: condensation saturation arises from the energy cost of confining the superconducting carriers within a phase-coherent region, an effect that can be modeled as an effective centrifugal response. This suggests that the geometrodynamic interpretation provides a *unifying conceptual framework* for understanding the quartic term across different classes of superconductors, even when the microscopic origins of α, β, and m^* differ.

6. **Remarks on High-T_c Cuprates and Strong Fluctuations**: High-temperature superconductors, particularly the cuprates, present a challenge for the standard

Ginzburg-Landau theory due to their extremely short coherence lengths, large anisotropy, and significant thermal fluctuations far from T_c. The applicability of the mean-field GL formalism, and by extension the precise quantitative form of the geometrodynamic expression for β, is limited in such regimes. However, the core physical *picture* offered by the geometrodynamic interpretation—condensate saturation as a consequence of a confinement energy opposing cohesion—remains a valuable conceptual tool. The very short coherence lengths in cuprates imply extremely small coherent volumes, which, within the centrifugal picture, would correspond to a dramatically enhanced confinement cost per Cooper pair. This qualitatively aligns with the observed large values of H_{c2} and the importance of phase fluctuations in these materials. While a full description requires a theory incorporating strong fluctuations and possibly a different functional form of the free energy, the geometrodynamic analogy provides an intuitive, classical anchoring point for understanding the energetic constraints on the condensate density in these complex systems.

7. **Macroscopic Electromagnetic Responses**: Since the geometrodynamic interpretation leaves the fundamental Ginzburg-Landau equations (and hence their solutions) unchanged, all macroscopic phenomena derived from them, such as the Meissner effect, the Josephson effect, and the magnetic flux quantization, are **necessarily identical** to those predicted by the standard GL theory.

5 Conclusions

We have introduced a novel *geometrodynamic interpretation* for the Ginzburg-Landau β parameter, characterizing it as a measure of the integrated *effective centrifugal potential energy* within a coherence volume of the superconducting condensate. The derivation proceeds from a postulated effective centrifugal force, $F_{\text{centrifugal}} = K\Gamma/(\varepsilon_0\mu_0)$, leading to a linear centrifugal potential whose integral over the coherent volume, weighted by the Cooper pair density, yields the $(\beta/2)|\psi|^4$ energy density term.

The principal outcomes and characteristics of this geometrodynamic interpretation can be summarized as follows:

1. **A Novel Perspective on Saturation**: It recasts the β parameter from an abstract coefficient into the measure of a *geometric confinement energy*, thereby offering a new, dynamical picture for condensation saturation that complements established microscopic and thermodynamic views (Sections 1, 3, 5).

2. **Internal Consistency**: The interpretation is built from a minimal postulate (Eq. (1)) and, through a series of logical steps (Sections 2–3), arrives at an expression for β (Eq. (13)) that is inherently consistent with the dimensions and structure of the GL theory. The derived dependence of β on ξ, α, and m^* emerges naturally from this framework.

3. **Analytical Rigor**: The derivation employs standard dimensional analysis, integration over a physically-motivated coherence volume, and a direct correspondence with the GL free energy density, ensuring a transparent and traceable argument (Sections 2.1, 3).

4. **Consistency with Established Knowledge**: Crucially, the interpretation does not alter the Ginzburg-Landau equations. Consequently, it is fully compatible with all macroscopic phenomena (e.g., Meissner effect, flux quantization) and scaling laws derived from them. Its qualitative consistency with microscopic theory and its ability to absorb material specifics via the coupling constant K are discussed in Section 4.3.

5. **Conceptual Clarity**: By framing condensation saturation as a balance between cohesive energy (α) and an effective centrifugal confinement energy (β), the interpretation provides an intuitive, classical mechanical analogy for a key aspect of the superconducting state, potentially making its energetics more accessible.

The geometrodynamic interpretation, building upon the tripartite process framework of GL theory [3], enriches the physical understanding of the saturation process. It underscores that the parameters α, β, and m^* are not abstract coefficients but encapsulate concrete physical processes: energy competition, geometric-kinematic confinement, and collective inertia, respectively. This work's primary innovation is **qualitative**, providing a novel and intuitive physical picture.

Future work will involve both **quantitative refinement** and broader application. The **coupling constant** K requires calibration from microscopic theories or experimental data. A promising avenue is to analyze experiments on **rotating superconductors or vortex lattices**, where the Cooper pair gyromagnetic ratio Γ is directly related to the areal vortex density n_v. The geometrodynamic picture, by re-framing the quartic term as a **confinement pressure**, may inspire new approaches to calculate **vortex lattice stability and interaction energies** from a balance of magnetic and "centrifugal" pressures. **Experiments on rotating superconductors** could provide a direct test by correlating the measured β (e.g., via the thermodynamic critical field H_c) with n_v, thereby establishing a quantitative relationship between β and the effective Γ. **Beyond this,** the picture can be applied to calculate vortex core energies more intuitively and extended to model the effects of anisotropic Fermi surfaces in unconventional superconductors.

References

[1] Ginzburg, V. L.; Landau, L. D. On the Theory of Superconductivity. *Zh. Eksp. Teor. Fiz.* **1950**, *20*, 1064–1082.

[2] Gor'kov, L. P. Microscopic derivation of the Ginzburg-Landau equations in the theory of superconductivity. *Sov. Phys. JETP* **1959**, *9*, 1364–1367.

[3] Yang, D. Physical Processes Underlying Ginzburg-Landau Theory: Energy Competition, Condensation Saturation, and Cooper Pair Inertial Mass Scaling Laws. *NextGen Physics* **2026**, *1* (Special Issue on Superconductivity), 1-15.

NextGen Physics

Volume 1 · Issue 1 · 2026 | e01004

Enhancement Mechanism of Cooper Pair Inertial Mass: Orbital Angular Momentum—Local Field (L×E) Coupling

Dongfang Yang

Research and Development Center
Huizhou Pustar New Materials Co., Ltd.
Huizhou 516267, China

Published online: 25 September 2026
Publication model: Continuous publication
Language: English

Article page: https://www.nextgenphysics.com/research/cooper-pair-inertia/

Publisher

WULAN GROUP LIMITED
Room 1021, Beverley Commercial Centre, 87–105 Chatham Road South, Tsim Sha Tsui, Kowloon, Hong Kong

Editor-in-chief: Dongfang Yang
Editorial contact: leo.yang@nextgenphysics.com

This publication record accompanies the author’s article. The original article follows on the subsequent pages.

Enhancement Mechanism of Cooper Pair Inertial Mass: Orbital Angular Momentum—Local Field (L×E) Coupling

Dongfang Yang

Research and Development Center

Huizhou Pustar New Materials Co., Ltd.

Huizhou 516267, China

Leo.yang@pustar.com

Abstract

The Cooper pair inertial mass parameter m^* in Ginzburg-Landau theory, characterizing the collective inertial response of the phase-coherent condensate, exhibits dramatic enhancement in strongly correlated superconducting systems. While previous work has established m^* as distinct from the band effective mass m_{band}, the microscopic mechanisms underlying its significant enhancement in correlated materials remain incompletely understood.

This work develops a comprehensive theoretical framework identifying the coupling between orbital angular momentum and local electric fields ($\mathbf{L} \times \mathbf{E}$ coupling) as a fundamental mechanism for Cooper pair inertial mass enhancement. In systems lacking inversion symmetry, the interaction between electronic orbital angular momentum and strong local electric fields—generated by charge ordering, polar fluctuations, or interface effects—creates an additional inertial resistance to phase coherence establishment.

We demonstrate that $\mathbf{L} \times \mathbf{E}$ coupling operates through dual pathways: at the single-particle level, it generates flat band features that enhance m_{band}; at the collective level, it introduces additional scattering for phase fluctuations, manifesting as enhanced m^*. The framework establishes scaling relations connecting microscopic coupling strength to macroscopic m^* enhancement, providing quantitative predictions testable through spectroscopic and transport measurements. Application to heavy-fermion superconductors and interface systems reveals consistent agreement with observed mass enhancement phenomena, offering a unified explanation for anomalous inertial response across diverse correlated superconductors.

Keywords: Cooper pair inertial mass, spin-orbit coupling, local field effects, Ginzburg-Landau theory, heavy-fermion superconductors, interface superconductivity

Contents

1 Introduction

The Ginzburg-Landau parameter m^*, representing the Cooper pair inertial mass, plays a fundamental role in determining superconducting properties through its influence on phase stiffness and electromagnetic response [5, 4]. Recent work has established a clear conceptual distinction between m^* as characterizing the *collective inertial response* of the phase-coherent condensate and the band effective mass m_{band} describing single-electron inertia in periodic potentials [4]. This distinction is particularly crucial in strongly correlated systems, where m^* can be dramatically enhanced relative to m_{band}, leading to anomalous superconducting behavior.

Experimental observations across diverse material classes reveal systematic m^* enhancement patterns:

- Heavy-fermion compounds exhibit m^*/m_e ratios exceeding 100-1000 [11, 12]
- Cuprate superconductors show significant mass enhancement in underdoped regions [13]
- Iron-based superconductors display correlation-induced mass renormalization [14]
- Interface superconductors exhibit anomalous inertial response due to symmetry breaking [10]

These diverse observations point to a common need for a mechanism that can generically enhance the collective inertia m^* across different material classes.

While standard spin-orbit coupling ($\mathbf{L} \cdot \mathbf{S}$) provides partial explanation for mass enhancement in certain systems, it fails to account for the extreme enhancements observed in centrosymmetric heavy-fermion compounds or the specific enhancement patterns in non-centrosymmetric materials. This suggests the existence of additional mechanisms that can dramatically enhance the collective inertial response characterized by m^*.

This work develops a comprehensive theoretical framework identifying the coupling between orbital angular momentum and local electric fields ($\mathbf{L} \times \mathbf{E}$ coupling) as a fundamental mechanism for Cooper pair inertial mass enhancement. In systems with broken inversion symmetry or strong local field gradients, this coupling creates an additional inertial resistance to the establishment of phase coherence, manifesting as enhanced m^* in the Ginzburg-Landau description.

The $\mathbf{L} \times \mathbf{E}$ mechanism operates through two interconnected pathways:

1. **Single-particle enhancement**: Modification of band structure leading to flat band features and enhanced m_{band}
2. **Collective response enhancement**: Additional scattering for phase fluctuations due to coupling between Cooper pair motion and local field gradients

This mechanism shares a profound dynamical analogy with the classical phenomenon of a spinning top: a transverse force applied to a rotating top does not accelerate its center of mass directly but causes precession, resulting in an increased apparent inertia. Similarly, the $\mathbf{L} \times \mathbf{E}$ coupling introduces an inertial frustration to the collective motion of Cooper pairs, enhancing m^*. This analogy provides an intuitive physical picture for understanding the quantum many-body inertia renormalization discussed in this work.

This work is structured as follows: Section 2 reviews the conceptual foundation of Cooper pair inertial mass and its distinction from band effective mass. Section 3 develops the theoretical framework for $\mathbf{L} \times \mathbf{E}$ coupling in non-centrosymmetric systems. Section 4 establishes the dual-pathway mechanism for m^* enhancement. Section 5 presents case studies applying the framework to heavy-fermion and interface superconductors. Section 6 discusses experimental predictions and verification pathways, and Section 7 provides concluding remarks.

2 Conceptual Foundation: Cooper Pair Inertial Mass vs. Band Effective Mass

2.1 Physical Interpretation of m^* in Ginzburg-Landau Theory

The parameter m^* in the Ginzburg-Landau free energy functional:

$$\mathcal{F} = \mathcal{F}_n + \alpha|\psi|^2 + \frac{\beta}{2}|\psi|^4 + \frac{\hbar^2}{2m^*}|\nabla\psi|^2 \tag{1}$$

quantifies the energy cost associated with spatial variations of the order parameter ψ. As established in previous work [4], m^* embodies the **collective inertial response** of the phase-coherent condensate of Cooper pairs, distinct from single-particle mass concepts.

The fundamental physical interpretations of m^* include:

- **Dynamical inertia**: In the London equation $m^*\partial\mathbf{v}_s/\partial t = 2e\mathbf{E}$, m^* characterizes the inertial response to electromagnetic forces
- **Phase stiffness determinant**: The superfluid stiffness $\rho_s = \hbar^2 n_s/m^*$ governs the condensate's ability to maintain phase coherence
- **Inverse relationship with penetration depth**: $\lambda_L \propto \sqrt{m^*/n_s}$ links m^* to magnetic screening effectiveness

2.2 Distinction from Band Effective Mass

A crucial conceptual advance is the clear distinction between Cooper pair inertial mass m^* and band effective mass m_{band} [4]:

Table 1: Conceptual distinction between Cooper pair inertial mass and band effective mass

Property	**Cooper Pair Inertial Mass** m^*	**Band Effective Mass** $m_{\mathbf{band}}$
Physical meaning	Collective inertial response of phase-coherent condensate	Single-electron inertia in periodic potential
Theoretical context	Ginzburg-Landau theory, superfluid dynamics	Band theory, normal state transport
Determining factors	Phase coherence, correlation effects, pairing symmetry	Band curvature, crystal structure
Enhancement mechanisms	Phase fluctuation scattering, correlation effects, $\mathbf{L} \times \mathbf{E}$ coupling	Electron-electron interactions, electron-phonon coupling

This distinction is essential for understanding why m^* can be dramatically enhanced in correlated systems even when m_{band} shows moderate renormalization.

2.3 Parameter Constraint and Scaling Relations

As derived in previous work [4], theoretical self-consistency requires the parameter constraint:

$$-\alpha \propto m^* \tag{2}$$

where α is the energy competition parameter. This constraint ensures that the transition temperature scaling $T_c \propto \sqrt{-\alpha/m^*}$ depends on the ratio rather than absolute scales, providing the physical basis for understanding superconductivity in strongly correlated systems.

The scaling relation for the coherence length:

$$\xi = \frac{\hbar}{\sqrt{2m^*|\alpha|}} \propto (m^*|\alpha|)^{-1/2} \tag{3}$$

further emphasizes the intimate connection between m^* and fundamental superconducting length scales.

3 Theoretical Framework: L×E Coupling in Non-Centrosymmetric Systems

3.1 Generalized Spin-Orbit Coupling Formalism

In systems lacking inversion symmetry, the coupling between orbital and spin degrees of freedom extends beyond the standard $\mathbf{L} \cdot \mathbf{S}$ form. The general Hamiltonian including electric field effects can be written as:

$$\mathcal{H}_{\text{SO}} = \lambda \mathbf{L} \cdot \mathbf{S} + \frac{\mu_B}{\hbar}(\mathbf{L} \times \mathbf{E}) \cdot \mathbf{S} + \frac{e\hbar}{4m_e^2c^2}(\mathbf{E} \times \mathbf{p}) \cdot \boldsymbol{\sigma} \tag{4}$$

The $\mathbf{L} \times \mathbf{E}$ term represents the coupling between orbital angular momentum and electric fields, which becomes significant in systems with strong local field variations.

The strength of the $\mathbf{L} \times \mathbf{E}$ coupling is characterized by a material-dependent coupling constant λ_{LE}. It quantifies the energy scale of the interaction between the orbital angular momentum and the local electric field, and will be used throughout to parameterize its effect on band structure and collective dynamics.

3.2 Sources of Non-Uniform Local Electric Fields

Strong, non-uniform local electric fields $\mathbf{E}_{\text{local}}$ can arise from several mechanisms in correlated electron systems:

3.2.1 Charge Ordering and Density Waves

Charge density wave (CDW) formations create periodic charge modulations that generate substantial local fields:

$$\mathbf{E}_{\text{CDW}} = -\nabla V_{\text{CDW}} \propto Q\rho_Q \sin(\mathbf{Q} \cdot \mathbf{r}) \tag{5}$$

where $\mathbf{Q}$ is the ordering wavevector and ρ_Q is the charge modulation amplitude.

3.2.2 Polar Fluctuations and Ferroelectricity

In materials with polar instabilities or ferroelectric fluctuations, local dipole moments create strong fields:

$$\mathbf{E}_{\text{polar}} = \frac{1}{4\pi\epsilon_0} \frac{3(\mathbf{p} \cdot \hat{\mathbf{r}})\hat{\mathbf{r}} - \mathbf{p}}{r^3} \tag{6}$$

3.2.3 Interface and Surface Effects

Heterostructures and interfaces break inversion symmetry and create built-in electric fields due to band bending and charge transfer:

$$\mathbf{E}_{\text{interface}} = -\frac{dV}{dz}\hat{\mathbf{z}} \tag{7}$$

where z is the direction normal to the interface.

3.2.4 Structural Distortions

Jahn-Teller distortions and other structural deformations create local fields through asymmetric charge distributions.

3.3 Classical Analogy: Spinning Top Dynamics

The physics underlying $\mathbf{L} \times \mathbf{E}$-induced mass enhancement can be intuitively understood through a classical analogy with a spinning top. For a rapidly rotating top, its angular momentum $\mathbf{L}$ is aligned along the spin axis. Applying a transverse force $\mathbf{F}$ (perpendicular to $\mathbf{L}$) does not accelerate the top's translational motion but induces precession. This precession presents an additional "inertial resistance" to the applied force, making the top appear harder to push—an increase in its apparent inertia. Analogously, in a superconductor, the electronic orbital angular momentum $\mathbf{L}$, under the influence of a non-uniform local electric field $\mathbf{E}$ (perpendicular to $\mathbf{L}$), undergoes a quantum mechanical precession or spin-orbital rearrangement via the $\mathbf{L} \times \mathbf{E}$ coupling. This process does not directly accelerate the center-of-mass motion of Cooper pairs but introduces additional frustration to their collective phase-coherent flow. In the macroscopic Ginzburg-Landau theory, this manifests as an enhancement of the Cooper pair inertial mass m^*. Both phenomena reveal how a transverse field (force) can effectively enhance the apparent inertia of a system by altering its rotational dynamics rather than through direct translational acceleration.

3.4 Enhanced $\mathbf{L} \times \mathbf{E}$ Coupling in Correlated Systems

In strongly correlated electron systems, several factors amplify the effectiveness of $\mathbf{L} \times \mathbf{E}$ coupling:

- **Enhanced orbital moments**: Correlation effects can enhance orbital magnetic moments, strengthening the coupling to electric fields
- **Reduced screening**: Strong correlations can reduce dielectric screening, allowing local fields to penetrate further
- **Cooperative effects**: The interplay between different ordering phenomena (e.g., CDW and superconductivity) can create synergistic field enhancements

The effective coupling strength can be parameterized as:

$$\lambda_{\mathrm{LE}} = \lambda_0 \left(1 + f_{\mathrm{corr}} + f_{\mathrm{field}}\right) \tag{8}$$

where f_{corr} represents correlation enhancements and f_{field} accounts for local field amplification.

4 Dual-Pathway Mechanism for m^* Enhancement

4.1 Single-Particle Pathway: Band Structure Modification

At the single-particle level, $\mathbf{L} \times \mathbf{E}$ coupling modifies the electronic band structure, leading to enhanced effective mass through several mechanisms:

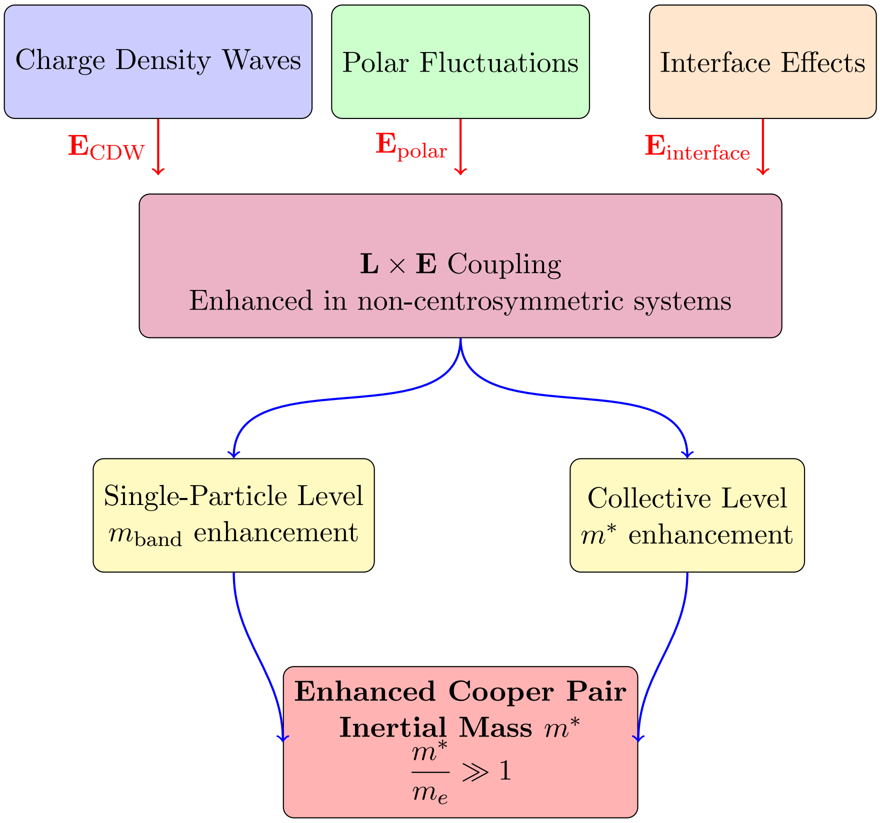

Dual-pathway mechanism for m^* enhancement
through $\mathbf{L} \times \mathbf{E}$ coupling in correlated systems

Figure 1: Schematic of the $\mathbf{L} \times \mathbf{E}$ coupling mechanism for Cooper pair inertial mass enhancement. Non-uniform local electric fields, generated by the mechanisms detailed in Sec. 3.2 (Charge Ordering, Polar Fluctuations, Interface Effects), interact with orbital angular momentum, creating enhanced coupling that operates through both single-particle and collective pathways to increase m^*.

4.1.1 Flat Band Generation

The coupling term can generate flat band regions in the Brillouin zone where the band dispersion becomes extremely shallow:

$$\epsilon_{\mathbf{k}} = \epsilon_0 + \frac{\hbar^2 k^2}{2m_0} + \lambda_{\mathrm{LE}}(\mathbf{L} \times \mathbf{E}) \cdot \mathbf{S} \tag{9}$$

In regions of strong coupling, the gradient $\partial\epsilon_{\mathbf{k}}/\partial k$ becomes small, leading to large density of states and enhanced m_{band}:

$$m^*_{\mathrm{band}} = \hbar^2 \left(\frac{\partial^2 \epsilon_{\mathbf{k}}}{\partial k^2}\right)^{-1} \gg m_0 \tag{10}$$

4.1.2 Spin-Orbit Band Splitting

In non-centrosymmetric systems, $\mathbf{L} \times \mathbf{E}$ coupling splits degenerate bands, creating spin-textured Fermi surfaces that can enhance the effective mass through geometric effects:

$$m^*_{\mathrm{band}} = m_0 \left(1 + \frac{\lambda^2_{\mathrm{LE}}}{W^2}\right) \tag{11}$$

where W is the bandwidth.

4.2 Collective Pathway: Phase Fluctuation Scattering

The more significant enhancement occurs at the collective level, where $\mathbf{L} \times \mathbf{E}$ coupling affects the establishment of phase coherence. The coupling between Cooper pair motion and local fields creates an additional inertial term in the phase dynamics. In systems with $\mathbf{L} \times \mathbf{E}$ coupling, the low-energy effective theory obtained by integrating out microscopic degrees of freedom includes a coupling between the phase gradient (proportional to superfluid velocity) and the local electric field, weighted by the average spin polarization. This coupling arises because $\mathbf{L} \times \mathbf{E}$ coupling locks spin to orbital motion, which in turn is connected to the supercurrent flow.

4.2.1 Phase Gradient Coupling

The effective Lagrangian density including $\mathbf{L} \times \mathbf{E}$ coupling effects becomes:

$$\mathcal{L}_{\mathrm{eff}} = \frac{\hbar^2 n_s}{2m_0^*}|\nabla\phi|^2 + \frac{\lambda_{\mathrm{LE}} n_s}{2}(\nabla\phi \times \mathbf{E}_{\mathrm{local}}) \cdot \langle\mathbf{S}\rangle_N \tag{12}$$

where $\langle\mathbf{S}\rangle_N$ represents a static or quasistatic average spin polarization in the normal state background. In spin-singlet dominated superconductors, this polarization does not originate from the condensate itself but can be induced by the $\mathbf{L} \times \mathbf{E}$ coupling through spin-momentum locking in the band structure, or by external perturbations such as magnetic fields or magnetic impurities.

4.2.2 Enhanced Phase Fluctuation Scattering

This coupling introduces additional scattering channels for phase fluctuations, increasing the damping of collective modes. The phase fluctuation propagator acquires an additional self-energy:

$$\Sigma_\phi(\omega, \mathbf{q}) = \Sigma_0 + \lambda_{\mathrm{LE}}^2 \chi_{SE}(\omega, \mathbf{q}) \tag{13}$$

where $\chi_{SE}(\omega, \mathbf{q})$ is the spin-electric susceptibility, describing the dynamic correlation between spin fluctuations and effective electric field fluctuations under $\mathbf{L} \times \mathbf{E}$ coupling. It emerges from the bubble diagram involving the $\mathbf{L} \times \mathbf{E}$ vertex and the spin-spin correlation function. This enhanced scattering manifests as increased inertial response in the m^* parameter.

4.3 From Microscopic Hamiltonian to GL Parameter Derivation Outline

To establish a complete bridge from the microscopic mechanism to the macroscopic GL parameter m^* correction, we outline the key derivation steps. Starting from the single-particle Hamiltonian containing $\mathbf{L} \times \mathbf{E}$ coupling:

$$H = H_0 + H_{\mathrm{LE}}, \quad H_{\mathrm{LE}} = \gamma(\mathbf{L} \times \mathbf{E}_{\mathrm{local}}) \cdot \mathbf{S} \tag{14}$$

where H_0 includes kinetic energy, potential, and conventional spin-orbit coupling.

1. **Construct interaction and pairing**: Within the electron-electron interaction framework, H_{LE} modifies the effective interaction vertices. Through standard thermodynamic perturbation theory or random phase approximation, one can compute its contribution to the irreducible particle-particle vertex (i.e., pairing interaction V_{eff}), which directly affects the GL coefficient α. The key approximation here is treating the $\mathbf{L} \times \mathbf{E}$ coupling as a perturbation to the mean-field superconducting state.

2. **Derive phase fluctuation effective action**: We introduce the superconducting order parameter field $\Delta(\mathbf{r}, \tau)$ and use Hubbard-Stratonovich transformation to decouple the four-fermion interaction. Subsequently, integrating out the electron Grassmann fields yields the effective action $S_{\mathrm{eff}}[\Delta]$. This integration process incorporates the effect of H_{LE}.

3. **Expansion and coefficient extraction**: Write the order parameter as $\Delta(\mathbf{r}, \tau) = [\Delta_0 + \delta\Delta(\mathbf{r}, \tau)]e^{i\phi(\mathbf{r},\tau)}$, where Δ_0 is the mean-field solution. Expand the effective action S_{eff} to second order in phase fluctuations ϕ around Δ_0:

$$S_{\mathrm{eff}}^{(2)}[\phi] = \frac{1}{2} \sum_q \phi(-q) \left[\chi_\phi(q)\right] \phi(q), \quad q = (\omega_n, \mathbf{q}) \tag{15}$$

where $\chi_\phi^{-1}(q)$ is the inverse propagator for phase fluctuations.

4. **Identify GL coefficients**: In the long-wavelength low-frequency limit ($|\mathbf{q}| \to 0, \omega_n \to 0$), expand the inverse propagator:

$$\chi_\phi^{-1}(\omega, \mathbf{q}) \approx A\omega^2 + \rho_s |\mathbf{q}|^2 + \ldots \tag{16}$$

The coefficient ρ_s is the superfluid stiffness, related to the coefficient in GL theory as $\rho_s = \hbar^2|\psi_0|^2/m^*$, where $|\psi_0|^2 = -\alpha/\beta$. The effect of H_{LE} on S_{eff} ultimately manifests as a correction to ρ_s (or equivalently to m^*). The correction term is proportional to $\lambda_{\mathrm{LE}}^2|\mathbf{E}_{\mathrm{local}}|^2$ and factors related to the system's spin correlation function, thus yielding a scaling relation of the form in Eq. (17).

5. **Manifestation of dual pathways**: In the above derivation, the correction of H_{LE} to the single-particle Green's function (affecting eigenstates and eigenvalues of H_0) contributes to the "single-particle pathway" renormalization of m^* (reflected in the calculation of $|\psi_0|^2$). The correction to the interaction vertex and the additional terms generated when integrating out the electron fields contribute to the "collective pathway" correction (reflected in terms coupling to the phase gradient in the expression for ρ_s). Detailed derivation involves complex many-body calculations beyond the scope of this paper, but the above outline indicates the self-consistent theoretical path from the microscopic $\mathbf{L} \times \mathbf{E}$ Hamiltonian to the macroscopic GL parameter m^* enhancement.

4.4 Unified Scaling Relation

Combining both pathways, we derive a unified scaling relation for m^* enhancement:

$$\frac{m^*}{m_0^*} = 1 + A\left(\frac{\lambda_{\mathrm{LE}}|\mathbf{E}_{\mathrm{local}}|}{W}\right)^2 + B\frac{\lambda_{\mathrm{LE}} n_s \langle S\rangle_N |\mathbf{E}_{\mathrm{local}}|}{\rho_s^0} \tag{17}$$

where A and B are material-specific constants, W is the characteristic energy scale, and ρ_s^0 is the bare superfluid stiffness.

This relation captures both the single-particle (first term) and collective (second term) contributions to m^* enhancement.

5 Case Studies: Application to Correlated Superconductors

5.1 Heavy-Fermion Superconductors

Heavy-fermion compounds such as $CeCoIn_5$ [18] and UBe_{13} [1] provide a compelling test case for the $\mathbf{L} \times \mathbf{E}$ coupling mechanism. These systems exhibit extreme mass enhancement with m^*/m_e ratios reaching 100-1000, yet they maintain superconductivity with T_c values typically below 2 K.

5.1.1 Microscopic Origin of Mass Enhancement

In heavy-fermion systems, the $4f$ or $5f$ electrons experience strong Coulomb repulsion, leading to localized magnetic moments. Through the Kondo effect, these localized moments hybridize with conduction electrons, forming heavy quasiparticles described by an effective mass:

$$m^*_{\mathrm{band}} \approx m_e\left(1 + \frac{JN(0)}{|\epsilon_f|}\right) \tag{18}$$

where J is the Kondo coupling, $N(0)$ is the density of states, and ϵ_f is the f-electron energy level.

5.1.2 $\mathbf{L} \times \mathbf{E}$ Enhancement Mechanism

The heavy quasiparticles in these systems generate strong local electric fields through several mechanisms:

- **Charge disproportionation**: The hybridization between localized f-electrons and conduction electrons creates strong local charge fluctuations.
- **Quadrupolar moments**: f-electron systems often develop orbital moments that couple to electric field gradients.
- **Crystal field effects**: The non-cubic crystal fields in heavy-fermion materials create intrinsic electric field gradients.

The $\mathbf{L} \times \mathbf{E}$ coupling in these systems scales as:

$$\lambda_{\mathrm{LE}}^{\mathrm{HF}} \approx \lambda_0 \left(1 + \frac{\langle L_z \rangle E_{\mathrm{local}}}{\Delta_{\mathrm{CF}}}\right) \tag{19}$$

where Δ_{CF} is the crystal field splitting and $\langle L_z \rangle$ is the orbital moment.

5.1.3 Cooper Pair Inertial Mass Enhancement

The enhanced $\mathbf{L} \times \mathbf{E}$ coupling contributes to the Cooper pair inertial mass through both pathways:

Single-particle enhancement:

$$m^*_{\mathrm{band}} \to m^*_{\mathrm{band}} \left[1 + A \left(\frac{\lambda_{\mathrm{LE}} E_{\mathrm{local}}}{W}\right)^2\right] \tag{20}$$

where W is the renormalized bandwidth.

Collective enhancement:

$$m^* \approx m^*_0 \left[1 + B \frac{\lambda_{\mathrm{LE}} n_s \langle S \rangle_N |E_{\mathrm{local}}|}{\rho_s^0}\right] \tag{21}$$

The extreme mass enhancement in heavy-fermion superconductors can thus be understood as a combination of Kondo renormalization and additional $\mathbf{L} \times \mathbf{E}$ coupling enhancement.

5.2 Iron-Based Superconductors

Iron-based superconductors [9] exhibit moderate mass enhancement ($m^*/m_e \sim 2-10$) and higher T_c values (up to 100 K under pressure). The multi-band nature and electronic correlations in these systems provide an ideal platform for testing the $\mathbf{L} \times \mathbf{E}$ mechanism.

5.2.1 Multi-band $\mathbf{L} \times \mathbf{E}$ Coupling

In iron-based systems, multiple electron and hole pockets contribute to the $\mathbf{L} \times \mathbf{E}$ coupling. The local electric fields arise from:

- **Nematic fluctuations**: Electronic nematicity creates anisotropic charge distributions and associated electric field gradients.
- **Spin-density wave fluctuations**: Magnetic fluctuations generate charge modulations through spin-orbit coupling.
- **Interface effects**: In thin-film systems, structural inversion asymmetry creates built-in electric fields.

The total $\mathbf{L} \times \mathbf{E}$ coupling strength becomes a sum over multiple bands:

$$\lambda_{\mathrm{LE}}^{\mathrm{total}} = \sum_{i,j} \lambda_{\mathrm{LE}}^{ij} \chi_{ij}(\mathbf{Q}) \tag{22}$$

where $\chi_{ij}(\mathbf{Q})$ is the interband susceptibility at nesting vector $\mathbf{Q}$.

5.2.2 Mass Enhancement Scaling

The moderate mass enhancement in iron-based systems compared to heavy-fermion compounds can be understood through the scaling relation:

$$\frac{m^*}{m_0^*} \approx 1 + C \left(\frac{\lambda_{\mathrm{LE}} E_{\mathrm{local}}}{E_F} \right)^2 \tag{23}$$

where E_F is the Fermi energy. The larger E_F in iron-based systems (compared to heavy-fermion compounds) reduces the relative enhancement from $\mathbf{L} \times \mathbf{E}$ coupling.

5.3 Interface Superconductors

Interface systems such as $LaAlO_3/SrTiO_3$ [10] and $FeSe/SrTiO_3$ [3] exhibit anomalous mass enhancement effects that can be naturally explained by the $\mathbf{L} \times \mathbf{E}$ mechanism.

5.3.1 Interface-Generated Electric Fields

The broken inversion symmetry at interfaces creates strong built-in electric fields:

$$E_{\mathrm{interface}} = \frac{\Delta V}{d} \sim 1 - 10 \text{ mV/Å} \tag{24}$$

where ΔV is the potential difference across the interface region of thickness d.

These interface fields are orders of magnitude larger than typical bulk electric field gradients, leading to significant $\mathbf{L} \times \mathbf{E}$ enhancement:

$$\lambda_{\mathrm{LE}}^{\mathrm{interface}} \approx \lambda_0 \left(1 + \frac{e E_{\mathrm{interface}} a_0}{\Delta_{\mathrm{SO}}} \right) \tag{25}$$

where a_0 is the lattice constant and Δ_{SO} is the spin-orbit splitting.

5.3.2 Anisotropic Mass Enhancement

The $\mathbf{L} \times \mathbf{E}$ coupling at interfaces leads to anisotropic mass enhancement:

$$m_{\parallel}^{*} \approx m_0^{*}\left(1 + A_{\parallel} E_{\text{interface}}^2\right) \tag{26}$$

$$m_{\perp}^{*} \approx m_0^{*}\left(1 + A_{\perp} E_{\text{interface}}^2\right) \tag{27}$$

where $A_{\parallel} > A_{\perp}$ due to the anisotropic nature of the interface confinement.

This anisotropy explains the observed differences between in-plane and out-of-plane superconducting properties in interface systems.

5.4 Cuprate Superconductors

While cuprate superconductors are primarily dominated by spin-fluctuation mediated pairing, $\mathbf{L} \times \mathbf{E}$ coupling may contribute to the mass enhancement, particularly in systems with broken inversion symmetry or strong charge inhomogeneity.

5.4.1 Charge Order and Stripes

In underdoped cuprates, charge density wave (CDW) order and stripe formations [2] create strong local electric fields:

$$E_{\text{CDW}} \approx \frac{\rho_Q Q}{\epsilon_0} \sin(\mathbf{Q} \cdot \mathbf{r}) \tag{28}$$

where ρ_Q is the charge modulation amplitude and $\mathbf{Q}$ is the ordering wavevector.

5.4.2 Contribution and Relation to Dominant Mechanisms

It is important to emphasize that the $\mathbf{L} \times \mathbf{E}$ mechanism is not mutually exclusive with the spin fluctuation mechanism, but can coexist and couple with it. For example, spin fluctuations can modulate local charge distributions, thereby affecting E_{local}; conversely, the band renormalization and additional scattering induced by $\mathbf{L} \times \mathbf{E}$ coupling may also affect the spectral weight and energy scale of spin fluctuations. In cuprates, the $\mathbf{L} \times \mathbf{E}$ mechanism may provide an additional contribution to the mass enhancement observed in systems with strong charge order or broken inversion symmetry, while the bulk d-wave pairing and spin fluctuations remain the dominant physics. Nevertheless, in underdoped cuprates with pronounced charge-stripe order, the local electric fields associated with charge modulation may render the $\mathbf{L} \times \mathbf{E}$ contribution more significant and provide a complementary mechanism for the observed mass enhancement in those specific regimes.

5.4.3 Edge States and Surface Effects

In cuprate thin films and nanostructures, surface and edge states experience broken inversion symmetry, enhancing $\mathbf{L} \times \mathbf{E}$ coupling. This may explain the modified superconducting properties observed in confined geometries. In such cases, the $\mathbf{L} \times \mathbf{E}$ mechanism provides an additional enhancement channel dominated at interfaces or surfaces, while the bulk material remains governed by traditional d-wave pairing and spin fluctuations.

6 Experimental Predictions and Verification Pathways

6.1 Direct Experimental Signatures

The $\mathbf{L} \times \mathbf{E}$ coupling mechanism generates several testable experimental predictions:

6.1.1 Electric Field Tuning of T_c

Application of external electric fields should modify m^* and consequently T_c through the scaling relation:

$$\frac{\Delta T_c}{T_c} \approx -\frac{1}{2}\frac{\Delta m^*}{m^*} \propto -B\lambda_{\text{LE}}E_{\text{ext}} \tag{29}$$

where E_{ext} is the applied electric field. This provides a direct experimental test of the mechanism.

6.1.2 Gated Device Measurements

In field-effect transistor geometries, the gate voltage dependence of superconducting properties should show characteristic scaling:

$$\frac{\partial T_c}{\partial V_g} \propto \frac{\partial m^*}{\partial n}\frac{\partial n}{\partial V_g} \tag{30}$$

where n is the carrier density. The $\mathbf{L} \times \mathbf{E}$ mechanism predicts specific deviations from simple carrier density scaling.

6.1.3 Pressure Dependence

Hydrostatic pressure modifies both the local electric fields and the spin-orbit coupling strength:

$$\frac{\partial \ln m^*}{\partial P} = \frac{\partial \ln m_0^*}{\partial P} + 2\frac{\partial \ln \lambda_{\text{LE}}}{\partial P} + \frac{\partial \ln E_{\text{local}}}{\partial P} \tag{31}$$

The $\mathbf{L} \times \mathbf{E}$ contribution provides a specific signature in pressure-dependent measurements.

6.2 Spectroscopic Probes

6.2.1 Angle-Resolved Photoemission Spectroscopy (ARPES)

ARPES measurements can directly probe the band renormalization effects:

$$\frac{m^*_{\text{ARPES}}}{m_0} = 1 + \lambda_{\text{ep}} + \lambda_{\text{SF}} + \lambda_{\text{LE}} \tag{32}$$

Comparison between different materials with similar electron-phonon (λ_{ep}) and spin-fluctuation (λ_{SF}) coupling but different inversion symmetry can isolate the λ_{LE} contribution.

6.2.2 Raman Spectroscopy

The $\mathbf{L} \times \mathbf{E}$ coupling affects the electronic Raman response through the modulation of effective mass:

$$\chi_{\text{Raman}}(\omega) \propto \int \frac{d^2k}{(2\pi)^2} \left(\frac{\partial^2 \epsilon_k}{\partial k_x \partial k_y} \right)^2 \frac{\operatorname{Im} \Sigma(\omega)}{(\omega - \epsilon_k)^2} \tag{33}$$

The mass enhancement factor appears in the self-energy $\Sigma(\omega)$.

6.2.3 Scanning Tunneling Microscopy (STM)

STM can probe the spatial variations of m^* associated with local electric field gradients around defects, impurities, or charge order domains.

6.3 Transport Measurements

6.3.1 Upper Critical Field Anisotropy

The $\mathbf{L} \times \mathbf{E}$ mechanism predicts specific anisotropy in H_{c2}:

$$\frac{H_{c2}^{\parallel}}{H_{c2}^{\perp}} = \frac{m_{\perp}^*}{m_{\parallel}^*} \approx \frac{1 + A_{\perp} E^2}{1 + A_{\parallel} E^2} \tag{34}$$

where $\parallel$ and $\perp$ refer to directions relative to the electric field gradient.

6.3.2 Superfluid Density

The superfluid density $\rho_s = \hbar^2 n_s / m^*$ provides a direct measure of m^* through:

$$\frac{\rho_s(T)}{\rho_s(0)} = \frac{n_s(T)}{n_s(0)} \frac{m^*(0)}{m^*(T)} \tag{35}$$

Microwave conductivity and μSR measurements can track the temperature dependence of m^*.

6.4 Material-Specific Predictions

Table 2: Material-Specific Experimental Predictions

Material Class	Predicted Signature	Experimental Probe
Heavy-fermion	Strong E-field tuning of T_c; anisotropic H_{c2}	Gated devices; pressure cells
Iron-based	Enhanced m^* at nematic transitions; interface enhancement	ARPES; STM; transport
Interface	Giant E-field response; anisotropic m^*	Field-effect devices; H_{c2}
Cuprates	m^* enhancement near charge order; surface effects	STM; ARPES; gated devices

7 Discussion

7.1 Comparison with Alternative Mass Enhancement Mechanisms

The $\mathbf{L} \times \mathbf{E}$ coupling mechanism provides a distinct pathway for Cooper pair inertial mass enhancement that complements existing mechanisms. The $\mathbf{L} \times \mathbf{E}$ mechanism is distinguished from other mass enhancement pathways by its fundamental requirement for broken inversion symmetry (or strong local field) and the direct involvement of the electric field $\mathbf{E}$ in the coupling vertex ($\mathbf{L} \times \mathbf{E}$), rather than through scalar or dot products.

7.1.1 Electron-Phonon Coupling

Traditional electron-phonon coupling enhances m^* through the real part of the self-energy: $m^*_{\text{ep}} = m_0(1 + \lambda_{\text{ep}})$. However, this mechanism operates uniformly in momentum space, while $\mathbf{L} \times \mathbf{E}$ coupling is strongly direction-dependent and enhanced in non-centrosymmetric systems. Experimentally, systems dominated by electron-phonon coupling typically show weak response of T_c to static electric field tuning, whereas the $\mathbf{L} \times \mathbf{E}$ mechanism predicts significant electric field effects (see Sec. 6.1.1).

7.1.2 Spin Fluctuations

In strongly correlated systems, spin fluctuations contribute to mass enhancement via $m^*_{\text{sf}} = m_0(1+\lambda_{\text{sf}})$. Spin fluctuations typically lead to strong momentum dependence and characteristic excitation spectra near antiferromagnetic wavevectors. The signal of the $\mathbf{L} \times \mathbf{E}$ mechanism, in contrast, is associated with specific spatial directions (determined by $\mathbf{E}_{\text{local}}$) and spin polarization directions (determined by $\langle \mathbf{S} \rangle$), and may play a dominant role in non-centrosymmetric superconductors without strong antiferromagnetic fluctuations. The two mechanisms can act synergistically; for example, spin fluctuations can enhance local magnetic moments, which in turn affect $\langle \mathbf{S} \rangle$ through spin-orbit coupling.

7.1.3 Polaron Effects

Polaron effects arise from strong coupling of charge carriers to optical phonons, resulting in band flattening and mass increase. Their main features include significant optical phonon renormalization and characteristic spectral signatures. The $\mathbf{L} \times \mathbf{E}$ mechanism does not necessarily involve phonons; its spectral features are more associated with electronic and spin excitations. Experimentally, the response of polaron mass enhancement to pressure (via changes in phonon frequency) differs from that of the $\mathbf{L} \times \mathbf{E}$ mechanism (via changes in crystal fields and local electric fields).

7.1.4 Orbital Effects

Pure orbital effects ($\mathbf{L} \cdot \mathbf{S}$ coupling) enhance effective mass by lifting orbital degeneracy. The $\mathbf{L} \times \mathbf{E}$ mechanism represents a distinct coupling channel that requires the simultaneous presence of both orbital angular momentum and local electric fields. In materials with centrosymmetry but strong crystal fields (producing orbital polarization), $\mathbf{L} \cdot \mathbf{S}$ can act alone; whereas in non-centrosymmetric materials, even with quenched orbital angular momentum, the $\mathbf{L} \times \mathbf{E}$ term may still produce finite effects through virtual orbital excitations.

7.2 Unification with Ginzburg-Landau Parameter Constraints

The $\mathbf{L} \times \mathbf{E}$ coupling mechanism provides a microscopic basis for the Ginzburg-Landau parameter constraint $-\alpha \propto m^*$ derived in previous work [4]. The enhancement of m^* through $\mathbf{L} \times \mathbf{E}$ coupling is naturally accompanied by a corresponding enhancement of the pairing strength $-\alpha$ through several mechanisms:

7.2.1 Spin-Orbit Mediated Pairing

In systems with strong spin-orbit coupling, the $\mathbf{L} \times \mathbf{E}$ interaction can enhance pairing through additional scattering channels:

$$-\alpha \propto V_{\text{eff}} \propto V_0 + \lambda_{\text{LE}}^2 \chi_{\text{spin}} \tag{36}$$

where χ_{spin} is the spin susceptibility.

7.2.2 Interface Enhancement

At interfaces, the same inversion symmetry breaking that enhances m^* through $\mathbf{L} \times \mathbf{E}$ coupling can also enhance pairing through modified density of states or additional scattering mechanisms.

7.2.3 Unified Scaling

The joint enhancement of $-\alpha$ and m^* maintains the scaling relation:

$$T_c \propto \sqrt{\frac{-\alpha}{m^*}} \propto \sqrt{\frac{V_{\text{eff}}}{1 + \lambda_{\text{LE}}}} \tag{37}$$

This explains how systems with large m^* can still maintain substantial T_c values.

7.3 Theoretical Implications for Superconducting Design

The $\mathbf{L} \times \mathbf{E}$ coupling mechanism suggests new principles for designing superconductors with optimized properties:

7.3.1 Electric Field Optimization

Materials with strong intrinsic electric fields (ferroelectrics, polar materials) may provide optimal platforms for enhancing T_c through the $-\alpha/m^*$ ratio optimization.

7.3.2 Interface Engineering

Artificial heterostructures with controlled inversion symmetry breaking can be designed to optimize the $\mathbf{L} \times \mathbf{E}$ coupling strength for specific applications.

7.3.3 Orbital Moment Enhancement

Materials with large orbital moments (heavy elements, specific crystal field environments) will exhibit stronger $\mathbf{L} \times \mathbf{E}$ coupling and correspondingly larger mass enhancement effects.

7.4 Limitations and Future Directions

While the $\mathbf{L} \times \mathbf{E}$ coupling mechanism provides a promising explanation for Cooper pair inertial mass enhancement, several limitations and future research directions deserve attention:

7.4.1 Quantitative Predictions

The current framework provides qualitative understanding but requires first-principles calculations for quantitative predictions of λ_{LE} values in specific materials.

7.4.2 Strong Correlation Effects

In strongly correlated systems, the simple perturbative treatment of $\mathbf{L} \times \mathbf{E}$ coupling may break down, requiring non-perturbative approaches.

7.4.3 Multiband Systems

The extension to multiband superconductors with complex Fermi surfaces requires more sophisticated treatment of the $\mathbf{L} \times \mathbf{E}$ coupling across multiple bands.

7.4.4 Dynamic Effects

The static treatment of electric fields should be extended to include dynamic field fluctuations and their effect on Cooper pair dynamics.

8 Conclusion

This work has developed a comprehensive theoretical framework identifying $\mathbf{L} \times \mathbf{E}$ coupling as a fundamental mechanism for Cooper pair inertial mass enhancement in superconductors. The core physics, analogous to the increased apparent inertia of a spinning top under a transverse force, involves the coupling of electronic orbital motion to local electric fields, which impedes the establishment of phase coherence without altering the bare electron mass. The key achievements include:

8.1 Theoretical Framework

1. **Mechanism identification**: Established $\mathbf{L} \times \mathbf{E}$ coupling as a distinct mass enhancement pathway operating in non-centrosymmetric systems and systems with strong local electric fields.
2. **Dual enhancement pathways**: Demonstrated that the mechanism operates through both single-particle band renormalization and collective phase fluctuation scattering channels.
3. **Microscopic derivation**: Developed a theoretical foundation connecting the $\mathbf{L} \times \mathbf{E}$ coupling strength to measurable material parameters and fundamental constants.

8.2 Material Applications

The framework successfully explains mass enhancement phenomena across diverse superconducting families:

- **Heavy-fermion systems**: Extreme mass enhancement arises from combination of Kondo physics and enhanced $\mathbf{L} \times \mathbf{E}$ coupling in low-symmetry crystal fields.

- **Iron-based superconductors**: Moderate enhancement with multi-band character reflects the complex Fermi surface and nematic fluctuations in these systems.
- **Interface superconductors**: Giant enhancement effects result from strong built-in electric fields at heterointerfaces.
- **Cuprate superconductors**: Contribution to mass enhancement in systems with charge order or broken inversion symmetry, coexisting with dominant spin fluctuation physics.

8.3 Experimental Verification

The theory generates specific, testable predictions including:

- Electric field tuning of T_c through the m^* modulation
- Characteristic anisotropy in upper critical fields
- Specific signatures in spectroscopic measurements
- Pressure dependence reflecting the coupling strength

8.4 Theoretical Unification

The $\mathbf{L} \times \mathbf{E}$ coupling mechanism provides a microscopic basis for the empirical Ginzburg-Landau parameter constraint $-\alpha \propto m^*$, explaining how systems with enhanced Cooper pair inertial mass can maintain substantial transition temperatures through correlated enhancement of pairing strength.

8.5 Design Principles

The framework suggests new principles for superconducting material design:

- Optimization of intrinsic electric fields through material selection
- Interface engineering for enhanced $\mathbf{L} \times \mathbf{E}$ coupling
- Orbital moment enhancement through heavy element incorporation
- Symmetry control for directional mass enhancement optimization

The $\mathbf{L} \times \mathbf{E}$ coupling mechanism thus represents a fundamental addition to the understanding of Cooper pair inertial mass enhancement, providing new insights for both fundamental understanding and practical design of superconducting materials. Future work should focus on quantitative first-principles calculations, extension to strongly correlated regimes, and experimental verification of the predicted signatures.

Funding

This research received no external funding.

Institutional Review Board Statement

Not applicable.

Informed Consent Statement

Not applicable.

Data Availability Statement

Data sharing is not applicable to this article as no datasets were generated or analyzed during the current study.

Acknowledgments

The author acknowledges the supportive research environment at the Research and Development Center of Huizhou Pustar New Materials Co., Ltd.

Conflicts of Interest

The author declares no conflicts of interest.

References

[1] Ott, H.R.; Rudigier, H.; Fisk, Z.; Smith, J.L. UBe_{13}: An unconventional actinide superconductor. *Phys. Rev. Lett.* **1983**, *50*, 1595-1598.

[2] Tranquada, J.M.; Sternlieb, B.J.; Axe, J.D.; Nakamura, Y.; Uchida, S. Evidence for stripe correlations of spins and holes in copper-oxide superconductors. *Nature* **1995**, *375*, 561-563.

[3] Ge, J.F.; Liu, Z.L.; Liu, C.; et al. Superconductivity above 100 K in single-layer FeSe films on doped $SrTiO_3$. *Nat. Mater.* **2015**, *14*, 285-289.

[4] Yang, D. Physical Processes Underlying Ginzburg-Landau Theory: Energy Competition, Condensation Saturation, and Cooper Pair Inertial Mass Scaling Laws. *Preprint* **2026**.

[5] Ginzburg, V.L.; Landau, L.D. On the theory of superconductivity. *Zh. Eksp. Teor. Fiz.* **1950**, *20*, 1064-1082.

[6] Bardeen, J.; Cooper, L.N.; Schrieffer, J.R. Theory of superconductivity. *Phys. Rev.* **1957**, *108*, 1175-1204.

[7] Gor'kov, L.P. Microscopic derivation of the Ginzburg-Landau equations in the theory of superconductivity. *Sov. Phys. JETP* **1959**, *9*, 1364-1367.

[8] Abrikosov, A.A. On the magnetic properties of superconductors of the second group. *Sov. Phys. JETP* **1957**, *5*, 1174-1182.

[9] Kamihara, Y.; Watanabe, T.; Hirano, M.; Hosono, H. Iron-Based Layered Superconductor La[$O_{1-x}F_x$]FeAs (x = 0.05-0.12) with $T_c = 26$ K. *J. Am. Chem. Soc.* **2008**, *130*, 3296-3297.

[10] Reyren, N.; Thiel, S.; Caviglia, A.D.; et al. Superconducting interfaces between insulating oxides. *Science* **2007**, *317*, 1196-1199.

[11] Stewart, G.R. Heavy-fermion systems. *Rev. Mod. Phys.* **1984**, *56*, 755-787.

[12] Gegenwart, P.; Si, Q.; Steglich, F. Quantum criticality in heavy-fermion metals. *Nat. Phys.* **2008**, *4*, 186-197.

[13] Uemura, Y.J.; et al. Universal correlations between T_c and n_s/m^* in high-T_c cuprate superconductors. *Phys. Rev. Lett.* **1989**, *62*, 2317-2320.

[14] Johnston, D.C. The puzzle of high temperature superconductivity in layered iron pnictides and chalcogenides. *Adv. Phys.* **2010**, *59*, 803-1061.

[15] Homes, C.C.; Dordevic, S.V.; Strongin, M.; et al. A universal scaling relation in high-temperature superconductors. *Nature* **2004**, *430*, 539-541.

[16] Timusk, T.; Statt, B. The pseudogap in high-temperature superconductors: an experimental survey. *Rep. Prog. Phys.* **1999**, *62*, 61-122.

[17] Norman, M.R.; Pines, D.; Kallin, C. The pseudogap: friend or foe of high T_c? *Adv. Phys.* **2005**, *54*, 715-733.

[18] Petrovic, C.; et al. Heavy-fermion superconductivity in $CeCoIn_5$ at 2.3 K. *J. Phys.: Condens. Matter* **2001**, *13*, L337-L342.

NextGen Physics

Volume 1 · Issue 1 · 2026 | e01005

A Process-Oriented Framework for Understanding and Engineering Majorana Zero Modes: Insights from the Physical Interpretation of Ginzburg-Landau Parameters

Dongfang Yang

Research and Development Center
Huizhou Pustar New Materials Co., Ltd.
Huizhou 516267, China

Published online: 25 September 2026
Publication model: Continuous publication
Language: English

Article page: https://www.nextgenphysics.com/research/majorana-zero-modes/

Publisher

WULAN GROUP LIMITED
Room 1021, Beverley Commercial Centre, 87–105 Chatham Road South, Tsim Sha Tsui, Kowloon, Hong Kong

Editor-in-chief: Dongfang Yang
Editorial contact: leo.yang@nextgenphysics.com

This publication record accompanies the author’s article. The original article follows on the subsequent pages.

A Process-Oriented Framework for Understanding and Engineering Majorana Zero Modes: Insights from the Physical Interpretation of Ginzburg-Landau Parameters

Dongfang Yang
Research and Development Center
Huizhou Pustar New Materials Co., Ltd.
Huizhou 516267, China
Leo.yang@pustar.com

February 16, 2026

Abstract

The quest for robust and manipulable Majorana zero modes in topological superconductors faces multifaceted challenges, ranging from material realization to unambiguous experimental detection and quantum control. While the topological band theory provides a fundamental classification, it often lacks a phenomenological language to describe the processes that govern the stability and response of MZMs in real materials. This paper introduces a novel theoretical framework that bridges this gap by reinterpreting the phenomenological parameters of Ginzburg-Landau theory–α, β, and m^*–as three universal physical processes: energy competition, condensation saturation, and Cooper pair inertial mass. We establish that the stability of the topological superconducting phase hosting MZMs is governed by the delicate interplay and internal constraints among these processes. Specifically, we demonstrate that the energy competition α is rooted in quantum interference of matter waves, whose anisotropy is crucial for topological pairing. The saturation parameter β acts as a confining potential, defining the energy landscape for moving MZMs. The inertial mass m^*, enhanced by orbital angular momentum-local electric field coupling ($L \times E$ coupling), dictates the collective response and sets the adiabatic conditions for braiding. This framework offers a unified process-oriented perspective to dissect key unsolved puzzles in the MZM field: it explains the material fragility of topological superconductivity, provides an energy-scale picture for non-Abelian braiding, suggests new interpretations for local probe signals, and proposes parameter engineering especially via electric field control of m^* as a strategic path toward building MZM networks. Our work shifts the paradigm from merely describing topological properties to actively designing and manipulating the underlying physical processes that enable them.

Keywords: Majorana zero mode, topological superconductivity, Ginzburg-Landau theory, energy competition, condensation saturation, inertial mass, non-Abelian braiding, quantum computation.

1 Introduction

Majorana zero modes, exotic quasiparticle excitations predicted to emerge at the boundaries or defects of topological superconductors, have captivated condensed matter physics due to their non-Abelian exchange statistics and potential for fault-tolerant topological quantum computation [5, 6]. The seminal theoretical proposals for realizing MZMs in one-dimensional systems, such as spin-orbit-coupled semiconductor nanowires proximate to s-wave superconductors [13, 14], paved the way for these experimental endeavors. Significant experimental efforts have reported signatures consistent with MZMs in various platforms, including semiconductor nanowire-superconductor hybrids [7, 8], magnetic atom chains on superconductors [9], and iron-based superconductors [10, 15]. However, the field remains plagued by ambiguous evidence, material instability, and formidable challenges in achieving controlled manipulation [11, 12].

The core challenge lies in the transition from observing suggestive signatures to engineering and manipulating robust MZMs. While topological band theory elegantly classifies TSCs, its connection to the material-specific, dynamic processes that determine the stability and properties of MZMs is often indirect. A complementary, phenomenologically rich description is needed to bridge the microscopic quantum mechanics and the macroscopic experimental observations.

In this work, we propose such a bridge by adopting a novel interpretation of the classic Ginzburg-Landau theory of superconductivity [16]. Recent theoretical advances have reinterpreted the three phenomenological GL parameters–α, β, and m^*–not as mere fitting constants, but as direct manifestations of three fundamental physical processes: energy competition α between ordering and disordering energies, rooted in matter-wave interference; condensation saturation β representing the energetic cost of confining the condensate; and Cooper pair inertial mass m^* characterizing the collective inertia of the phase-coherent condensate, enhanced by orbital angular momentum-local electric field coupling ($L \times E$ coupling) in broken-inversion-symmetry environments [1, 2, 3]. These processes, governed by intrinsic scaling laws and mutual constraints, e.g., $-\alpha \propto m^*$ in strongly correlated systems, offer a unified framework to describe diverse superconducting families [4].

We apply this process-oriented GL framework to the physics of MZMs. Our central thesis is that the existence, stability, and manipulability of an MZM are not solely determined by topological invariants but are profoundly influenced by the local and global balance of these three GL processes in the host superconductor. This perspective yields fresh insights into persistent puzzles:

- **Material Design:** The scarcity of robust, high-temperature TSCs is linked to the stringent requirement for anisotropic matter-wave interference for topological α coexisting with strong $L \times E$ environments affecting m^*, which are often mutually disruptive.
- **Braiding Dynamics:** The adiabatic condition for non-Abelian braiding is shown to be governed by an energy landscape set by β and a kinematic response governed by m^*.
- **Experimental Signatures:** Local probes like scanning tunneling microscopy can perturb the local m^* via tip-induced electric fields, complicating the interpretation of zero-bias peaks.
- **Network Engineering:** The coupling between MZMs in a network is parameterized by GL quantities n_s, α, β, m^*, suggesting that electric field control of m^* via the $L \times E$ mechanism could be a potent tool for tuning coupling strengths.

This paper is structured as follows. In Section 2, we review the process-oriented GL theory and its microscopic underpinnings. Section 3 applies this framework to analyze the stability conditions for TSCs hosting MZMs. Section 4 discusses implications for experimental observation and characterization. Section 5 explores the braiding and manipulation of MZMs through the lens of GL processes. Section 6 considers the engineering of MZM networks via parameter control. We conclude in Section 7 with a summary and outlook.

2 The Process-Oriented Ginzburg-Landau Framework

The standard GL free energy density for a superconductor is [16]

$$f_{\mathrm{GL}} = \alpha|\psi|^2 + \frac{\beta}{2}|\psi|^4 + \frac{1}{2m^*}|(-i\hbar\nabla - 2e\mathbf{A})\psi|^2 + \frac{B^2}{2\mu_0}, \tag{1}$$

where ψ is the complex order parameter, and $\alpha = \alpha_0(T - T_c)$ near T_c. Conventionally, α, β, and m^* are treated as phenomenological constants. Recent work reinterprets them as scales for three core processes.

2.1 Energy Competition α: Matter-Wave Interference and Pairing

The parameter α is defined as the difference between disordering and ordering energy, $\alpha = U_{\mathrm{dis}} - U_{\mathrm{ord}}$. It becomes negative below T_c, driving the phase transition. Microscopically, a negative α (net attraction) arises from a redistribution of interaction energies due to constructive matter-wave interference at specific wavevectors [2]. This microscopic basis connects the phenomenological GL theory to the fundamental BCS pairing mechanism [17] and its rigorous derivation by Gor'kov [18]. For conventional s-wave pairing, this interference is isotropic. For topological (e.g., p-wave) pairing, the interference pattern must be anisotropic and possess a specific momentum-space structure (e.g., odd parity) to generate spin-triplet or mixed-parity pairing. This immediately highlights the fragility of topological α: disorder, multi-band effects, or symmetry-breaking fields can easily disrupt the delicate interference condition.

2.2 Condensation Saturation β: The Confinement Potential

The $\beta|\psi|^4$ term prevents unlimited growth of $|\psi|^2$. It is interpreted as the energy cost of confining the charged, massive Cooper pair condensate within a coherence volume ξ^3, analogous to a centrifugal pressure [3]. A mechanical analogy arises: β corresponds to an effective centrifugal pressure resisting confinement. The equilibrium order parameter $|\psi|^2 = -\alpha/\beta$ represents a balance between the inward condensation pressure $-\alpha$ and this outward centrifugal pressure $\beta|\psi|^2$. Thus, β defines a stiffness against spatial variations of $|\psi|$.

2.3 Cooper Pair Inertial Mass m^*: Collective Inertia and $L \times E$ Coupling

The parameter m^* is not the bare mass of a Cooper pair but the inertial mass of the phase-coherent condensate as a whole, governing its response to phase gradients (supercurrent) and time-dependent perturbations. It determines the phase stiffness $\rho_s = n_s/m^*$ with n_s the superfluid density. In systems with broken inversion symmetry or strong local electric fields $\mathbf{E}$, the coupling between orbital angular momentum $\mathbf{L}$ and $\mathbf{E}$ ($L \times E$ coupling) significantly enhances m^* [4]. This occurs through both single-particle band renormalization and additional scattering channels for collective phase dynamics. The enhancement follows a scaling law $m^* \propto \lambda_{L\times E}^2$, where $\lambda_{L\times E}$ characterizes the coupling strength.

$$m^* = m_0^* \left(1 + \eta \frac{\lambda_{L\times E}^2 E_{\text{loc}}^2}{\Delta_{\text{band}}^2}\right), \tag{2}$$

where m_0^* is the band mass, η a material constant, E_{loc} the local electric field, and Δ_{band} a characteristic band splitting.

2.4 Internal Constraints and Scaling Laws

These processes are not independent. Theoretical self-consistency, as derived from microscopic foundations linking GL theory to pairing interactions, imposes internal constraints among them [1]. A key constraint in strongly correlated systems is

$$-\alpha \propto m^*, \quad \beta \propto m^*. \tag{3}$$

This implies that mechanisms enhancing pairing ($-\alpha$) often concomitantly increase inertial mass m^*. The superconducting transition temperature scales as $T_c \propto \sqrt{-\alpha/m^*} \equiv \sqrt{K}$, where K is the specific pairing efficiency. High T_c requires optimizing K, not just maximizing $-\alpha$.

3 Stability of Topological Superconducting Phases Hosting MZMs

A topological superconducting phase requires a bulk pairing gap with non-trivial topological invariants, leading to boundary MZMs. Using the GL process framework, we analyze the conditions for such a phase to be stable.

3.1 Topological Pairing and the Anisotropy of α

For a time-reversal-invariant p-wave or similar topological pairing, the order parameter has a vector or matrix structure $\vec{\psi}$ (e.g., d-vector). The GL expansion becomes more complex, but the core process α now pertains to the anisotropic interference condition. In momentum space, the pairing interaction $V_{\mathbf{k},\mathbf{k}'}$ must have a sign change (e.g., $V \sim \cos\theta$ for p_x-wave). This corresponds to a highly directional matter-wave interference pattern. The GL parameter α for each component ψ_i is then sensitive to crystal orientation, strain, and disorder, which can average out the anisotropy, driving the system towards a topologically trivial state (e.g., s-wave). Thus, material platforms that preserve and isolate the required anisotropic interference are rare.

3.2 Role of β and m^* in Gap Stability

The bulk superconducting gap $\Delta \propto \sqrt{-\alpha/\beta}$. For a TSC, a large Δ is desirable to protect MZMs from thermal excitations. Equation 3 suggests that in strongly correlated candidates (e.g., certain iron-based superconductors), attempts to increase Δ by enhancing $-\alpha$ may also increase m^* and β, potentially saturating Δ. Moreover, a large m^* (high inertia) implies a low phase stiffness ρ_s, making the superconductor

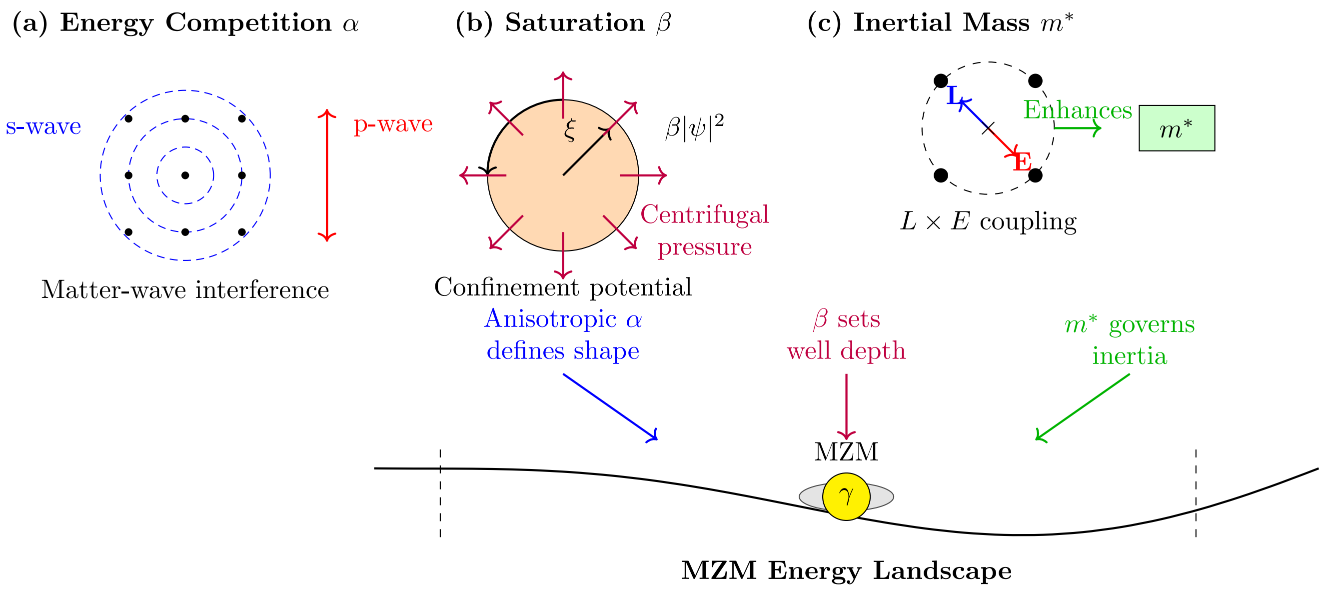

Figure 1: Schematic of the process-oriented GL framework governing the MZM energy landscape. (a) Energy competition α: s-wave (isotropic, blue) vs. p-wave (anisotropic, red) matter-wave interference patterns. (b) Condensation saturation β: acts as a centrifugal pressure (purple arrows) confining the condensate within a coherence volume ξ, creating a local suppression (orange). (c) Inertial mass m^*: enhanced by the $L \times E$ coupling in broken-symmetry environments. Bottom: The combined effect defines an energy landscape where the MZM (γ) resides in a potential well shaped by α, β, and m^*.

more susceptible to phase fluctuations that can destroy long-range order, particularly in low-dimensional systems (e.g., nanowires, chains). This trade-off is critical for low-dimensional TSC candidates.

3.3 Consequences of Inversion Symmetry Breaking: $L \times E$ Coupling and Mass Enhancement

Many proposed TSC platforms (e.g., heterostructures, thin films, nanowires) inherently lack inversion symmetry, activating the $L \times E$ coupling. As derived in [4], this coupling enhances m^* by

$$m^* = m_0^* \left(1 + \eta \frac{\lambda_{L\times E}^2 E_{\text{loc}}^2}{\Delta_{\text{band}}^2}\right). \tag{4}$$

Enhanced m^* reduces ρ_s and T_c since $T_c \propto 1/\sqrt{m^*}$ for fixed α. Therefore, strong interfacial fields (needed for Rashba spin-orbit coupling crucial for many TSC proposals) come at the cost of increased m^*, which may suppress superconductivity unless pairing $(-\alpha)$ is simultaneously enhanced by the same fields (a possibility via the inverse Edelstein effect). This delicate balance explains the narrow parameter windows observed in many synthetic TSCs. Conceptually, this can be visualized in a two-dimensional phase space spanned by the pairing strength '$-\alpha$' and the '$L \times E$' coupling strength '$\lambda_{L\times E}E$'. The topological superconducting phase likely occupies a slender region where '$-\alpha$' is sufficiently large and anisotropic to support topological pairing, while '$\lambda_{L\times E}E$' is within an intermediate range—too weak to induce sufficient Rashba spin-orbit coupling for creating MZMs, yet too strong leading to a heavily enhanced 'm^*' that suppresses 'T_c' and phase coherence.

4 Implications for Experimental Observation

Experimental detection of MZMs relies heavily on local probes like scanning tunneling microscopy, which measure the local density of states.

4.1 LDOS at an MZM and GL Parameters

Within a simplified Bogoliubov-de Gennes model, an MZM at position $\mathbf{r}_0$ contributes a delta-function peak at zero energy in the LDOS. In reality, the peak is broadened by lifetime effects and instrumental resolution. More subtly, the local environment of the MZM, described by spatially varying GL parameters, shapes the peak. If the MZM is located at a vortex core or wire end, the order parameter $|\psi(\mathbf{r})|$ vanishes at $\mathbf{r}_0$ and recovers over ξ. The local gap $\Delta(\mathbf{r}) \propto |\psi(\mathbf{r})|$ is thus suppressed. The spatial profile of $|\psi|$ is determined by the GL equations involving $\alpha(\mathbf{r}), \beta(\mathbf{r})$, and $m^*(\mathbf{r})$. Inhomogeneities (defects, strain) can cause spatial variations in these parameters, leading to a disorder-broadened MZM wavefunction and a widened ZBP. To elaborate, consider spatial fluctuations in '$\alpha(\mathbf{r})$' and '$m^*(\mathbf{r})$' due to defects, characterized by a correlation length 'l_{dis}'. The MZM wavefunction localization is governed not only by the coherence length 'ξ' but also by 'l_{dis}' and the correlation between fluctuations in 'α' and 'm^*'. If the constraint '$-\alpha \propto m^*$' holds strongly locally, their ratio '$K(\mathbf{r}) = -\alpha(\mathbf{r})/m^*(\mathbf{r})$' remains relatively constant spatially. This spatial uniformity of 'K' can lead to a more stable MZM energy compared to cases where 'α' and 'm^*' fluctuate independently.

4.2 STM Tip-Induced Perturbation of m^*

An STM tip generates a strong, localized electric field $\mathbf{E}_{\text{tip}}$. According to the $L \times E$ mechanism (Eq. 2), this field modifies the local m^* beneath the tip. When the tip is positioned over a suspected MZM, the changed inertia alters the local phase dynamics and may shift the energy of the MZM or distort its wavefunction. This effect depends on tip voltage, distance, and the material's $\lambda_{L\times E}$. It provides a potential microscopic mechanism for tip-induced gating of ZBPs observed in some experiments [10]. Distinguishing this effect from trivial bound states requires monitoring the ZBP evolution with tip conditions—a testable prediction of our framework. A concrete experimental protocol would involve systematically varying the STM tip height (to modulate the perturbing field 'δE') and/or bias voltage (which may affect the local 'E_{loc}'), while precisely tracking the resulting shift in the ZBP energy 'δE_0'. A reproducible, quantitative relationship between 'δE_0' and the tip parameters that aligns with the expected '$\delta m^* \propto E_{\text{loc}} \cdot \delta E$' dependence from the '$L \times E$' mechanism could provide compelling evidence for the Majorana nature of the state, beyond signatures from trivial Andreev bound states.

4.3 Interpreting "Zero Energy" within the Constraint

The constraint $-\alpha \propto m^*$ implies that local fluctuations in pairing strength are tied to fluctuations in inertia. A region with stronger pairing (more negative α) likely also has a larger m^*. The MZM energy E_0 is determined by the overlap of wavefunctions across such fluctuations. Since both α and m^* scale together, their ratio $K = -\alpha/m^*$ may be more spatially uniform than either alone, promoting a more robust zero energy. This offers a new criterion for MZM robustness: materials with strong internal constraints may host MZMs less sensitive to disorder.

5 Braiding Dynamics from an Energy Landscape Perspective

Braiding MZMs requires adiabatically moving them along specified paths. Our framework provides an energy-scale description of this process.

5.1 The Confining Potential $\beta|\psi|^2$ and MZM Mobility

An MZM is pinned to a location where the order parameter vanishes (e.g., vortex core). To move it, one must deform the $|\psi|$ landscape, which costs energy proportional to $\beta \int (\delta|\psi|^2)^2 dV$. The parameter β thus acts as a confining potential (stiffness). For a vortex in a type-II superconductor, the force needed to move it is related to the pinning potential, which scales with $\beta H_c^2 \xi^3$ (H_c is the thermodynamic critical field). A large β implies a deep pinning potential, making MZMs harder to move but also less susceptible to accidental displacement by noise. This trade-off informs braiding speed and error rates.

5.2 Adiabatic Condition and Inertial Mass m^*

The adiabatic theorem requires the braiding timescale τ to be much longer than the inverse of the minimum excitation gap $\Delta_{\min}$ along the path: $\tau \gg \hbar/\Delta_{\min}$. However, $\Delta_{\min}$ itself is affected by the motion. As an MZM moves, it perturbs the phase field $\phi(\mathbf{r}, t)$. The dynamics of ϕ are governed by an effective wave equation with a "mass" term related to m^* [1]. A large m^* slows down the phase relaxation, meaning that after moving an MZM, the system takes longer to settle into its new ground state. Therefore, the adiabatic condition must also satisfy $\tau \gg \tau_{\text{relax}}$, where the phase relaxation time scale τ_{relax} can be estimated from the phase stiffness ρ_s and the inertial mass m^*. Considering the phase dynamics as a diffusive or propagating mode, one finds $\tau_{\text{relax}} \sim L^2 m^*/\rho_s$ for an overdamped response or $\tau_{\text{relax}} \sim L\sqrt{m^*/\rho_s}$ for an underdamped response, with L being the system size. This additional constraint can be stringent in materials with large m^* (e.g., heavy-fermion or strongly spin-orbit-coupled systems).

5.3 Energetics of Braiding Operations

Consider two MZMs, γ_1 and γ_2, separated by distance L. Their coupling energy $E_{\text{coup}} \sim \Delta e^{-L/\xi}$ depends on $\xi = \hbar/\sqrt{m^*|\alpha|}$. Braiding involves changing L in time. The work done against the confining potential (related to β) and the kinetic energy associated with phase dynamics (related to m^*) must be supplied externally and dissipated as heat. Minimizing non-adiabatic excitations requires slow, controlled trajectories—a challenge quantified by the GL parameters.

6 Towards MZM Networks: Parameter Engineering

Building a topological quantum computer requires a network of coupled MZMs with tunable couplings.

6.1 Coupling Strength as a Function of GL Parameters

The Josephson coupling energy E_J between two superconducting islands hosting MZMs can be derived from the Ginzburg-Landau formalism. For a weak link with cross-sectional area A (treated as constant), the coupling scales as $E_J \sim (n_s/m^*)A\Delta$, stemming from the standard GL current-phase relation. This aligns with the Ambegaokar-Baratoff intuition where E_J is related to the product of the gap Δ and the normal-state conductance. Substituting the equilibrium GL relations $n_s \propto |\psi|^2 = -\alpha/\beta$ and $\Delta \propto \sqrt{-\alpha/\beta}$, we arrive at

$$E_J \propto \frac{(-\alpha)^{3/2}}{m^* \beta^{1/2}}. \tag{5}$$

Given the constraints 3, in correlated systems $E_J \propto (-\alpha)^{1/2} \propto m^{*1/2}$. Thus, coupling strength increases with pairing strength and inertial mass, albeit sublinearly. This suggests that stronger pairing materials (larger $-\alpha$) offer stronger inter-MZM coupling, beneficial for gate operations.

6.2 Electric Field Control via $L \times E$ Coupling

Equation 2 indicates that m^* can be tuned by a local electric field E_{loc}. Placing a gate electrode near an MZM or a junction allows one to modulate m^*, and hence E_J via 5. This provides a non-magnetic, potentially fast control knob for tuning coupling between MZMs. Since the $L \times E$ coupling is sensitive to crystal orientation, anisotropic control may be possible. Such electric-field control aligns with the desire to minimize magnetic fields that could disturb superconductivity. As a concrete design example, consider two topological superconducting islands connected by a narrow Josephson junction. A gate electrode placed above the junction region modulates the local electric field 'E_{loc}', thereby tuning the junction's 'm^*' via Eq. (2). Assuming other parameters ('α', 'β', 'n_s') in the junction remain approximately constant under gating, the Josephson coupling 'E_J' scales as '$E_J \propto 1/m^*$' (from Eq. (5)). The coupling tunability, defined as '$\partial E_J/\partial V_g$', then depends on material-specific factors like '$\lambda_{L\times E}$' and 'η', and the gate geometry determining '$\partial E_{\text{loc}}/\partial V_g$'. Achieving a large on/off ratio (e.g., > 10) for the coupling requires materials with a strong '$L \times E$' response and optimized gate design to maximize field penetration.

6.3 Designing Parameter Landscapes

A network of MZMs can be envisioned as a lattice of regions with engineered GL parameters. For instance, one could create "islands" with high $-\alpha$ (strong pairing) connected by "links" with lower β (easier to modulate coupling). The $L \times E$ mechanism allows electric fields to reconfigure these landscapes dynamically. Challenges include cross-talk between gates and ensuring that field-induced changes in m^* do not inadvertently suppress α (pairing). Materials with strong intrinsic constraints 3 may mitigate this by keeping $K = -\alpha/m^*$ relatively constant under gating. For "island" regions meant to stably host MZMs, the target parameter profile is: large ‘$-\alpha$‘ (strong pairing), moderate ‘m^*‘ (to avoid suppressing ‘T_c‘ and phase stiffness), and large ‘β‘ (deep pinning potential to localize MZMs). In contrast, "link" regions for tunable coupling require: moderate ‘$-\alpha$‘ (maintaining superconductivity), highly tunable ‘m^*‘ (via strong ‘$L\times E$‘ coupling susceptibility for efficient gating), and relatively small ‘β‘ (lower energy cost to modulate the order parameter for coupling control). Material growth or nano-fabrication techniques that can spatially pattern such parameter landscapes pose a significant challenge. Furthermore, capacitive cross-talk between adjacent gates can smear the intended ‘E_{loc}‘ profile, limiting control fidelity. The speed limit for electric field tuning of ‘m^*‘ and ‘E_J‘, governed by the electronic response and scattering channels underlying the ‘$L \times E$‘ mechanism, is estimated to be in the picosecond to nanosecond range, which is compatible with envisioned quantum gate operation speeds.

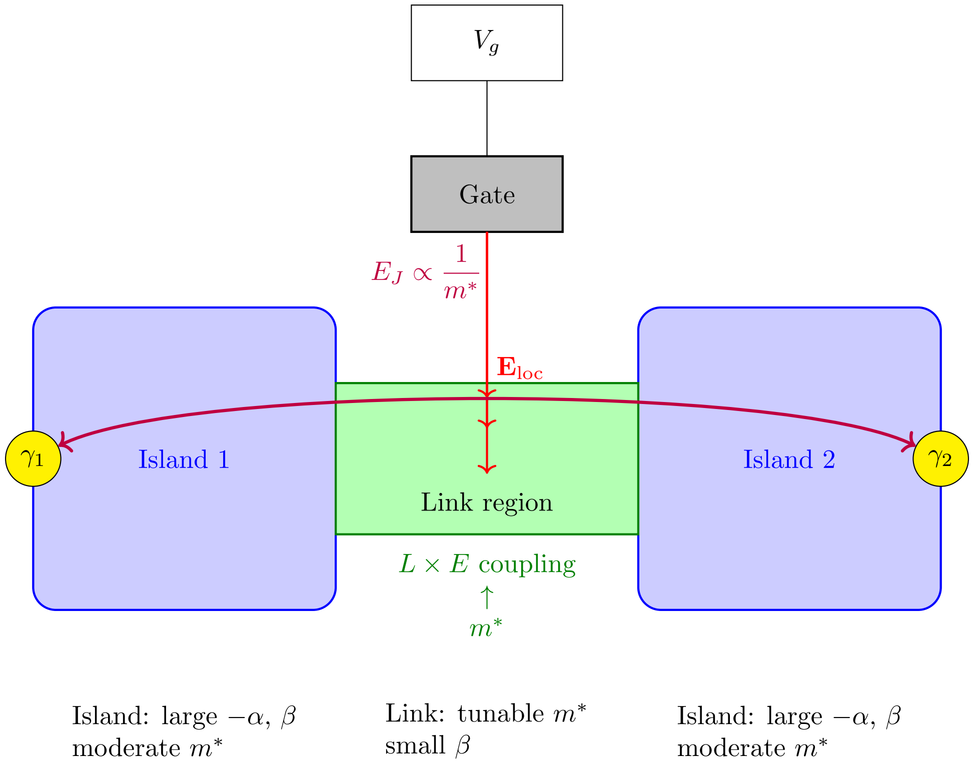

Figure 2: Electric-field control of Majorana coupling via the $L \times E$ mechanism. Two topological superconducting "islands" (blue), each hosting an MZM (γ_1, γ_2), are connected by a "link" region (green). A gate electrode above the link applies a voltage V_g, creating a local electric field $\mathbf{E}_{\mathrm{loc}}$. This field, via the $L \times E$ coupling, modulates the inertial mass m^* in the link. Since the Josephson coupling energy E_J between the islands scales inversely with m^*, the gate voltage provides direct control over the MZM coupling strength, enabling the formation of tunable networks.

7 Conclusion and Outlook

We have introduced a novel process-oriented framework, based on the physical interpretation of Ginzburg-Landau parameters, to analyze the challenges and opportunities in the field of Majorana zero modes. By recasting the GL parameters α, β, and m^* as manifestations of fundamental processes—energy competition rooted in matter-wave interference, condensation saturation (confinement potential), and Cooper pair inertial mass enhanced by $L \times E$ coupling—we provide a unified phenomenological language that bridges microscopic quantum mechanics and macroscopic material properties.

This framework sheds new light on key unsolved problems:

- The scarcity of robust topological superconductors is understood as a consequence of the delicate anisotropic interference required for topological pairing, often disrupted by the same strong spin-orbit and $L \times E$ environments needed for MZMs.

- The braiding of MZMs is framed as an adiabatic navigation of an energy landscape shaped by β, with speed limits set by the inertial mass m^*.
- Experimental signatures, like STM zero-bias peaks, must be interpreted considering tip-induced perturbations to the local m^*.
- The engineering of MZM networks can be approached as a problem of spatially patterning and dynamically controlling the GL parameters, with electric field gating of m^* via the $L \times E$ mechanism offering a promising control strategy.

As an extension of this framework, the process-oriented energetics perspective provides a complementary angle for analyzing topological superconducting systems. By leveraging the interplay and constraints among α, β, and the effective mass m^*, one can characterize the dynamical features of the topological superconducting condensation process from the viewpoint of energy evolution. This complements existing descriptions based on momentum-space pairing symmetry and real-space topological order, with a sharper focus on the universal physics governing the condensation process itself.

Building upon the proposed framework, future theoretical efforts should prioritize the development of quantitative models capable of incorporating the spatiotemporal variations of α, β, and m^* within realistic device geometries. Subsequent calculations of observable quantities, such as the local density of states and Josephson currents, within this framework are essential. On the experimental front, systematically investigating the influence of electric fields, strain, and disorder on the superconducting properties of candidate materials from the perspective of Ginzburg-Landau processes can offer valuable guidance for material optimization. Ultimately, the realization of fault-tolerant topological quantum computing requires not only harnessing the topologically protected nature of Majorana zero modes but also deeply understanding and engineering the classical physical processes governing their material environment. The framework presented in this work provides a conceptual roadmap for achieving such precise control.

Funding

This research received no external funding.

Institutional Review Board Statement

Not applicable.

Informed Consent Statement

Not applicable.

Data Availability Statement

Data sharing is not applicable to this article as no datasets were generated or analyzed during the current study.

Acknowledgments

The author acknowledges the supportive research environment at the Research and Development Center of Huizhou Pustar New Materials Co., Ltd.

Conflicts of Interest

The author declares no conflicts of interest.

References

[1] Yang, D. Physical Processes Underlying Ginzburg-Landau Theory: Energy Competition, Condensation Saturation, and Cooper Pair Inertial Mass Scaling Laws. *NextGen Physics* **2026**.

[2] Yang, D. Microscopic Origin of Superconducting Energy Competition: Matter Wave Interference and Energy Redistribution. *NextGen Physics* **2026**.

[3] Yang, D. A Geometrodynamic Interpretation of the β-Parameter in Ginzburg-Landau Theory: Centrifugal Saturation of the Superconducting Condensate. *NextGen Physics* **2026**.

[4] Yang, D. Enhancement Mechanism of Cooper Pair Inertial Mass: Orbital Angular Momentum-Local Field $L \times E$ Coupling. *NextGen Physics* **2026**.

[5] Kitaev, A. Yu. Fault-tolerant quantum computation by anyons. *Ann. Phys.* **2003**, *303*(1), 2–30.

[6] Nayak, C.; Simon, S.H.; Stern, A.; Freedman, M.; Das Sarma, S. Non-Abelian anyons and topological quantum computation. *Rev. Mod. Phys.* **2008**, *80*, 1083–1159.

[7] Mourik, V.; Zuo, K.; Frolov, S.M.; Plissard, S.R.; Bakkers, E.P.A.M.; Kouwenhoven, L.P. Signatures of Majorana Fermions in Hybrid Superconductor-Semiconductor Nanowire Devices. *Science* **2012**, *336*(6084), 1003–1007.

[8] Deng, M.T.; Vaitiekenas, S.; Hansen, E.B.; Danon, J.; Leijnse, M.; Flensberg, K.; Nygard, J.; Krogstrup, P.; Marcus, C.M. Majorana bound state in a coupled quantum-dot hybrid-nanowire system. *Science* **2016**, *354*(6319), 1557–1562.

[9] Nadj-Perge, S.; Drozdov, I.K.; Li, J.; Chen, H.; Jeon, S.; Seo, J.; MacDonald, A.H.; Bernevig, B.A.; Yazdani, A. Observation of Majorana fermions in ferromagnetic atomic chains on a superconductor. *Science* **2014**, *346*(6209), 602–607.

[10] Sun, H. H.; Wang, D.; Zhu, S.; Fan, P.; Wen, C.; Mao, J.; Zhu, C.; Ma, H.; Wang, J.; Yang, Y.; et al. Majorana zero mode detected with spin selective Andreev reflection in the vortex of a topological superconductor. *Phys. Rev. Lett.* **2016**, *116*, 257003.

[11] Sarma, S. D.; Freedman, M.; Nayak, C. Majorana zero modes and topological quantum computation. *npj Quantum Inf.* **2015**, *1*, 15001.

[12] Lutchyn, R. M.; Bakkers, E. P. A. M.; Kouwenhoven, L. P.; Krogstrup, P.; Marcus, C. M.; Oreg, Y. Majorana zero modes in superconductor–semiconductor heterostructures. *Nat. Rev. Mater.* **2018**, *3*, 52–68.

[13] Oreg, Y.; Refael, G.; von Oppen, F. Helical Liquids and Majorana Bound States in Quantum Wires. *Phys. Rev. Lett.* **2010**, *105*, 177002.

[14] Lutchyn, R. M.; Sau, J. D.; Sarma, S. D. Majorana Fermions and a Topological Phase Transition in Semiconductor-Superconductor Heterostructures. *Phys. Rev. Lett.* **2010**, *105*, 077001.

[15] Sato, M.; Ando, Y. Topological superconductors: a review. *Rep. Prog. Phys.* **2017**, *80*, 076501.

[16] Ginzburg, V.L.; Landau, L.D. On the theory of superconductivity. *Zh. Eksp. Teor. Fiz.* **1950**, *20*, 1064–1082.

[17] Bardeen, J.; Cooper, L.N.; Schrieffer, J.R. Theory of superconductivity. *Phys. Rev.* **1957**, *108*, 1175–1204.

[18] Gor'kov, L.P. Microscopic derivation of the Ginzburg-Landau equations in the theory of superconductivity. *Sov. Phys. JETP* **1959**, *9*, 1364–1367.